UNIVERSITAT POLITÈCNICA DE CATALUNYA

Programa de Doctorat:
AUTOMÀTICA, ROBÒTICA I VISIÓ

Tesi Doctoral

DIGITAL REPETITIVE CONTROL UNDER VARYING FREQUENCY CONDITIONS

Germán Andrés Ramos Fuentes

Director: Ramon Costa Castelló

Maig, 2012

Abstract

The tracking/rejection of periodic signals constitutes a wide field of research in the control theory and applications area and Repetitive Control (RC) has proven to be an efficient way to face this topic; however, in some applications the period of the signal to be tracked/rejected changes in time or is uncertain, which causes and important performance degradation in the standard repetitive controller. This thesis presents some contributions to the open topic of repetitive control working under varying frequency conditions. These contributions can be organized as follows:

One approach that overcomes the problem of working under time varying frequency conditions is the adaptation of the controller sampling period, nevertheless, the system framework changes from Linear Time Invariant (LTI) to Linear Time-Varying (LTV) and the closed-loop stability can be compromised. This work presents two different methodologies aimed at analysing the system stability under these conditions. The first one uses a Linear Matrix Inequality (LMI) gridding approach which provides necessary conditions to accomplish a sufficient condition for the closed-loop Bounded Input Bounded Output (BIBO) stability of the system. The second one applies robust control techniques in order to analyse the stability and yields sufficient stability conditions. Both methodologies yield a frequency variation interval for which the system stability can be assured. Although several approaches exist for the stability analysis of general time-varying sampling period controllers few of them allow an integrated controller design which assures closed-loop stability under such conditions. In this thesis two design methodologies are presented, which assure stability of the repetitive control system working under varying sampling period for a given frequency variation interval: a μ-synthesis technique and a pre-compensation strategy.

On a second branch, High Order Repetitive Control (HORC) is mainly used to improve the repetitive control performance robustness under disturbance/reference signals with varying or uncertain frequency. Unlike standard repetitive control, the HORC involves a weighted sum of several signal periods. Furthermore, the use of an odd-harmonic internal model will make the system more appropriate for applications where signals have only odd-harmonic components, as in power electronics systems. Thus an Odd-harmonic High Order Repetitive Controller suitable for applications involving odd-harmonic type signals with varying/uncertain frequency is presented. The open loop stability of internal models used in HORC and the one presented here is analysed. Additionally, as a consequence of this analysis, an Anti-Windup (AW) scheme for repetitive control is proposed. This AW proposal is based

on the idea of having a small steady state tracking error and fast recovery once the system goes out of saturation.

The experimental validation of these proposals has been performed in two different applications: the Roto-magnet plant and the active power filter application. The Roto-magnet plant is an experimental didactic plant used as a tool for analysing and understanding the nature of the periodic disturbances, as well as to study the different control techniques used to tackle this problem. This plant has been adopted as experimental test bench for rotational machines. On the other hand, shunt active power filters have been widely used as a way to overcome the power quality problems caused by nonlinear and reactive loads. These power electronics devices are designed with the goal of obtaining a power factor close to 1 and achieving current harmonics and reactive power compensation. The implementation on this plant shows the experimental behaviours of the here proposed repetitive controllers under constant and varying network frequency. Also this performance is presented and analysed in terms of the Total Harmonic Distortion (THD), Power Factor (PF) and $cos\phi$.

Acknowledgements

I would like to acknowledge my family for their support and love. My parents, Marlene and Germán, who have always believed in me and supported me in all of my endeavours.

I would especially like to thank my Advisor, Ramon Costa, for his invaluable support and guidance.

I would like to express my gratitude to Josep Olm whose knowledge and assistance were crucial in this work.

I would like to acknowledge the Advanced Control of Energy Systems (ACES) research group for their support and help.

I would like to acknowledge Maarten Steinbuch and Sjirk Koekebakker for their help during my stay in Technische Universiteit Eindhoven.

I would like to thank Universidad Nacional de Colombia for supporting me during all levels of my professional career.

Finally, I would like to thank all of my IOC colleagues for their company and especially for the pleasant talks and debates we share during all this time.

Contents

Part II HORC approach

Part III Experimental validation

List of Tables

List of Symbols

Repetitive control structure

$H(z)$	Robustness filter
$G_p(z)$	Discrete time plant model
$G_x(z)$	Stabilizing filter
k_r	Repetitive control gain
$\tilde{G}_x(z)$	Re-designed stabilizing filter
$G_c(z)$	Loop controller
$S(z)$	Closed-loop sensitivity function
$G_o(z)$	Closed-loop system without repetitive control
$S_o(z)$	Closed-loop sensitivity function without repetitive control
$S_{Mod}(z)$	Modifying sensitivity function for odd-harmonic high order repetitive control
$S_{Mod}^{hodd}(z)$	Modifying sensitivity function
$I(z)$	Generic internal model
$I_{st}(z)$	Standard internal Model
$I_{odd}(z)$	Odd-harmonic internal model
$I_{ho}(z)$	High order repetitive control internal model
$I_{hodd}(z)$	Odd-harmonic high order repetitive control internal model
N	Discrete time signal period
T_p	Continuous time signal period
$W(z)$	Delay function
M	Number of delay blocks
w_k	Weights for high order repetitive control
σ	Determines full or odd harmonic action
T_s	Generic sampling period
$\bar{T}$	Nominal sampling period
T_k	Sampling period at instant k
$\mathscr{T}$	Sampling period interval of variation
θ_k	Sampling period variation variable
$\Delta(\cdot)$	Uncertainty function
Δ_{T_s}	Sampling period variation seen as an uncertainty
Δ_d	Delay function seen as an uncertainty
$C_{aw}(z)$	Anti-windup compensator
$sat(\cdot)$	Saturation function
r_k	Reference signal

e_k	Error signal
u_k	Control signal
$\hat{u}_k$	Control signal output of saturation block
$\bar{u}_k$	Control signal input to saturation block
y_k	System output signal
η_k	Ideal output signal
x_k	State space variable
(A,B,C,B)	State space system representation

Electrical variables

i_n	Current at the source
i_l	Load current
i_f	Inductor current
v_n	Voltage source
L	Inductor
C	Capacitor
r_L	Inductor parasitic resistance
r_C	Capacitor parasitic resistance
$cos\phi$	Current-voltage phase difference
E_C	Energy stored in the capacitors

General symbols

$\mathbb{N}$	Natural numbers
$\mathbb{R}$	Real numbers
$\mathbb{R}^+$	Positive real numbers
$\|\cdot\|$	2-norm of a matrix, i.e. the matrix norm induced by the euclidean vector norm
$\|\cdot\|_\infty$	Infinite norm
$\rho(\cdot)$	Spectral radius
$X(s)$	Continuous time transfer function of system X
$X(z)$	Discrete time transfer function of system X
$\mathscr{Z}\{X(s)\}$	Z-transform of a continuous time transfer function
x^*	Steady state value of signal $x(t)$
$< x >_0$	DC value, or mean value, of the signal $x(t)$
$< x >_{T_n}$	Mean value of the signal $x(t)$ in a period T_n

Abbreviations

AW	Anti-Windup
BIBO	Bounded Input Bounded Output
DLAW	Direct Linear Anti-Windup
DSP	Digital Signal Processor
FIR	Finite Impulse Filter
HORC	High Order Repetitive Control
IEC	International Electrotechnical Commission
IEEE	Institute of Electrical and Electronics Engineers
ILC	Iterative Learning Control
IM	Internal Model
IMC	Internal Model Control
IMP	Internal Model Principle

LMI	Linear Matrix Inequality
LTI	Linear Time Invariant
LTV	Linear Time Varying
LQ	Linear Quadratic
MRAW	Model Recovery Anti-Windup
PF	Power Factor
PI	Proportional Integral
PWM	Pulse Width Modulation
RC	Repetitive Control
RMS	Root Medium Squared
SISO	Single Input Single Output
THD	Total Harmonic Distortion

Chapter 1
Introduction

1.1 Motivation and problem statement

Repetitive control [6, 11, 17, 19] is an Internal Model Principle-based control technique [7] that yields perfect asymptotic tracking and rejection of periodic signals. Essentially, this is achieved by including a generator of the reference/disturbance signal in the control loop. Periodic signals are present in many real-world applications and repetitive control has been successfully used in different control areas, such as CD and disk arm actuators [20], robotics [16], electro-hydraulics [13], tubular heat exchangers [2], electronic rectifiers [23], pulse-width modulated inverters [22, 21] and shunt active power filters [8].

It is usual to design repetitive controllers assuming a fixed period T_p for the signals to be tracked/rejected. Then, a fixed sampling period T_s is selected and, eventually, the value of the ratio $N = T_p/T_s$ is structurally embedded in the control algorithm. However, it is well known that even slight changes in the frequency of the tracked/rejected signals result in a dramatic decay of the controller performance [14]. A large number of practical applications can be affected by this phenomena, these include disturbance period changes caused by speed variations in rotational mechanical systems [4] (CD roms, printers, peristaltic pumps, machining tools, etc.), and frequency variations experimented by power devices (shunt active filters, inverters, rectifiers) connected to the electric distribution network [5].

Several approaches have been introduced to overcome this problem and we can differentiate three groups:

- A first set of proposals dealing with this problem maintain the sampling period T_s constant and adapt the value of N according to the time variation of T_p [12, 18]. This renders a variable structure internal model with an integer approximation N of the ratio T_p/T_s which, under the variations of T_p, is generally a non integer number.
- The following two sets of approaches work with a fixed value of N, its main advantage being quality preservation in signal reconstruction. Thus, the second set of proposals also maintain the initially selected sampling period, and robustness against frequency variations is achieved by means of large memory elements [14, 15] or introducing a fictitious sampler operating at a variable sampling rate and later using a fixed frequency internal model [1, 3]. The former idea works well for small frequency variations at the cost of increasing the computational burden and the later constitutes a very simple method with less computational

load but presents some performance degradation in the high frequency range due to the use of interpolation.
- The third set of schemes proposes to adapt the controller sampling rate according to the reference/disturbance period [9, 10, 18]. This allows the preservation of the steady-state performance while maintaining a low computational cost but, on the other hand, the original LTI system becomes LTV. This structural change requires a new stability study, but no formal proofs regarding this issue are reported in the quoted references.

1.2 Contribution

This thesis presents some contributions to the open topic of repetitive control working under varying frequency conditions. These contributions are developed in the single-input single-output systems framework and can be organized as follows:

- **Stability analysis methods for repetitive control under varying sampling time**. As mentioned before, an efficient way to deal with frequency variations is to adapt the controller sampling time; however a stability analysis should be carried out in order to establish the formal validity of this technique. Two different methodologies are presented: LMI gridding and robust stability analysis. The first method yields necessary conditions for a sufficient stability condition and the second one renders sufficient stability conditions. In both methods, the stability conditions are given for a sampling time variation interval, using the LMI gridding method the stability is rigorously guaranteed only in open neighbourhoods of selected points within the interval while employing the robust control method the stability is assured for the entire variation interval.

- **Design methods for repetitive controllers dealing with varying frequency conditions**. In the frame of a variable sampling time strategy the design problem can be stated as finding a repetitive controller that assures the system stability and performance for a given frequency variation interval. Following this premise, two designs are proposed: a plant pre-compensation, where an additional compensator is added to the standard scheme to provide compensation for the sampling time variation and a robust μ-synthesis design where the part of the system affected by the sampling period variation is treated as a bounded structured uncertainty, thus obtaining a controller that stabilizes the system and preserves the performance for the required frequency interval.

- **Robust performance of repetitive control using high order internal models**. High order repetitive controllers are robust against frequency variation; however they imply a higher computational load compared with the standard controller. Additionally, in some applications like active power filters it is necessary the rejection of disturbance signals with only odd harmonic components. In this sense, an odd-harmonic high order repetitive control is proposed which is able to reject odd-harmonic components and can be implemented to obtain the equivalent computational burden of the standard repetitive controller. Finally, due to the characteristics of the obtained internal models an anti-windup compensation is

added. The design involves an optimal Linear Quadratic approach to obtain the anti-windup filter.

1.3 Outline

This thesis starts with two introductory chapters: Chapter 1 presents and discusses the state of the art, motivation and contributions of this work and Chapter 2 summarizes the RC concepts, basics and drawbacks. Following theses chapters this thesis is divided in three parts. The first part is dedicated to develop contributions based on the varying sampling period approach, the second part is devoted to propose a robust performance strategy and the final part presents the experimental validation of the previously described proposals. The first part, is in turn, divided in two chapters. Chapter 3 presents two stability analysis for systems that work with varying sampling period: an LMI gridding approach and a robust theory-based analysis. In Chapter 4 two control design methods are described: a pre-compensation scheme and a robust control theory-based design. The second part contains Chapter 5, which introduces the odd-harmonic HORC and includes an AW scheme for this type of controller. The third part includes the experimental validation trough two different plants: Chapter 6 presents the Roto-magnet didactic plant experimental results and Chapter 7 describes an active power filter application. Finally, general conclusions an suggested future work are presented in Chapter 8.

References

1. J. Álvarez, L. Yebra, and M. Berenguel. Adaptive repetitive control for resonance cancellation of a distributed solar collector field. *International Journal of Adaptive Control Signal Processing*, 23(4):331–352, 2007.
2. J. Álvarez, L. Yebra, and M. Berenguel. Repetitive control of tubular heat exchangers. *Journal of Process Control*, 17(9):689–701, 2007.
3. Z. Cao and G. F. Ledwich. Adaptive repetitive control to track variable periodic signals with fixed sampling rate. *IEEE/ASME Transactions on Mechatronics*, 7(3):374–384, September 2002.
4. K. Chew and M. Tomizuka. Digital control of repetitive errors in disk drive systems. *IEEE Control Systems Magazine*, pages 16–19, January 1990.
5. R. Costa-Castelló, S. Malo, and R. Griñó. High performance repetitive control of an active filter under varying network frequency. In *Proceedings of the 17th IFAC World Congress*, pages 3344–3349, 2008.
6. R. Costa-Castelló, J. Nebot, and R. Griñó. Demonstration of the internal model principle by digital repetitive control of an educational laboratory plant. *IEEE Transactions on Education*, 48(1):73–80, 2005.
7. B. Francis and W. Wonham. Internal model principle in control theory. *Automatica*, 12:457–465, 1976.
8. R. Griñó, R. Cardoner, R. Costa-Castelló, and E. Fossas. Digital repetitive control of a three-phase four-wire shunt active filter. *IEEE Transactions on Industrial Electronics*, 54(3):1495–1503, 2007.
9. R. D. Hanson and T.-C. Tsao. Periodic sampling interval repetitive control and its application to variable spindle speed noncircular turning process. *Journal of Dynamic Systems, Measurement, and Control*, 122(3):560–566, 2000.
10. G. Hillerström. *On Repetitive Control*. PhD thesis, Lulea University of Technology, November 1994.

11. G. Hillerström and K. Walgama. Repetitive control theory and applications - A survey. In *Proceedings of the 13th IFAC World Congress, Vol. D*, pages 1–6, 1996.
12. J. Hu. Variable structure digital repetitive controller. In *Proceedings of the American Control Conference*, volume 2, pages 2686–2690, 1992.
13. D. H. Kim and T. Tsao. Robust performance control of electrohydraulic actuators for electronic cam motion generation. *IEEE Transactions on Control Systems Technology*, 8(2):220–227, 2000.
14. M. Steinbuch. Repetitive control for systems with uncertain period-time. *Automatica*, 38(12):2103–2109, 2002.
15. M. Steinbuch, S. Weiland, and T. Singh. Design of noise and period-time robust high order repetitive control, with application to optical storage. *Automatica*, 43:2086–2095, 2007.
16. A. Tayebi, S. Abdul, M. Zaremba, and Y. Ye. Robust iterative learning control design: Application to a robot manipulator. *IEEE/ASME Transactions on Mechatronics*, 13(5):608–613, 2008.
17. M. Tomizuka. Dealing with periodic disturbances in controls of mechanical systems. *Annual Reviews in Control*, 32(2):193 – 199, 2008.
18. T.-C. Tsao, Y.-X. Qian, and M. Nemani. Repetitive control for asymptotic tracking of periodic signals with an unknown period. *Journal of Dynamic Systems, Measurement, and Control*, 122(2):364–369, 2000.
19. Y. Wang, F. Gao, and F. J. D. III. Survey on iterative learning control, repetitive control, and run-to-run control. *Journal of Process Control*, 19(10):1589 – 1600, 2009.
20. S.-C. Wu and M. Tomizuka. An iterative learning control design for self-servowriting in hard disk drives. *Mechatronics*, 20(1):53 – 58, 2010.
21. B. Zhang, K. Zhou, Y. Wang, and D. Wang. Performance improvement of repetitive controlled pwm inverters: A phase-lead compensation solution. *International Journal of Circuit Theory and Applications*, 38:453–469, June 2010.
22. K. Zhou and D. Wang. Digital repetitive learning controller for three-phase CVCF PWM inverter. *IEEE Transactions on Industrial Electronics*, 48(4):820–830, August 2001.
23. K. Zhou, D. Wang, and G. Xu. Repetitive controlled three-phase reversible PWM rectifier. In *Proceedings of the American Control Conference*, pages 125–129, 2000.

Chapter 2
Repetitive control

2.1 Introduction

This Chapter describes the concepts and basics of Repetitive Control. The standard internal model and the plug-in scheme structure are used to introduce the design, stability and robustness concepts that are traditionally employed in this technique. The performance of the RC regarding frequency variations or uncertainty is analysed using the magnitude response of the internal model and the closed loop phase behaviour of the system. These response characteristics are evidence of the dramatic lose of performance that occurs when the period of the reference/disturbance signal is time varying or uncertain. Section 2.2 introduces the internal model, the controller structure, stability conditions and design criteria in RC while in Section 2.3, the performance degradation under varying frequency conditions is analysed.

2.2 Basics

2.2.1 The Internal Model

As an Internal Model Principle (IMP) [6] based strategy, Repetitive Control uses an internal model which corresponds with the model of a periodic signal. In order to derive this model, recall that the trigonometric Fourier series expansion of a T_p-periodic signal $r(t)$ reads as:

$$r(t) = a_0 + \sum_{k=1}^{\infty} a_k \cos\frac{2k\pi}{T_p}t + b_k \sin\frac{2k\pi}{T_p}t. \tag{2.1}$$

By the IMP, the inclusion of the model of (2.1) in the control loop results in the tracking/rejection of any T_p-periodic reference/disturbance signal. Hence, following [17], the transfer function of a periodic signal generator may be written as

$$\hat{G}_r(s) = \frac{1}{s}\prod_{k=1}^{\infty}\frac{\left(\frac{2k\pi}{T_p}\right)^2}{s^2+\left(\frac{2k\pi}{T_p}\right)^2} = \frac{T_p e^{-\frac{T_p s}{2}}}{1-e^{-T_p s}}. \tag{2.2}$$

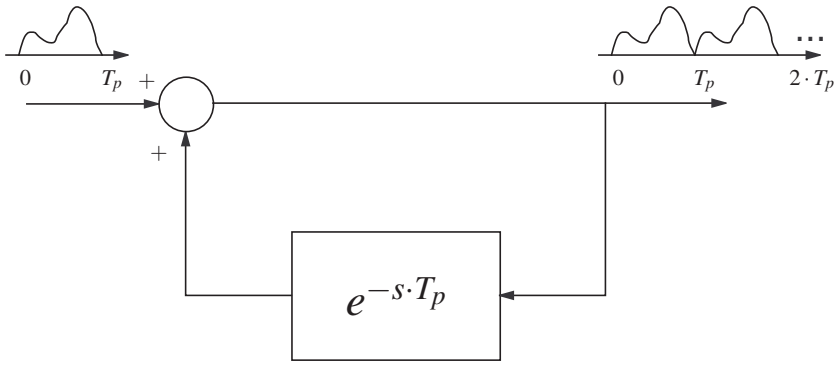

Fig. 2.1 Basic structure for a continuous-time repetitive controller.

However, $T_p e^{-T_p s/2}$ being a delay term with a gain T_p, it is sufficient to include the following continuous time internal model:

$$\bar{G}_r(s) = \frac{1}{1 - e^{-T_p s}}$$

inside the control loop, which can be implemented as $e^{-T_p s}$ with a positive feedback, as depicted in Figure 2.1. Notice that the internal model (2.2) has poles at $s = \pm jk/T_p$, $k \in \mathbb{N}$. Therefore, from a frequency point of view, $\bar{G}_r(s)$ exhibits infinite gain at frequencies k/T_p, $\forall\ k \in \mathbb{N}$. This assures zero tracking error at these frequencies in closed loop if the closed-loop system is stable.

It is also worth mentioning that some studies relate repetitive control with learning control techniques (see, for example, [17]). This is due to the fact that the basic repetitive structure learns a signal of length T_p and repeats it as a periodic signal of period T_p if the input to the system is set to zero (see Figure 2.1).

The implementation of a time delay in continuous-time is a complicated point [11]. Fortunately, in discrete time it is an easier task: if the reference/disturbance signal period T_p is a multiple of the sampling period T_s, the digital implementation is reduced to a circular queue. Therefore, the discrete internal model that should be included in the loop is:

$$G_r(z) = \frac{z^{-N}}{1 - z^{-N}} = \frac{1}{z^N - 1}, \tag{2.3}$$

where $N = T_p/T_s \in \mathbb{N}$.

In addition to the constraint that represents the demand of a constant ratio between T_p and T_s, it is important to point out that T_s should be selected taking into account that discrete-time implementations can only deal with those harmonics which are below the Nyquist frequency $\omega_s/2 = \pi/T_s$. A magnitude response of the internal model 2.3 designed for a 50 Hz periodic signal is depicted in Figure 2.4. It can be noticed that the response presents high gain at the fundamental and harmonic frequencies.

Several types of internal models are used depending on the specific periodic signal to deal with [3, 10, 7, 4]. In this work the following generic internal model will

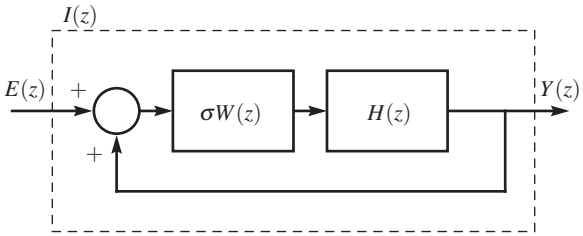

Fig. 2.2 Generic repetitive control internal model scheme, where $W(z)$ is a delay function, $H(z)$ a null-phase low pass filter, and $\sigma \in \{-1,1\}$.

be used

$$I(z) = \frac{\sigma W(z)H(z)}{1-\sigma W(z)H(z)}, \tag{2.4}$$

where $W(z)$ is a time delay function, $H(z)$ is a low pass filter for robustness improvement at high frequencies [2] and σ determines the feedback sign i.e. $\sigma = 1$ and $\sigma = -1$ for positive and negative feedback respectively. Figure 2.2 shows the feedback scheme of this internal model. From the generic model 2.4 the so-called standard, odd-harmonic, high order and odd-harmonic high order internal models can be derived as will be shown in the following chapters. Table 2.1 summarizes different internal models commonly used in RC.

2.2.2 The repetitive controller

Repetitive controllers are composed by two main elements: the internal model, $I(z)$, and the stabilizing controller, $G_x(z)$. The internal model is the one in charge of guaranteeing null or small error in steady state, while the stabilizing controller assures closed-loop stability. The standard internal model is constructed using (2.4) and setting $W(z) = z^{-N}$ and $\sigma = 1$, resulting in:

$$I_{st}(z) = \frac{H(z)}{z^N - H(z)}. \tag{2.5}$$

IM / Action	Full-harmonic	Odd-harmonic	$6l \pm 1$
RC	$I_{st}(z) = \frac{H(z)}{z^N - H(z)}$ $W(z) = z^{-N}, \sigma = 1$	$I_{odd}(z) = \frac{-H(z)}{z^{\frac{N}{2}} + H(z)}$ $W(z) = z^{-\frac{N}{2}}, \sigma = -1$	$I_{6l\pm1}(z) = \frac{W(z)H(z)}{1+W(z)H(z)}$ $W(z) = z^{-\frac{N}{3}} - z^{-\frac{N}{6}}, \sigma = -1$
HORC	$I_{ho}(z) = \frac{W(z)H(z)}{1-W(z)H(z)}$ $W(z) = 1-(1-z^{-N})^M, \sigma = 1$	$I_{hodd}(z) = \frac{-W(z)H(z)}{1+W(z)H(z)}$ $W(z) = -1+\left(1+z^{-\frac{N}{2}}\right)^M, \sigma = -1$	

Table 2.1 Some internal models used in repetitive control.

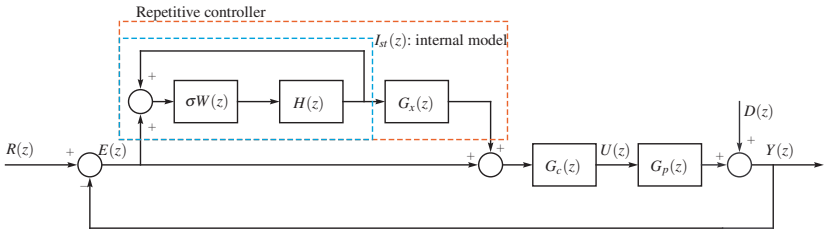

Fig. 2.3 Discrete-time block-diagram of the proposed repetitive transfer function.

When $H(z) = 1$, the poles of (2.5) are uniformly distributed over the unit circle[1], $z = \exp(2k\pi j/N)$, providing infinite gain at frequencies $\omega_k = 2k\pi/N$, with $k = 0, 2, ..., N-1$.

Although the internal model and the stabilizing controller can be arranged in different ways, most repetitive controllers are usually implemented in a "plug-in" fashion, as depicted in Figure 2.3: the repetitive compensator is used to augment an existing nominal controller, $G_c(z)$. This nominal compensator is designed to stabilize the plant, $G_p(s)$, and provides disturbance attenuation across a broad frequency spectrum.

Assume that both T_p and T_s are constant, which makes $N = T_p/T_s$ also constant, and let $G_p(z)$ stand for the corresponding z-transform of $G_p(s)$. Sufficient stability criteria are given in the next Proposition:

Proposition 2.1. *The closed-loop system of Figure 2.3 is stable if the following conditions are fulfilled [10, 3]:*

1. *The closed-loop system without the repetitive controller $G_o(z)$ is stable, where*

$$G_o(z) = \frac{G_c(z)G_p(z)}{1 + G_c(z)G_p(z)}. \tag{2.6}$$

2. $\| W(z)H(z)[1 - G_o(z)G_x(z)] \|_\infty < 1$, *where $G_x(z)$ is a design filter to be chosen.*

The sensitivity function of the closed-loop system in Figure 2.3, using the generic internal model (2.4) is:

$$S(z) = \frac{E(z)}{R(z)} = S_o(z)S_{Mod}(z), \tag{2.7}$$

where

$$S_o(z) = \frac{1}{1 + G_c(z)G_p(z)} \tag{2.8}$$

stands for the sensitivity function of the system without repetitive controller and $S_{Mod}(z)$ is the modifying sensitivity function

$$S_{Mod}(z) = \frac{1 - \sigma W(z)H(z)}{1 - \sigma W(z)H(z)(1 - G_x(z)G_o(z))}. \tag{2.9}$$

[1] Note that, since there is also a pole in $z = 1$, there is infinite gain in dc-frequency, i.e. an integral action.

The closed-loop system poles are the poles of the system without repetitive controller, i.e. poles of $S_o(z)$ and the poles of $S_{Mod}(z)$ defined in equations (2.8) and (2.9), respectively. For the case in which $G_x(z) = k_r(G_o(z))^{-1}$, $\sigma = 1$, $W(z) = z^{-N}$ and $H(z) = 1$, the poles of $S_{Mod}(z)$ result

$$z = \sqrt[N]{|1-k_r|}e^{\frac{2k\pi j}{N}},\ k = 0,\ldots,N-1. \tag{2.10}$$

These poles are uniformly distributed over a circle of radius $\sqrt[N]{|1-k_r|}$. To render stability these poles should be within the unit circle, namely $k_r \in (0,2)$. Although the introduction of $H(z) \neq 1$ and designs that involve nonminimum-phase plants affect the location of the closed-loop poles and also the convergence speed of the system as a function of k_r, this analysis gives a simple and intuitive approximation of the distribution of the poles [18].

Stability filter $G_x(z)$

Condition 2 of Proposition 2.1 should be fulfilled with an appropriate design of the filter $G_x(z)$. The fundamental issue is to provide enough leading phase to cancel out the phase of $G_o(z)$ [9]. In case of minimum phase systems $G_x(z)$ is implemented as the inverse of the complementary sensitivity function $G_o(z)$. In general, it would be sufficient that $G_x(z)$ approximates the inverse of $G_o(z)$ in the passband of the filter $H(z)$ [9, 12].

Gain k_r

The design of the gain k_r involves a trade-off between stability robustness and steady state performance [8]. Furthermore, it has been proved that an appropriate selection of k_r decreases the error caused by non harmonic components [9], and a tuning algorithm has been proposed in [1].

Robustness filter $H(z)$

The cancellation performed by the filter $G_x(z)$ is not perfect, specially at high frequencies, due to model uncertainty and unmodelled dynamics. Moreover, the allowable model uncertainty is smaller at harmonic frequencies where the internal model brings infinite gain, which is more critical at high frequencies [15]. Therefore, the filter $H(z)$ is used to limit the infinite gain mainly at high frequencies, thus improving the stability robustness. In this way, $H(z)$ should provide enough band limitation in accordance with the frequency interval where model uncertainty exists. In general, $H(z)$ is chosen to be a null phase low pass FIR filter [9, 14, 15]. If conventional low pass filters are used it will be necessary to compensate for the phase shifting they provoke [16, 5].

When limiting the gain by means of the filter $H(z)$ the tracking/rejecting performance decreases mainly at high frequencies and slight deviation of the generated harmonic frequencies is caused due to pole shifting. As in other components, design of filter $H(z)$ implies a trade off between stability robustness and performance.

Design characteristics

The following remark summarizes the above described characteristics:

Remark 2.1. The design of $H(z)$, $G_x(z)$ and $G_c(z)$ should also consider the following issues [10, 3]:

- It is advisable to design the controller $G_c(z)$ with a high enough robustness margin.
- $H(z)$ is designed to have gain close to 1 in the desired bandwidth and attenuate the gain out of it.
- A trivial structure which is often used for $G_x(z)$ in case that $G_o(z)$ is minimum-phase is [13]:

$$G_x(z) = k_r \left[G_o(z)\right]^{-1}.$$

  Otherwise, alternative techniques should be applied in order to avoid unstable pole-zero cancellations [13] (see Appendix A). Moreover, there is no problem with the improperness of $G_x(z)$ because the internal model provides the repetitive controller with a high positive relative degree. Finally, as argued in [8], k_r must be designed looking for a trade-off between robustness against plant uncertainty and transient response.

2.3 Performance under varying frequency

The theoretical basics and the design developed above assume that the frequency of the signal to be tracked/rejected is well known or constant. However for most of the practical implementations it is important to analyse the system performance in the face of frequency variations or frequency uncertainty.

The repetitive controller introduced in Section 2.2 contains the ratio $N = T_p/T_s$, which is embedded in the controller implementation. This setting renders a well-known good performance if the reference/disturbance periodic signal has a known constant period T_p. However, the controller performance decays dramatically when a variation of T_p appears. As an example, Figure 2.4 shows the magnitude response of a open-loop internal model designed for a 50 Hz periodic signal, with the gain for 49 Hz and 51 Hz (and some of their harmonics) highlighted. Note that the gain is large at the fundamental and harmonic frequencies, but it is highly reduced when the frequency is slightly deviated from these frequencies. Consequently, the tracking/rejection capabilities are dramatically reduced. Also, it is worth noticing that the gain reduction is even worse for higher harmonics.

Something similar occurs with the phase lag of the closed loop control system. Figure 2.5 portrays the closed loop phase response of a RC implementation using the settings of Section 7.3 but using the full harmonic internal model (2.5). It can be seen that while for the nominal frequency the phase is almost zero, this does not happen with the other frequencies. It is worth emphasizing that this would imply a reduction of the reference signal tracking capabilities. Clearly, this effect would contribute to the reduction of the system performance. Furthermore, it can be seen that the phase difference worsens for higher harmonics.

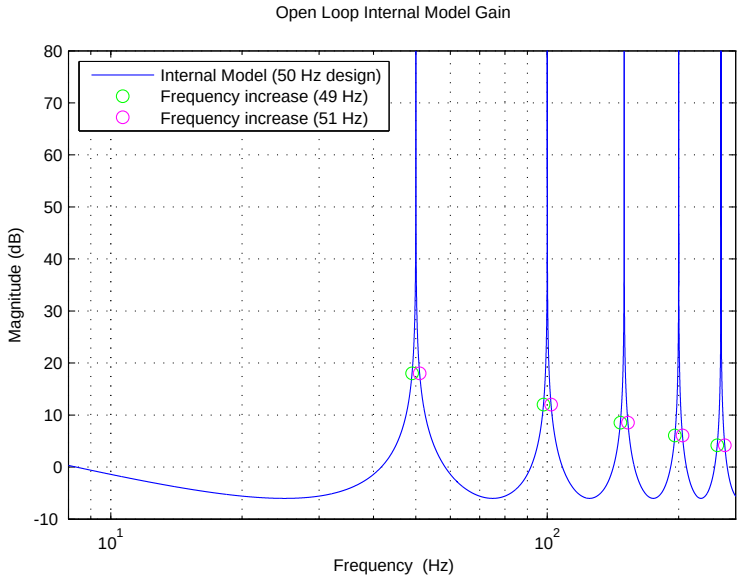

Fig. 2.4 Open-loop internal model gain diagram.

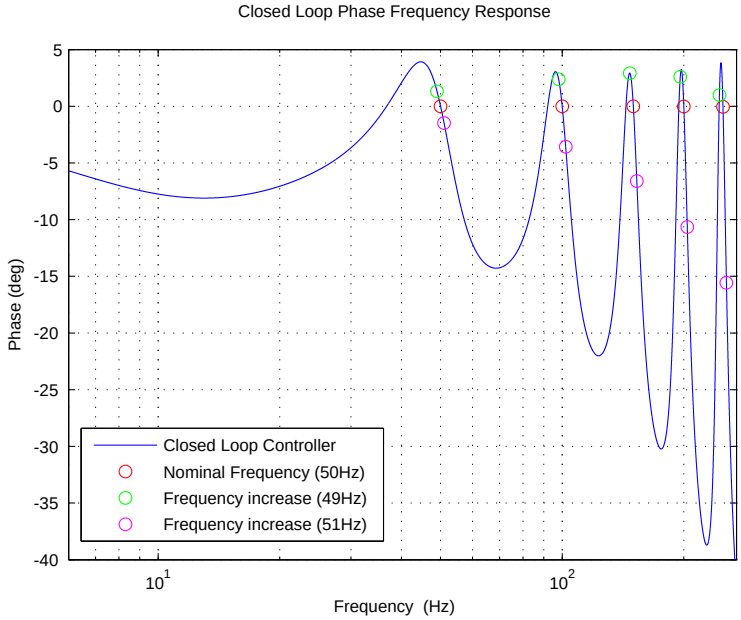

Fig. 2.5 Closed-loop transfer function phase diagram.

References

1. W. S. Chang, I. H. Suh, and T. W. Kim. Analysis and design of two types of digital repetitive control systems. *Automatica*, 31(5):741–746, 1995.
2. K. K. Chew and M. Tomizuka. Steady-state and stochastic performance of a modified discrete-time prototype repetitive controller. *Journal of Dynamic Systems, Measurement, and Control*, 112:35–41, March 1990.
3. R. Costa-Castelló, J. Nebot, and R. Griñó. Demonstration of the internal model principle by digital repetitive control of an educational laboratory plant. *IEEE Transactions on Education*, 48(1):73–80, 2005.
4. G. Escobar, P. Hernandez-Briones, R. Torres-Olguin, and A. Valdez. A repetitive-based controller for the compensation of $6l \pm 1$ harmonic components. In *Proceedings of the IEEE International Symposium on Industrial Electronics*, pages 3397–3402, 2007.
5. G. Escobar, R. Torres-Olguin, A. Valdez, M. Martinez-Montejano, and P. Hernandez-Briones. Practical modifications of a repetitive-based controller aimed to compensate 6l+1 harmonics. In *Proceedings of the 11th IEEE International Power Electronics Congress, 2008. CIEP 2008.*, pages 90 –95, aug. 2008.
6. B. Francis and W. Wonham. Internal model principle in control theory. *Automatica*, 12:457–465, 1976.
7. R. Griñó and R. Costa-Castelló. Digital repetitive plug-in controller for odd-harmonic periodic references and disturbances. *Automatica*, 19(4):1060– 1068, July 2004.
8. G. Hillerström and R. C. Lee. Trade-offs in repetitive control. Technical Report CUED/F-INFENG/TR 294, University of Cambridge, June 1997.
9. T. Inoue. Practical repetitive control system design. In *Proceedings of the 29th IEEE Conference on Decision and Control*, pages 1673–1678, 1990.
10. T. Inoue, M. Nakano, T. Kubo, S. Matsumoto, and H. Baba. High accuracy control of a proton synchroton magnet power supply. In *Proceedings of the 8th IFAC World Congress*, pages 216–220, 1981.
11. J. Leyva-Ramos, G. Escobar, P. Martinez, and P. Mattavelli. Analog circuits to implement repetitive controllers for tracking and disturbance rejection of periodic signals. *IEEE Transactions on Circuits and Systems II: Express Briefs*, 52(8):466 – 470, aug. 2005.
12. G. Pipeleers, B. Demeulenaere, and S. Sewers. Robust high order repetitive control: Optimal performance trade offs. *Automatica*, 44:2628–2634, 2008.
13. M. Tomizuka, T.-C. Tsao, and K.-K. Chew. Analysis and synthesis of discrete-time repetitive controllers. *Journal of Dynamic Systems, Measurement, and Control*, 111:353–358, September 1989.
14. T.-C. Tsao and M. Tomisuka. Adaptive and repetitive digital control algorithms for non circular machining. In *Proceedings of the 1988 American Control Conference*, 1988.
15. T.-C. Tsao and M. Tomizuka. Robust adaptive and repetitive digital tracking control and application to a hydraulic servo for noncircular machining. *Journal of Dynamic Systems, Measurement, and Control*, 116(1):24–32, 1994.
16. G. Weiss and M. Häfele. Repetitive control of MIMO systems using H_∞ design. *Automatica*, 35(7):1185 – 1199, 1999.
17. Y. Yamamoto. Learning control and related problems in infinite-dimensional systems. In *Proceedings of the European Control Conference*, pages 191–222, 1993.
18. J. W. Yeol, R. W. Longman, and Y. S. Ryu. On the settling time in repetitive control systems. In *Proceedings of 17th International Federation of Automatic Control (IFAC) World Congress*, July 2008.

Part I
Varying sampling approach

Chapter 3
Stability analysis methods

3.1 Introduction

3.1.1 State of the Art

The idea of adapting the sampling rate of the repetitive controller according to the reference/disturbance period (see [7, 6]) allows the preservation of a constant value for N and the steady-state performance of the controller. Also, two additional advantages are obtained: the computational cost is kept low and, since the number of samples per period is maintained constant, the quality of the continuous-time signal reconstruction is preserved. However, as mentioned before, this approach implies that the structure of the system changes from LTI to LTV, which may result in closed-loop instability. Indeed, no formal stability proofs are provided in the existing literature for this case. The approach in [7] tries to ensure stability using different controllers according to the value of T_s, but stability is not formally proved. Differently, [6] deals with the specific case of periodic variations of T_p and proves stability after transforming the periodic system into an LTI one by means of lifting techniques. The third proposal [14] considers the adaptation of both N and T_s, and stability is claimed arguing that changes in T_s are small enough.

In a more general context, the stability analysis of sampled-data linear systems with time-varying sampling rates is a challenging problem which may follow several approaches. The first one [11] uses an LMI gridding approach that allows to establish necessary conditions to fulfil a discrete time Lyapunov stability criterion, which in LTV framework constitutes a sufficient condition. Sufficient stability conditions are reported in [2], where the aperiodic sampling operation is modelled as a piecewise continuous delay in the control input; less conservative conditions are given in [8] after interpreting the derived stability condition in terms of the small gain theorem, while the exploitation of passivity-type properties yields a further improvement of the technique [5]. The third approach [9] is based on a hybrid modelling of sampled-data systems and a search of discontinuous Lyapunov functions. In all the above reported works the different stability conditions are established in an LMI format. However, computational issues may arise when trying to solve LMI problems that involve high order systems, and repetitive controllers use to share this feature.

Recently, a different insight has been considered in [3, 13]. The main idea in both contributions, which use a static controller, is to model the non-uniform sampling

time effect as a nominal system affected by an additive, norm-bounded time-varying disturbance. Hence, small-gain theorem-based robust control tools may ensure stability in closed neighborhoods of the nominal sampling period.

3.1.2 Contribution

This Chapter describes the tools developed with the aim of analysing the stability of a system containing a digital repetitive controller working under time-varying sampling period.

In this way, an accurate study of stability margins is performed where reliable performance may ensured without specifically requiring T_p to be periodic, thus improving the results in [7] and generalizing the ones in [6]. The stability test is carried out twofold, the first proposed methodology uses a LMI gridding approach [1, 11] that allows to assess conditions for the BIBO stability of the closed-loop system in a known, bounded interval where the reference/disturbance period is assumed to vary. The second one, is based on robust control techniques, which allows to overcome intrinsic lacks of the LMI gridding approach and presents an adaptation and improvement of the approach introduced in [3, 13] for digital repetitive control systems. The key point of the improvement lies in the fact that the proposed technique uses a discrete-time dynamic controller that yields a degenerate disturbance matrix. This allows to carry out an optimal decomposition with regard to the expected stability interval. Furthermore, additional discussion that may help towards a conservatism reduction of the stability intervals is provided.

3.1.3 Outline

Section 3.2 describes an adaptation procedure for the sampling period according to the time-variation of the reference/disturbance signal. Section 3.3 analyses the stability of the closed-loop system using the LMI gridding approach and Section 3.4 studies the stability of the system using robust control techniques while conclusions and further research lines are presented in Section 3.5.

3.2 Repetitive control under varying frequency conditions

In this approach the controller sampling time T_s is adapted according to the reference/disturbance period variation T_p, and thus maintaining a constant value for N. Hence, on the one hand, $I(z)$, $G_x(z)$ and $G_c(z)$ are designed and implemented to provide closed-loop stability for a nominal sampling time $T_s = \bar{T}$ (see Chapter 2 for stability criteria and design issues). In this way, their structures remain always invariant, i.e. they undergo no further structural changes. On the other hand, the period of the sampling device preceding the plant, $G_p(s)$, is accommodated to the variation of T_p. Therefore, its discrete-time representation is that of an LTV system. The accommodation scheme is detailed in Figure 3.1.

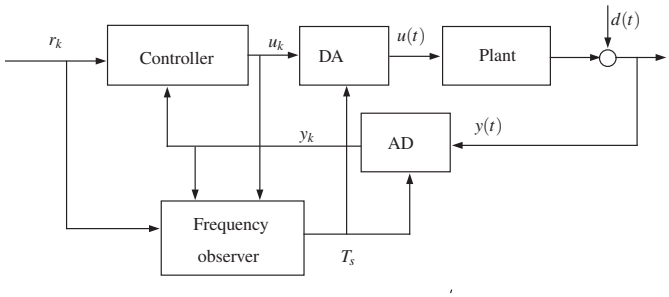

Fig. 3.1 Accommodation of the sampling period T_s to possible variations of T_p.

Although the proposed technique allows to adapt the system to the specific signal frequency to be tracked/rejected without changing the digital controller, the sampling rate change may compromise closed-loop stability. In what follows, a closed-loop stability analysis of the system under varying sampling rate condition is carried out. For the rest of the chapter it is assumed that the original continuous-time plant is controllable and observable, and also that these properties are not lost due to sampling.

Regarding the time-varying nature of the plant sampling period, the stability analysis is carried out in the state-space formalism. The final part of the Section is devoted to obtaining the state equations of the system.

Let the discrete-time state-space representations of blocks $I(z)$, $G_x(z)$, $G_c(z)$ and $G_p(z)$ (see Figure 2.3) be denoted by (A_i, B_i, C_i, D_i), with the subindex i replaced by I, x, c and p, respectively. The closed-loop system state equations are derived under the following assumptions:

- The internal model, $I(z)$, of Figure 2.3 is such that $D_I = 0$.
- The continuous-time plant $G_p(s)$ has at least relative degree 1, so $D_p = 0$.
- The representations corresponding to blocks $I(z)$, $G_x(z)$ and $G_c(z)$ are obtained from the nominal sampling time $T_s = \bar{T}$.
- Only the discrete-time plant model matrices A_p, B_p vary according to sampling rate updating: $A_p = A_p(T_s)$, $B_p = B_p(T_s)$ while C_p is kept constant. Hence, assuming that $(A,B,C,0)$ stands for the continuous-time plant state-space representation, i.e. $G_p(s) = C(s\mathbb{I} - A)^{-1}B$, then

$$A_p(T) \triangleq e^{AT}, \;\; B_p(T) \triangleq \int_0^T e^{Ar} B dr. \tag{3.1}$$

Let the system be sampled at time instants $\{t_0, t_1, \ldots\}$ with $t_0 = 0$, $t_{k+1} > t_k$, the sampling periods being $T_k = t_{k+1} - t_k$. Let also $x_k \triangleq x(t_k)$, $r_k \triangleq r(t_k)$, $y_k \triangleq y(t_k)$. The state equations are given by the discrete-time LTV system:

$$x_{k+1} = \Phi(T_k)x_k + \Pi(T_k)r_k, \quad y_k = \Upsilon x_k, \tag{3.2}$$

where

$$\Phi(T) \triangleq \begin{pmatrix} K & L \\ B_p(T)M & A_p(T) + B_p(T)Q \end{pmatrix}, \tag{3.3}$$

with

$$K \triangleq \begin{pmatrix} A_I & 0 & 0 \\ B_x C_I & A_x & 0 \\ B_c D_x C_I & B_c C_x & A_c \end{pmatrix}, \; L \triangleq \begin{pmatrix} -B_I C_p \\ 0 \\ -B_c C_p \end{pmatrix},$$

$$M \triangleq \begin{pmatrix} D_c D_x C_I & D_c C_x & C_c \end{pmatrix}, \; Q \triangleq -D_c C_p$$

and

$$\Pi(T) \triangleq \begin{pmatrix} B_I^\top & 0 & B_c^\top & (B_p(T) C_c)^\top \end{pmatrix}^\top, \; \Upsilon \triangleq \begin{pmatrix} 0 & 0 & 0 & C_p \end{pmatrix}.$$

Remark 3.1. When T_k remains constant, i.e. $T_k = \bar{T}$, $\forall k \geq 0$, (3.2) becomes a discrete-time LTI system with z-transfer function

$$G(z) = \Upsilon \left[z\mathbb{I} - \Phi(\bar{T}) \right]^{-1} \Pi(\bar{T}).$$

In an aperiodic sampling time framework, $\Phi(T_k)$ and $\Pi(T_k)$ vary with k, and the z-transform representation is no longer valid.

In repetitive control systems, the internal model is designed to ensure a null error in the steady state provided that closed-loop stability is guaranteed. Hence, assuming that $I(z)$, $G_x(z)$ and $G_x(z)$ are constructed to provide stability for a nominal sampling time $T_s = \bar{T}$, the aim is to prove both internal and BIBO stability for the non-uniformly sampled system (3.2).

Throughout this thesis $\| \cdot \|$ denotes the 2-norm of a matrix, i.e. the matrix norm induced by the euclidean vector norm. Hence, for any real matrix R, $\|R\| = \left[\rho(R^\top R) \right]^{1/2}$, with $\rho(\cdot)$ standing for the spectral radius. Moreover, recall that given a discrete-time LTI system with constant sampling time T_s and transfer function matrix $G(z)$, its H_∞-norm is defined as

$$\|G(z)\|_\infty = \max \left\{ \left\| G\left(e^{j\omega T_s} \right) \right\|, \; \forall \omega \in \mathbb{R} \right\}.$$

Proposition 3.1. *Let the sampling period, T_k, take values in a compact subset $\mathscr{T} \subset \mathbb{R}^+$. Then, the uniform exponential stability of*

$$x_{k+1} = \Phi(T_k) x_k \tag{3.4}$$

implies the uniform BIBO stability of (3.2).

Proof. According to Lemma 27.4 in [10], the result follows if $\Pi(T_k)$ and Υ are uniformly bounded matrices, $\forall k \geq 0$. This is indeed true: $\Pi(T_k)$ depends continuously on T_k, which belongs to a compact set $\mathscr{T}$, while Υ is a constant matrix because so is C_p. □

Proposition 3.2 ([10]). *Let the sampling period, T_k, take values in a compact subset $\mathscr{T} \subset \mathbb{R}^+$. If there exists a matrix P such that*

$$\Phi(T_k)^\top P \Phi(T_k) - P < 0, \; \forall T_k \in \mathscr{T}, \; \text{s.t.} \; P = P^\top > 0, \tag{3.5}$$

then (3.4) is uniformly exponentially stable.

3.3 LMI gridding approach

It is immediate to realize that relation (3.5) in Proposition 3.2 yields an infinite set of LMIs. The gridding approach introduced in [1, 11] allows a simplified stability analysis that may be performed in two stages, if necessary.

In a first stage, advantage is taken from the fact that the system (3.2) is stable by construction for $T_k = \bar{T}$, $\forall k$.

Proposition 3.3. *Assume that the stability conditions of Proposition 2.1 are satisfied for a nominal sampling period $\bar{T} \in \mathscr{T}$. Then,*

1. *The zero state of the LTI system (3.4) with $T_k = \bar{T}$, $\forall k$, is uniformly exponentially stable.*
2. *The LMI problem*
$$L_{\bar{T}}(P) \leq -\alpha\mathbb{I}, \;\; s.t. \;\; P = P^\top > 0, \tag{3.6}$$
with $L_{\bar{T}}(P)$ constructed from (3.5) and $\alpha \in \mathbb{R}^+$, is feasible.
3. *Let $P = P_N$ be a solution of the LMI problem (3.6) for a fixed $\alpha \in \mathbb{R}^+$. Then, there exists an open neighborhood of $\bar{T}$, say $\mathscr{I}_\mathscr{N}$, such that (3.4) is BIBO stable in $\mathscr{I}_\mathscr{N}$.*

Proof. It follows from the stability hypothesis that all the eigenvalues of $\Phi(\bar{T})$ have modulus less that 1, which yields immediately item 1 [10]. Item 2 stems from the fact that the sufficient condition for uniform exponential stability established in Proposition 3.2 is also necessary for a discrete-time LTI system. Finally, item 3 follows immediately from Propositions 3.1 and 3.2 once the continuity of the matrix elements of $\Phi(T_k)$ with respect to T_k is taken into account. □

Assume that we are interested in analyzing the stability of (3.4) for all sampling periods $T_k \in \mathscr{T}$. Let $P = P_N$ be a feasible solution of the LMI problem (3.6) for a fixed $\alpha \in \mathbb{R}^+$: its existence is guaranteed by Proposition 3.3. Let also $\{\tau_0, \ldots, \tau_q\}$, with $\tau_{i+1} > \tau_i$, be a sufficiently fine grid of $\mathscr{T}$. Then, one has to check that $L_{\tau_i}(P_N) < 0$, $\forall i = 0, \ldots, q$: see Figure 3.2.

In case that there exists at least a single τ_i such that $L_{\tau_i}(P_N) \geq 0$, the gridding procedure proposed in [11] may be carried out as follows. Let $\{\tau_0, \ldots, \tau_r\}$, be a sorted set of candidate sampling periods suitably distributed in $\mathscr{T}$. Then, one may solve the following finite set of LMIs:

$$L_{\tau_i}(P) \leq -\alpha\mathbb{I}, \;\; i = 0, \ldots, r, \;\; \text{s.t.} \;\; P = P^\top > 0, \tag{3.7}$$

for a fixed $\alpha \in \mathbb{R}^+$. In case that the problem is feasible and a solution, $P = P_G$, is encountered, the negative-definite character of $L_{T_k}(P_G)$ is to be checked for intermediate values of T_k in each open subinterval (τ_i, τ_{i+1}), i.e. for all $\{\tau_{ij}; i = 0, \ldots, r-1, \;\; j = 1, \ldots, p\}$, with $\tau_i < \tau_{i1} < \cdots < \tau_{ip} < \tau_{i+1}$, for all $i = 0, \ldots, r-1$; see Figure 3.3. If this fails to be accomplished, (3.7) has to be solved again for a finer grid of $\mathscr{T}$. Otherwise, the procedure should be relaunched for a new interval $\mathscr{T}' \subset \mathscr{T}$.

Remark 3.2. Notice that:

(i) Comparatively, in the first approach a shorter stability radius may be reasonably expected.

(ii) An important drawback of both analysis paths is associated to the fact that stability is rigorously guaranteed just in open neighbourhoods of each sampling time τ_i

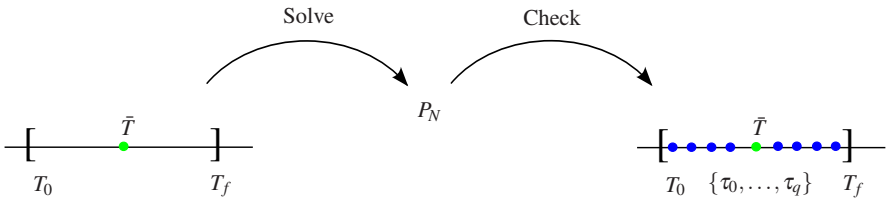

Fig. 3.2 Graphical scheme of the LMI gridding-based stability analysis in $\mathscr{T} = [T_0, T_f]$ from the solution of (3.6).

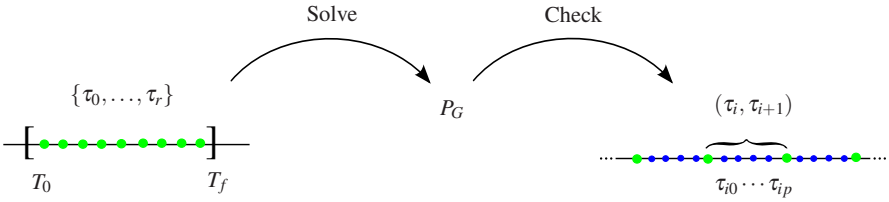

Fig. 3.3 Graphical scheme of the LMI gridding-based stability analysis in $\mathscr{T} = [T_0, T_f]$ from the solution of (3.7).

or τ_{ij} where either $L_{\tau_i}(P_N) < 0$ or $L_{\tau_{ij}}(P_G) < 0$ are satisfied, respectively, thus indicating a partial fulfilment of the sufficient stability condition. However, the distance between these intervals may be reduced at will by increasing the number of grid points. Furthermore, it is important to note that in a real application the sampling time variation is defined by a finite precision digital clock which yields a variation interval with a finite number of points, therefore, including these points to check the Lyapunov condition may guarantee the stability of the digital implementation in a defined interval.

(iii) Repetitive systems use to be high order systems, and this fact may yield computational issues when solving LMIs. Hence, in the next subsection an alternative tool for stability analysis is introduced.

(iv) A faulty estimation of T_p and/or an error in the implementation of T_s may yield important performance degradation [12]. However, closed-loop BIBO stability is not threatened unless the plant is actually sampled with T_s values lying outside the region $\mathscr{T}$ where stability is guaranteed.

3.4 Robust analysis

The stability analysis follows the approach proposed in [13, 4], where the non-uniform sampling is viewed as a nominal sampling period affected by an additive disturbance. Thus, the problem is faced from a robustness analysis viewpoint and is solved by means of a simple application of the small-gain theorem. In the present case, the repetitive control system is designed to provide closed-loop stability for a nominal case. Then, the actual problem is to quantify the "amount" of disturbance due to aperiodic sampling that the system can accommodate while preserving stability.

Proposition 3.4. *Let $\bar{T}$ be a nominal sampling period and define $\theta_k = T_k - \bar{T}$. Then, the matrix $\Phi(T_k)$ may be written as*

$$\Phi(T_k) = \Phi(\bar{T}) + \Gamma\tilde{\Delta}(\theta_k)\Psi(\bar{T}), \tag{3.8}$$

where

$$\tilde{\Delta}(\theta_k) \triangleq \begin{pmatrix} 0 & 0 \\ 0 & \Delta(\theta_k) \end{pmatrix}, \quad \Delta(\theta_k) \triangleq \int_0^{\theta_k} e^{Ar}dr, \tag{3.9}$$

$$\Psi(T_k) \triangleq \begin{pmatrix} 0 & 0 \\ A_p(T_k)A & A_p(T_k)B \end{pmatrix} \begin{pmatrix} 0 & \mathbb{I} \\ M & Q \end{pmatrix} \tag{3.10}$$

and $\Gamma \in \Xi$, with

$$\Xi := \left\{\Gamma;\, \Gamma\tilde{\Delta}(\theta) = \tilde{\Delta}(\theta)\right\} = \left\{ \begin{pmatrix} \Gamma_1 & 0 \\ \Gamma_2 & \mathbb{I} \end{pmatrix} \right\}. \tag{3.11}$$

Proof. Recalling (3.1) and using the well known fact that

$$e^{A\theta} = \mathbb{I} + \int_0^{\theta} e^{Ar}Adr,$$

one has that

$$A_p(T_k) = e^{A(\theta_k+\bar{T})} = \left(\mathbb{I} + \int_0^{\theta_k} e^{Ar}Adr\right) A_p(\bar{T}) = A_p(\bar{T}) + \Delta(\theta_k)A_p(\bar{T})A; \tag{3.12}$$

on the other hand,

$$\begin{aligned} B_p(T_k) &= \int_0^{T_k} e^{Ar}Bdr = \int_0^{\bar{T}} e^{Ar}Bdr + \int_{\bar{T}}^{T_k} e^{Ar}Bdr = B_p(\bar{T}) + \int_0^{\theta_k} e^{A(s+\bar{T})}Bds = \\ &= B_p(\bar{T}) + \Delta(\theta_k)A_p(\bar{T})B. \end{aligned} \tag{3.13}$$

The result follows immediately taking (3.12) and (3.13) to (3.3). □

Notice that, using Proposition 3.4, (3.4) becomes

$$x_{k+1} = \left[\Phi(\bar{T}) + \Gamma\tilde{\Delta}(\theta_k)\Psi(\bar{T})\right] x_k, \tag{3.14}$$

which allows the following interpretation [4]: (3.14) can be regarded as the LTI system

$$\Sigma := \begin{cases} x_{k+1} = \Phi(\bar{T})x_k + \Gamma u_k \\ v_k \quad\;\; = \Psi(\bar{T})x_k \end{cases}, \tag{3.15}$$

$G_{\bar{T}}(z) = \Psi(\bar{T})\left[z\mathbb{I} - \Phi(\bar{T})\right]^{-1}\Gamma$ being its associated discrete-time transfer function, receiving the time-varying output feedback control action $u_k = \tilde{\Delta}(\theta_k)v_k$ as shown in Figure 3.4.

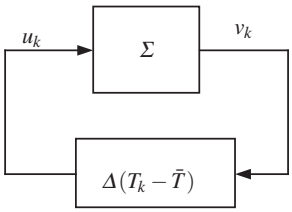

Fig. 3.4 The resulting feedback system.

Theorem 3.1. *Assume that $\bar{T}$ is a nominal sampling period. Let*

$$\gamma_{\bar{T}} = (1+\varepsilon)\|G_{\bar{T}}(z)\|_\infty, \;\; \varepsilon > 0, \tag{3.16}$$

be an upper bound of the H_∞-norm of system Σ (3.15), and let also $\mathscr{T} \subset \mathbb{R}^+$ be compact. If

$$\gamma_{\bar{T}}\|\Delta(T_k - \bar{T})\| \leq 1, \;\; \forall T_k \in \mathscr{T}, \tag{3.17}$$

then system (3.2) is uniformly BIBO stable in $\mathscr{T}$.

Proof. The fact that $\bar{T}$ be a nominal sampling period ensures that $\rho\,[\Phi(\bar{T})] < 1$, and the particular block-diagonal structure of $\tilde{\Delta}(\theta_k)$ (see (3.9)) indicates that $\|\Delta(T_k - \bar{T})\| = \|\Delta(\theta_k)\| = \|\tilde{\Delta}(\theta_k)\|$. According to Lemma 2 in [4], the stated hypotheses are sufficient for the LMI problem (3.5) to be feasible $\forall T_k \in \mathscr{T}$. Then, Proposition 3.2 yields the uniform exponential stability of (3.4) and, therefore, Proposition 3.1 entails the uniform BIBO stability of (3.2). □

Remark 3.3. In sight of Theorem 3.1, the obtention of better stability regions (i.e. wider intervals $\mathscr{T}$) may depend on the following issues:

1. Minimization of $\gamma_{\bar{T}}$.
   It may be achieved through the selection a matrix $\Gamma \in \Xi$ that minimizes $\|G_{\bar{T}}(z)\|_\infty = \|G_{\bar{T}}(z,\Gamma)\|_\infty$. This problem is faced in Proposition 3.5 below.
2. Reduction of conservatism in the calculation of the interval $\mathscr{T}$ where $\|\Delta(T - \bar{T})\| \leq \gamma_{\bar{T}}^{-1}$ is ensured.
   Recalling (3.9), it is immediate that the repetitive control system has no influence in this is point; indeed, it depends exclusively on the plant.

Proposition 3.5. *A solution of the problem*

$$\min\left\{\|\Psi(T)\,[z\mathbb{I} - \Phi(T)]^{-1}\Gamma\|_\infty, \;\; \Gamma \in \Xi\right\},$$

is given by

$$\Gamma = \begin{pmatrix} 0 & 0 \\ 0 & \mathbb{I} \end{pmatrix}. \tag{3.18}$$

Proof. Assuming that $\Gamma \in \Xi$ (see (3.11)) and writing $\Psi(T)$, $[z\mathbb{I} - \Phi(T)]^{-1}$, in block form as

$$\Psi(T) = \begin{pmatrix} 0 & 0 \\ \Psi_1 & \Psi_2 \end{pmatrix}, \quad [z\mathbb{I} - \Phi(T)]^{-1} = \begin{pmatrix} F_{11} & F_{12} \\ F_{21} & F_{22} \end{pmatrix},$$

where $\Psi_i = \Psi_i(T)$ and $F_{ij} = F_{ij}(z,T)$, it results that

$$G_T(z,\Gamma) = \begin{pmatrix} 0 & 0 \\ G_{T1}(z,\Gamma_1,\Gamma_2) & G_{T2}(z) \end{pmatrix},$$

with

$$G_{T1} = (\Psi_1 F_{11} + \Psi_2 F_{21})\Gamma_1 + (\Psi_1 F_{12} + \Psi_2 F_{22})\Gamma_2,$$
$$G_{T2} = \Psi_1 F_{12} + \Psi_2 F_{22}.$$

Hence, the definition of the H_∞-norm and the well known fact that matrix expansion does not decrease norms yield straightforward that $\|G_T(z)\|_\infty \geq \|G_{T2}(z)\|_\infty$. □

Remark 3.4. In [3, 13], the decomposition (3.8) uses $\Gamma = \mathbb{I}$. This is indeed the only possibility when $\tilde{\Delta}(\theta)$ is a non-singular matrix, but it becomes a non optimal selection when that is not the case, as shown in Proposition 3.5. Hence, the proposed procedure is generalizable to any system matching (3.8) and possessing a degenerate disturbance matrix (3.9). This encompasses the class of systems that exhibit the block structure depicted in Figure 2.3 but operate with a generic discrete-time dynamic controller.

Finally, the procedure to calculate the sampling period variation intervals based on Theorem 3.1 using numeric calculation and norm bounds is described in Appendix B.

3.5 Conclusions

This Chapter analyses the stability of digital repetitive control systems subjected to references/disturbances with time-varying period T_p. The approach proposes a real-time adaptation of the sampling time of the system, T_s, in order to maintain the ratio $N = T_p/T_s$ at a constant level. The stability issue is studied by means of an LMI gridding method and also using robust control techniques.

The LMI gridding approach is rather simple, but it just provides necessary conditions for a sufficient stability condition and becomes unsuitable for high order systems and/or large analysis intervals due to computational problems. On the contrary, the robust control approach provides better quality results, i.e. sufficient conditions and wider stability margins, for the adaptation structure proposed.

Finally, it is worth mentioning that in this framework the repetitive controller and the frequency observer that allows the real-time updating of T_s are completely decoupled from a stability analysis viewpoint, which allows an independent design of such components.

In future work, the analysis criteria for repetitive controllers that may provide further reduction of conservatism in the obtained stability intervals will be studied. Also, a formal transient study in the LTV framework is an open research topic especially when a frequency observer is needed.

References

1. P. Apkarian and R. Adams. Advanced gain-scheduling techniques for uncertain systems. *IEEE Transactions on Control Systems Technology*, 6(1):21–32, 1998.
2. E. Fridman, A. Seuret, and J. Richard. Robust sampled-data stabilization of linear systems: An input delay approach. *Automatica*, 40(8):1441–1446, 2004.
3. H. Fujioka. Stability analysis for a class of networked-embedded control systems: A discrete-time approach. In *Proceedings of the American Control Conference*, pages 4997–5002, 2008.
4. H. Fujioka. A discrete-time approach to stability analysis of systems with aperiodic sample-and-hold devices. *IEEE Trans. Automat. Control*, 54(10):2440–2445, 2009.
5. H. Fujioka. Stability analysis of systems with aperiodic sample-and-hold devices. *Automatica*, 45(3):771–775, 2009.
6. R. D. Hanson and T.-C. Tsao. Periodic sampling interval repetitive control and its application to variable spindle speed noncircular turning process. *Journal of Dynamic Systems, Measurement, and Control*, 122(3):560–566, 2000.
7. G. Hillerström. *On Repetitive Control*. PhD thesis, Lulea University of Technology, November 1994.
8. L. Mirkin. Some remarks on the use of time-varying delay to model sample-and-hold circuits. *IEEE Trans. Autom. Control*, 52(6):1109–1112, 2007.
9. P. Naghshtabrizi, J. Hespanha, and A. Teel. On the robust stability and stabilization of sampled-data systems: A hybrid system approach. In *Proceedings of the 45th IEEE Confecence on Decision and Control*, pages 4873–4878, 2006.
10. W. Rugh. *Linear system theory, 2nd Ed.* Prentice-Hall, Inc., Upper Saddle River, NJ, 1996.
11. A. Sala. Computer control under time-varying sampling period: An LMI gridding approach. *Automatica*, 41(12):2077–2082, 2005.
12. M. Steinbuch. Repetitive control for systems with uncertain period-time. *Automatica*, 38(12):2103–2109, 2002.
13. Y. Suh. Stability and stabilization of nonuniform sampling systems. *Automatica*, 44(12):3222–3226, 2008.
14. T.-C. Tsao, Y.-X. Qian, and M. Nemani. Repetitive control for asymptotic tracking of periodic signals with an unknown period. *Journal of Dynamic Systems, Measurement, and Control*, 122(2):364–369, 2000.

Chapter 4
Design methods

4.1 Introduction

The previous chapter analyses the stability of repetitive control systems in which the sampling period is adjusted as a way to preserve the performance under varying frequency conditions. As a result, a frequency variation interval can be found where the stability of the system can be established. As an opposite problem, it would be desirable to establish a methodology in which a controller can be designed that allow us to assure the stability and performance of the system for a given frequency variation range. Thus, this chapter describes the design methodologies developed in order to obtain a repetitive controller that assures the stability and steady-state performance in a frequency variation interval. Two different strategies are presented: a μ-synthesis technique and a pre-compensation strategy.

4.1.1 State of the art

This section propounds an adaptive variation of the sampling period T_s of the repetitive control system [5, 4, 11, 2] aiming at maintaining a constant value for N. This means that the number of samples per period is kept constant, which preserves the continuous-time signal reconstruction quality. However, it implies changes in the system dynamics and, specifically, in the plant model. Therefore, it is important to check that these changes do not threat stability. Although several approaches exist for the stability analysis of time-varying sampling period controllers [3, 8], few of them allow an integrated controller design which assures closed-loop stability under such conditions. An H_∞ Linear Parameter Varying (LPV) design is proposed in [7, 6]: the system sampling period dependency is approximated and later a sampling period dependent controller is obtained through Linear Matrix Inequalities (LMI) optimization. However, the application of these approaches in the repetitive control field is constrained by the high order usually exhibited by repetitive controllers and the limitations of current LMI solvers.

4.1.2 Contribution

The main contribution of this section involves two designs:

First, the re-design of a original repetitive controller in such a way that the effect of time-varying sampling is modelled as an structured uncertainty. Under this fact, Bounded Input-Bounded Output (BIBO) stability can be assured when the uncertainty belongs to a known bounded set using small-gain theorem-based standard robust control methodologies. Also, steady-state performance is guaranteed when T_s remains constant for sufficiently large time intervals.

Alternatively, a pre-compensation scheme that forces the inner plant to remain invariant despite sampling rate changes is proposed. As a consequence, standard LTI methods can be used in the control design and the stability analysis. Thus, this adaptation strategy includes an additional compensator placed between the controller and the plant that, under the assumption of internal stability, annihilates the effect of the time-varying period and forces the closed-loop behaviour to match that of a preselected nominal sampling period. Since this strategy involves a plant inversion it is only applicable in case of stable and minimum phase plants.

4.1.3 Outline

This Chapter is organized as follows: Section 4.2 presents the design that uses robust control techniques to ensure the stability of the repetitive control system for a pre-defined frequency variation interval, Section 4.3 describes a pre-compensation based design to compensate the sampling time variation effects and finally the conclusions are stated in Section 4.4.

4.2 Robust stability design

In this Section, a repetitive control design method is described in which the controller is obtained to assure stability in a predefined sampling period variation interval $\mathscr{T}$. Thus, it is proposed to re-design the original repetitive controller in order to achieve that

$$\|G_{\bar{T}_s}(z)\|_\infty < (1+\varepsilon)^{-1}\|\Delta\left(T_s-\bar{T}\right)\|_\infty^{-1}$$

(recall that $G_{\bar{T}_s}(z)$ is the transfer function of the system Σ that corresponds to the system rearrangement in Figure 3.4).

In order to calculate $\|\Delta\left(T_s-\bar{T}\right)\|_\infty$, it is assumed that BIBO stability is to be preserved $\forall\ T_s \in \mathscr{T}$, $\mathscr{T}$ being a closed interval[1], then, a Schur decomposition-derived bound [10] for the matrix exponential (see (3.9)) may be used to compute $\|\Delta\left(T_s-\bar{T}\right)\|_\infty$ in $\mathscr{T}$.

The repetitive controller elements $G_c(z)$ and $G_x(z)$, i.e. the nominal controller and the stabilizing controller, will be re-designed using robust control methods so as to achieve BIBO stability of the closed-loop system in the overall interval

[1] From an assumed frequency variation expected in the interval $[f_{min}, f_{max}]$ Hz, recalling the relation $T_p = N \cdot T_s$, one finds out that $\mathscr{T} = \left[(f_{max}N)^{-1}, (f_{min}N)^{-1}\right]$.

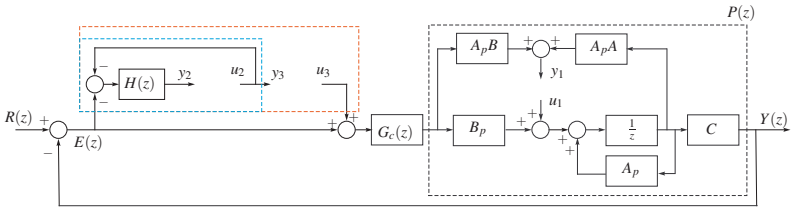

Fig. 4.1 Adaptation of the repetitive control loop to the H_∞ formulation.

of expected variation of the sampling period, $\mathscr{T}$. However, as $G_x(z)$ depends on $G_c(z)$, this results in a coupled problem which may not be easily solved. Hence, the procedure proposed here is to carry out a two-stage re-desing: firstly of $G_c(z)$ -if necessary-, and then of $G_x(z)$.

Remark 4.1. Notice that the use of the z-transform in an LTV framework is not formally correct. In this chapter the notation is preserved for simplicity and compactness. Hence, z^{-1} should be read as a one sample period delay, but with a possible change of sampling interval length from sample to sample.

The possible re-design of the nominal controller, $G_c(z)$, aims at making easier the solution of the optimization problem that will be later posed to obtain $G_x(z)$. Recalling Section 2.2, the first condition required for the stability of the current control block is that the closed-loop without the repetitive controller is stable, i.e. that $G_o(z)$ defined in (2.6) is stable. Therefore, one should check that the nominal controller $G_c(z)$ proposed yields stability of $G_o(z)$ not only for the nominal sampling period, $\bar{T}$, but for all $T_s \in \mathscr{T}$. This can be worked out using the approach in Subsection 3.4, that is, modelling the plant variation due to sampling period changes as an uncertainty and assessing the fulfilment of a (3.17)-like inequality. If this were not the case, $G_c(z)$ should be re-designed using a traditional H_∞ problem formulation.

The second stage deals with the re-design of $G_x(z)$, aiming at providing stability when including the internal model in the closed-loop system using the plug-in architecture introduced in Section 2.2 and taking into account the uncertainty due to sampling period variation. Notice that this could be tackled through an H_∞ problem, but the inclusion of the internal model might result in a very high order controller. This problem will be overcome using the approach introduced in [12]. The important delay present in the internal model will be treated as an external uncertainty. Although this might introduce certain conservativeness, it will also generate a lower order controller.

To apply this scheme to the complete control-loop, it will be opened in the internal model delay and the uncertainty due to sampling period variation, as shown in Figure 4.1. This representation contains three pairs of input-output variables: (u_1, y_1) and (u_2, y_2), which are used to define the system performance, and (u_3, y_3), which is used to apply the control law. In order to assure closed-loop stability it is sufficient that the H_∞ norm from u_1 to y_1 is less than the uncertainty bound in the desired sampling interval, $\mathscr{T}$, and also that the H_∞ norm from u_2 to y_2 is less than one. Reducing these two norms will generate a more robust system in the face of sampling period variations and will make the system faster.

Figure 4.2 shows the Linear Fractional Transformation (LFT) formulation of this problem, the generalized plant being

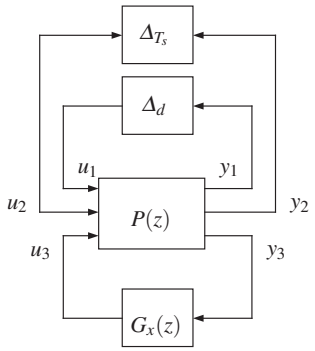

Fig. 4.2 Equivalent Scheme.

$$\begin{bmatrix} Y_1(z) \\ Y_2(z) \\ Y_3(z) \end{bmatrix} = P(z) \begin{bmatrix} U_1(z) \\ U_2(z) \\ U_3(z) \end{bmatrix}, \tag{4.1}$$

with

$$P(z) = \begin{bmatrix} A_pAM(z) - (A_pB + A_pAM(z)B_p)G_1(z)CM(z) & 0 & (A_pB + A_pAM(z)B_p)G_1(z) \\ H(z)CM(z)(G_o(z) - 1) & H(z) & -H(z)G_o(z) \\ 0 & 1 & 0 \end{bmatrix} \tag{4.2}$$

being $M(z) = (z\mathbb{I} - A_p)^{-1}$, $G_o(z) = G_p(z)G_c(z)/(1 + G_p(z)G_c(z))$ and $G_1(z) = G_c(z)/(1 + G_p(z)G_c(z))$, considering the two last transfer functions Single Input Single Output (SISO) systems. Although this could be addressed using a mixed H_∞ formulation, a μ-synthesis approach can take advantage from the problem structure [9].

Finally, it is worth mentioning that, according to the Internal Model Principle, steady-state performance will be guaranteed when T_p (and, consequently, T_s) remains constant for sufficiently large time intervals.

4.3 Plant pre-compensation

This Section presents a design strategy for a digital repetitive controller operating under time-varying sampling period which allows to neutralize the structural changes originated by the adaptation of the sampling rate. This is achieved with the introduction of a compensator that annihilates the effect of the time-varying sampling and forces the closed-loop behaviour to coincide with that of the system operating under constant and a priori selected nominal sampling period. Hence, once internal stability of the compensator-plant subsystem is ensured, both time and frequency responses of the overall closed-loop system can be characterized using standard LTI tools.

Let us now detail the basic issues that support the proposed adaptive compensation scheme:

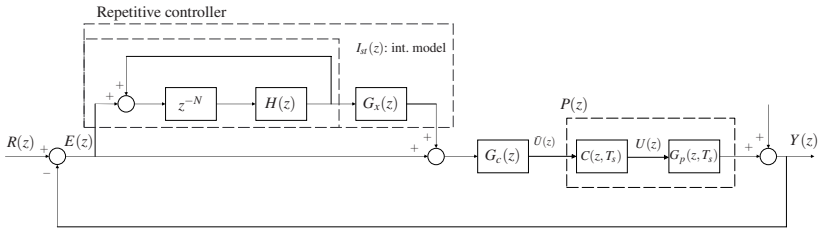

Fig. 4.3 Discrete-time block-diagram of the closed-loop system with the proposed repetitive controller structure.

1. The repetitive controller is designed and implemented to provide closed-loop stability for an a priori selected nominal sampling time $T_s = \bar{T}$ to the nominal, LTI plant
$$G_p(z,\bar{T}) \triangleq \frac{Num(z,\bar{T})}{Den(z,\bar{T})}, \tag{4.3}$$
in accordance with Proposition 2.1 and Remark 2.1. Hence, $I_{st}(z)$, $G_x(z)$ and $G_c(z)$ are kept invariant.
2. Aiming for the maintenance of a constant value N for the ratio T_p/T_s, which preserves the reference/disturbance signal reconstruction quality, the controller sampling time T_s is accommodated to the time variation of the reference/disturbance period T_p, i.e. $T_s = T_p/N$. Therefore, the discrete-time representation of the plant $G_p(s)$ is that of a LTV system
$$G_p(z,T_s) = \frac{Num(z,T_s)}{Den(z,T_s)}. \tag{4.4}$$
3. The structural changes caused by the sampling time variation of T_s are annihilated through the additional compensator
$$C(z,T_s) = G_p(z,\bar{T})G_p^{-1}(z,T_s), \tag{4.5}$$
which pre-multiplies the LTV plant $G_p(z,T_s)$. Thence, under the assumption of internal stability for the compensator-plant system, its behavior is that of the nominal LTI system $G_p(z,\bar{T})$. Figure 4.3 depicts the overall system, while Figure 4.4 details the compensator-plant subsystem.

Remark 4.2. The compensation strategy yields
$$P(z) \triangleq C(z,T_s)G_p(z,T_s) = G_p(z,\bar{T}), \tag{4.6}$$
i.e. a time-invariant block representing the nominal plant for which the repetitive controller provides of closed-loop stability. Furthermore, when T_s remains constant at the nominal sampling time $\bar{T}$, the compensator is such that $C(z,T_s) = C(z,\bar{T}) = 1$.

It is also worth mentioning that the compensator has no causality problems. Indeed, the use of (4.3) and (4.4) in (4.5) allows to write

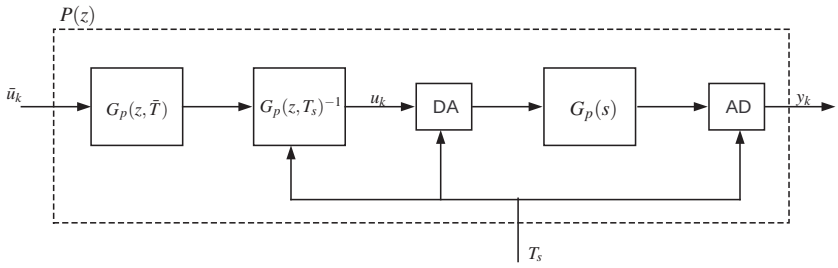

Fig. 4.4 Detail of the compensator-plant system.

$$C(z,T_s) = \frac{Num(z,\bar{T})}{Den(z,\bar{T})} \cdot \frac{Den(z,T_s)}{Num(z,T_s)}. \tag{4.7}$$

Therefore, the possible improperness of the second factor is removed by the properness of the first factor.

One last consequence is that the response of $P(z)$ at the sample instants $\{t_k\}_{k\geq 0}$ for a fixed sampling period is the same in spite of the sampling rate value. This corresponds to a time-scaling effect as a result of forcing the system to stay invariant in the discrete-time space.

The stability of the proposed control scheme is ensured by the following result:

Proposition 4.1. *Assume that the repetitive controller elements $I_{st}(z)$, $G_x(z)$, $G_c(z)$ are designed according to Proposition 2.1 and Remark 2.1 in order to provide of closed-loop stability for the LTI system $G_p(z,\bar{T})$. If the subsystem $P(z)$ detailed in Figure 4.4 is internally stable for all $T_s \in \mathscr{T} \subset \mathbb{R}^+$, then the overall closed-loop system depicted in Figure 4.3 is stable for all $T_s \in \mathscr{T}$.*

Proof. Recalling (4.6), the internal stability of $P(z)$ for all sampling periods $T_s \in \mathscr{T}$ guarantees that compensation is effectively carried out in $\mathscr{T}$. Hence, the overall subsystem $P(z)$ is ensured to behave as the LTI system $G_p(z,\bar{T})$ and, as the repetitive controller is assumed to provide of closed-loop stability to this block, the result follows. □

Remark 4.3. (i) The internal stability of the compensator-plant subsystem $P(z)$ can be checked using an LMI gridding approach [1, 8]. Also notice that a necessary condition for the internal stability of $P(z)$ is that $G_p(z,T_s)$ be minimum phase for all $T_s \in \mathscr{T}$. (ii) In many practical applications the plant $G_p(z)$ admits a relative degree 1, first order model description, which ensures internal stability for $P(z)$ whenever $G_p(z)$ is stable. (iii) The proposed procedure guarantees the expected behaviour at the sampling time instants. However, for extremely large values of $|\theta_k| = |T_k - \bar{T}|$, undesirable intersampling oscillations might appear.

4.4 Conclusions

The adaptation of the sampling period of a repetitive controller in case of reference/disturbance periodic signals with time-varying period allows to maintain its tracking/rejection performance; however, this strategy may negatively affect the closed-loop stability. In this direction, two repetitive control designs that assure the stability of the system working with sampling period adaptation are presented.

First, a controller was obtained through a small-gain theorem-based robust control design technique that assures BIBO stability in the required sampling period interval, with no restrictions on its rate of change. This interval is set from the expected interval of variation which is assumed to be known. Further research will study the problem in the time-varying sampling period framework.

Second, the pre-compensation design strategy presented in this work propounds to neutralize the structural changes caused by the sampling period adjustment by means of an additional compensator which makes the system LTI from an input-output viewpoint. This allows the characterization of time and frequency responses of the overall closed-loop system using standard LTI tools, provided that internal stability of the compensator-plant subsystem is ensured. Furthermore, with this approach, the repetitive controller design defined for a constant sampling period remains valid also in case of aperiodic sampling. The proposed method guarantees closed-loop stability independently of the frequency observer dynamics; thence, a decoupled independent design is feasible.

In case of perfect estimation of the signal frequency, the model invariance obtained with the pre-compensation scheme makes possible to preserve the performance during frequency transients. Furthermore, the proposed scheme allows transient analysis in a LTI framework.

The pre-compensation scheme is subject to the following limitations:
(i) As an inversion is carried out, it cannot be used with nonminimum phase plants. The extension of the pre-compensation approach to this case is currently under study.
(ii) Internal stability is required for the compensator-plant subsystem, which in general needs a non-trivial stability analysis regarding its LTV nature. As the subsystem does not usually exhibit high order, the LMI gridding procedure described in Section 3.3 is suitable for the stability analysis.

References

1. P. Apkarian and R. Adams. Advanced gain-scheduling techniques for uncertain systems. *IEEE Transactions on Control Systems Technology*, 6(1):21–32, 1998.
2. R. Costa-Castelló, S. Malo, and R. Griñó. High performance repetitive control of an active filter under varying network frequency. In *Proceedings of the 17th IFAC World Congress*, pages 3344–3349, 2008.
3. H. Fujioka. A discrete-time approach to stability analysis of systems with aperiodic sample-and-hold devices. *IEEE Transactions on Automatic Control*, 54(10):2440–2445, 2009.
4. R. D. Hanson and T.-C. Tsao. Periodic sampling interval repetitive control and its application to variable spindle speed noncircular turning process. *Journal of Dynamic Systems, Measurement, and Control*, 122(3):560–566, 2000.
5. G. Hillerström. *On Repetitive Control*. PhD thesis, Lulea University of Technology, November 1994.

6. D. Robert, O. Sename, and D. Zsimon. Synthesis of a sampling period dependent controller using LPV approach. In *Proceedings of the 5th IFAC Symposium on Robust Control Design*, Toulouse, France, 2006.
7. D. Robert, O. Sename, and D. Zsimon. An H_∞ LPV design for sampling varying controllers: experimentation with a T inverted pendulum. *IEEE Transactions on Control Systems Technology*, 18(3):741 – 749, May 2010.
8. A. Sala. Computer control under time-varying sampling period: An LMI gridding approach. *Automatica*, 41(12):2077–2082, 2005.
9. R. S. Sánchez-Peña and M. Sznaier. *Robust Systems Theory and Applications*. Adaptive and Learning Systems for Signal Processing, Communications and Control Series. Wiley-Interscience, August 1998.
10. Y. S. Suh. Stability and stabilization of nonuniform sampling systems. *Automatica*, 44(12):3222–3226, 2008.
11. T.-C. Tsao, Y.-X. Qian, and M. Nemani. Repetitive control for asymptotic tracking of periodic signals with an unknown period. *Journal of Dynamic Systems, Measurement, and Control*, 122(2):364–369, 2000.
12. G. Weiss and M. Häfele. Repetitive control of MIMO systems using H_∞ design. *Automatica*, 35(7):1185 – 1199, 1999.

Part II
HORC approach

Chapter 5
Odd-harmonic high order repetitive control

5.1 Introduction

5.1.1 State of the art

The aim of the High-Order Repetitive Control (HORC) has been focused on two aspects: improve the interharmonic behaviour by reducing the gain of the sensitivity function at these frequency intervals or provide robustness against frequency variation/uncertainty by enlarging the interval around the harmonics for which the the internal model provides high gain.

The internal model used in HORC can be defined from the generic internal model (2.4) setting $\sigma = 1$ and

$$W(z) = \sum_{l=1}^{M} w_l z^{-lN}, \tag{5.1}$$

thus yielding:

$$I_{ho}(z) = \frac{\sum_{l=1}^{M} w_l z^{-lN} H(z)}{1 - \sum_{l=1}^{M} w_l z^{-lN} H(z)}. \tag{5.2}$$

It can be seen that the delay function is now a weighted addition of M delays. The controller architecture follows the scheme depicted in Figure 5.1. Stability conditions for the closed-loop system of Figure 5.1 using (5.2) as the internal model are derived in the same way as conditions given in Section 2.2. Thus, condition 1 and 2 in Proposition 2.1 need to be fulfilled.

The weights w_l in (5.1) can be selected according to the desired performance. With this purpose, several criteria have been introduced and usually they are formulated through an optimization procedure. In order to assure high gain at harmonic frequencies, the following constraint is commonly demanded:

$$\sum_{l=1}^{M} w_l = 1. \tag{5.3}$$

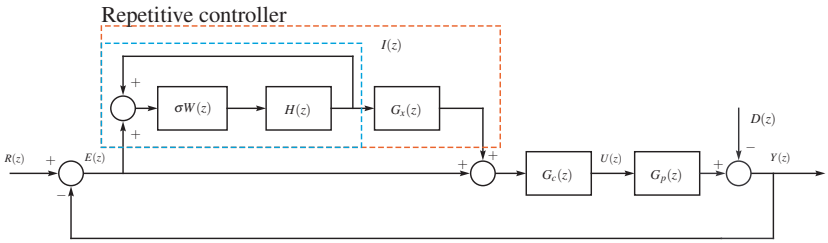

Fig. 5.1 Block-diagram of the repetitive controller plug-in approach.

In case of $H(z) = 1$, condition (5.3) guarantees that the poles of the internal model (5.2) are located at harmonic frequencies.

In HORC, the robustness analysis against frequency variations is usually based on the modifying sensitivity transfer function of the system $S_{Mod}(z)$, see equation (2.9).

In [11], HORC is used to improve the non-harmonic performance by means of $\min_{w_l} \|S_{Mod}(z)\|_2$ and $w_l = 1/M$, $\forall\ l$ is found to be the analytical solution of this problem. In [1], the problem of finding the weights w_l is solved by means of an error spectrum minimization via $\min_{w_l} \|S_{Mod}(z)\|_\infty$.

In [19], in order to minimize sensitivity against frequency variations, $W(z)$ is selected to have the first $M-1$ derivatives equal to zero at harmonic frequencies, and an analytical solution is obtained. A generalization of the results in [1] is found in [20], where $\min_{w_l} \|G(z)S_{Mod}(z)\|_\infty$ is solved using the weight function $G(z)$ as a way to determine the frequency region for which $S_{Mod}(z)$ will be minimized; results in [1, 19] can be obtained using this generic formulation.

In [15], the constraint (5.3) is eliminated. This diminishes the gain obtained at harmonic frequencies. Although this reduces the performance at nominal frequency it makes possible to obtain a lower interharmonic gain. In this way, the optimization problem proposed considers both components. It can be shown that the results in [1, 19, 20] can be obtained under particular settings of this formulation.

Figure 5.2 compares the results obtained for $G_x(z) = 1/(G_o(z))^{-1}$, $H(z) = 1$ and $M = 3$ when using the different tuning techniques previously introduced. The obtained weights are summarized in Table 5.1. As can be seen, [1, 11] enhance the interharmonic performance, but they do not improve robustness against frequency variations. It is also shown that results from [19] obtain perfect tracking, that is, the modifying sensitivity function gain at the harmonic frequencies is zero, and at the same time make flatter the zone around them, which reflects the robustness improvement against small variation in the signal frequency. However, the frequency interval between the harmonics is notoriously amplified. Finally, although the re-

Delay blocks	$M = 3$
Inoue (1990)	$w_1 = w_2 = w_3 = 1/3$
Chang (1996)	$w_1 = 3/6$, $w_2 = 2/6$, $w_3 = 1/6$
Steinbuch (2002)	$w_1 = 3$, $w_2 = -3$, $w_3 = 1$
Pipeleers (2008)	$w_1 = -1.654588$, $w_2 = 1.521402$, $w_3 = -0.654055$

Table 5.1 Obtained weights using the proposals [11], [1], [19] and [15] $M = 3$.

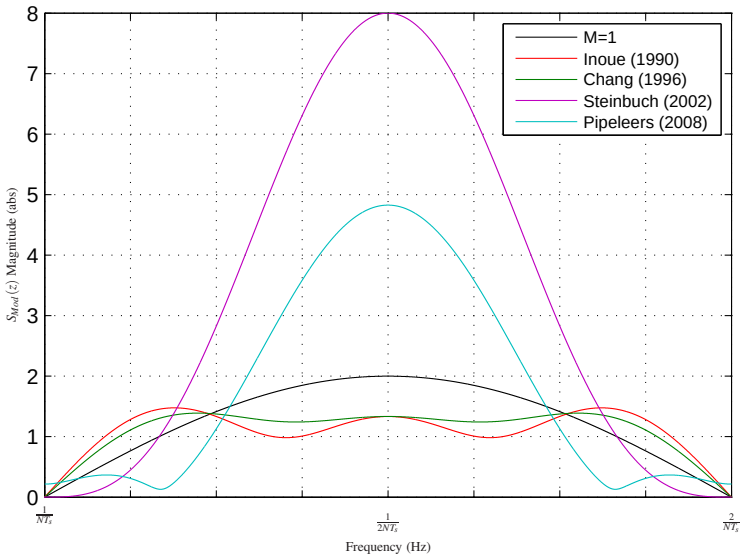

Fig. 5.2 Magnitude response of $S_{Mod}(z)$: comparison of [11], [1], [19] and [15] for $G_x = 1/(G_o(z))^{-1}$, $H(z) = 1$ and $M = 3$.

sult in [15] has no perfect tracking the gain around harmonics is kept small and the interharmonic amplification is lower than the one obtained in the previous case.

It is worth noticing that having too much gain at interharmonic frequencies can yield the amplification of undesirable signals that have frequency components at those regions, such as noise or flicks, and thus compromising the performance of the system.

5.1.2 Contribution

The main contribution of this part is based on proposing an odd-harmonic HORC. This controller is intended for systems that are exposed to periodic signals with only odd harmonic components, like those ones in power electronics applications, and at the same time providing them with robustness against frequency variations. Two additional issues have been developed to complete the proposal: the stability analysis of the internal models used in HORC and, viewed as consequence of this, an anti-windup synthesis for repetitive control.

5.1.3 Outline

This Chapter is organized as follows: Section 5.2 analyses the stability of the internal models used in HORC which is carried out by means of the internal model pole analysis, Section 5.3 develops the Odd-harmonic High Order Repetitive Controller which constitutes the main matter of this Chapter, Section 5.4 proposes and anti-

windup synthesis as response to the analysis presented in Section 5.2 and finally conclusions and future work are presented in Section 5.5.

5.2 Internal model poles analysis

In this section, the stability of the internal models used in HORC is analysed. This is an important issue since the practical implementation of the controller becomes more complex in case of unstable internal models. The stability of the models referenced in Section 5.1.1 is analysed and we are particularly interested in the internal models proposed in [19] and [15] since those approaches provide robustness in face to frequency variation/uncertainty.

Proposition 5.1. *The procedure followed in [19] yields*

$$W(z) = 1 - (1 - z^{-N})^M$$

and, as a consequence, the internal model resulting from (2.4) with $\sigma = 1$ *and* $H(z) = 1$ *is*

$$I_{ho}(z) = \frac{1 - (1 - z^{-N})^M}{(1 - z^{-N})^M}, \tag{5.4}$$

its poles being $z = \sqrt[N]{1}$ *with multiplicity M.*

Proof. By straightforward calculation. □

From Proposition 5.1 it is immediate that the poles coincide with those of the traditional repetitive controller ($M = 1$).

The increment of the pole multiplicity improves robustness against frequency variations [19] (i.e. with $M > 1$) but it makes the real implementation harder. For example a system with actuator saturation in which the multiplicity of the poles located over the unit circle is larger than 1, will experiment a substantially harder wind-up effect.

Figure 5.3 shows the Nyquist plot of $-\sigma W(z)H(z)$ with $\sigma = 1, H(z) = 1$ and $N = 400$ for the options previously analyzed[1]. The Nyquist plot of the standard repetitive controller, i.e. with $M = 1$, is over the unit circle and, therefore, it is marginally stable[2]. It can be noticed that the results obtained in [11, 1] which do not improve robustness under frequency uncertainty, generate a Nyquist plot contained inside the unit circle, except at tangential points corresponding to the harmonic frequencies poles, whilst those methods which improve robustness, [19], encircle the -1 point many times.

Remark 5.1. Although, as shown in Proposition 5.1, the internal models obtained following the procedure in [19], for $H(z) = 1$, do not contain poles outside the unit circle, with the introduction of a low pass filter $H(z)$ inside the internal model the Nyquist plot will vary slightly. Using the traditional design of $H(z)$, this variation will change the number of the encirclements around $z = -1$ and, consequently, poles outside the unit circle appear in most cases.

[1] Note that, as the internal model is composed of a positive feedback, the Nyquist criterion has to be applied to $-W(z)H(z)$.

[2] Marginally stable in the sense that it has poles over the unit circle with multiplicity one.

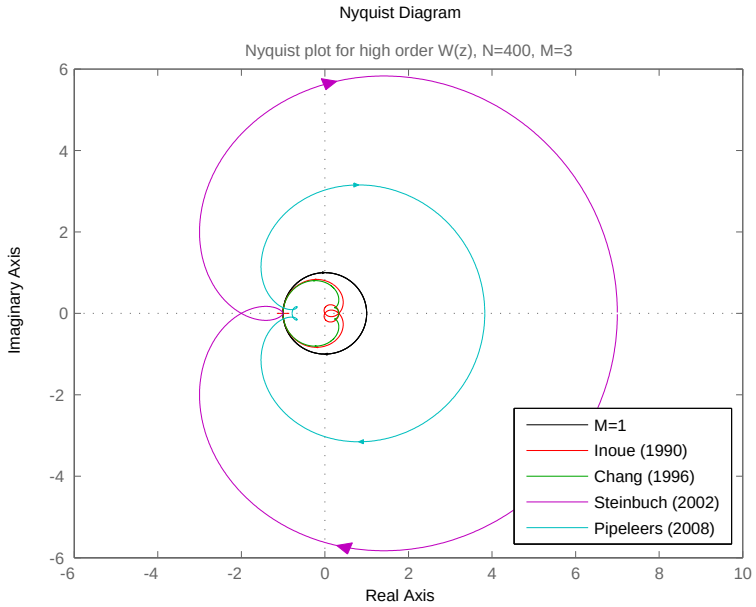

Fig. 5.3 Nyquist plot of $-W(z)$ for traditional repetitive control ($M = 1$) and the high order repetitive control ($M = 3$) tuned according to [11], [1], [19] and [15].

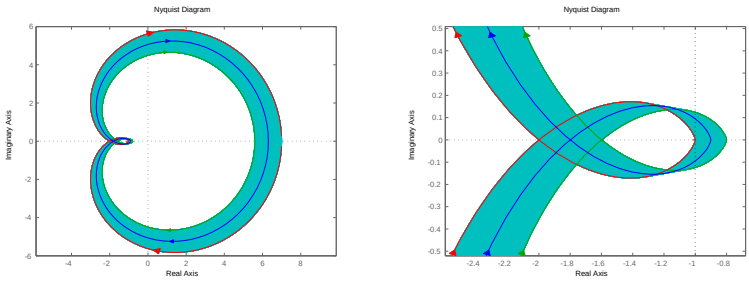

Fig. 5.4 Nyquist plot of $-W(z)H(z)$ for high order repetitive control ($M = 3$) tuned according to [19] and using $H(z) = 0.05z^{-1} + 0.9 + 0.05z$.

As an example, Figure 5.4 shows the Nyquist plot of $-W(z)H(z)$ with $H(z) = 0.05z^{-1} + 0.9 + 0.05z$, $N = 400$ and $M = 3$, for the approach in [19]. As it can be seen, the addition of the filter $H(z)$ increases encirclements around $z = -1$ and the internal model has poles outside the unit circle.

The optimization based tuning [15] generates internal models with poles outside the unit circle depending on the selected filter $H(z)$ and weight function. It is important to note that, for the specific tuning shown in Figure 5.2, these internal models do not contain integrators or poles at the harmonic frequencies which generates an internal model without poles outside the unit circle. As an example, Figure 5.5 shows the Nyquist plot of $-W(z)H(z)$ with $H(z) = 0.05z^{-1} + 0.9 + 0.05z$, $N = 400$ and $M = 3$, for the approach in [15] but using a different setup from the previous one. As it can be seen, the addition of the filter $H(z)$ and the new setup causes now encir-

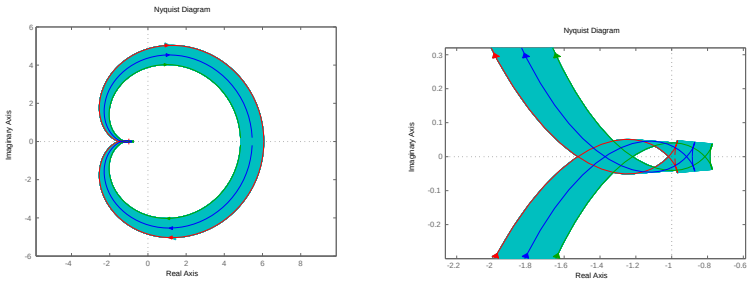

Fig. 5.5 Nyquist plot of $-W(z)H(z)$ for high order repetitive control ($M = 3$) tuned according to [15] and using $H(z) = 0.05z^{-1} + 0.9 + 0.05z$.

clements around $z = -1$ and the resulting internal model has poles outside the unit circle.

From the theoretical point of view, the existence of poles outside the unit circle in the internal model does not compromise the closed-loop stability; however, unstable controllers yield an unpredictable behaviour in practical implementations where nonlinearities, actuator saturation or sensor failure can be present. As an example, sophisticated anti-windup schemes must be included in order to avoid problems with saturated control actions [5]. Furthermore, regarding the interharmonic behaviour, an additional problem arises due to the water-bed effect which becomes harder for unstable open loop systems [18], such as those obtained with these internal models.

5.3 Odd-harmonic HORC

5.3.1 Odd-harmonic repetitive control

From the generic function (2.4) the standard internal model [11] can be defined using $W(z) = z^{-N}$ with N the discrete period of the signal, $H(z) = 1$ and $\sigma = 1$. This internal model provides infinite gain at certain fundamental frequency and all its harmonics until the $(N/2-1)$-th. On the other hand, an odd-harmonic internal model, which only introduces infinite gain at odd-harmonics of the fundamental frequency [8], can be obtained using $W(z) = z^{-N/2}$, $H(z) = 1$ and $\sigma = -1$, yielding

$$I_{odd}(z) = \frac{-H(z)}{z^{\frac{N}{2}} + H(z)}. \tag{5.5}$$

When $H(z) = 1$, the poles of (5.5) are uniformly distributed over the unit circle[3], $z = \exp(2(2k-1)\pi j/N)$, providing infinite gain at frequencies $\omega_k = 2(2k-1)\pi/N$, with $k = 1, 2, ..., N/2$.

The closed-loop system poles are the poles of the system without repetitive controller, i.e. poles of $S_o(z)$, and the poles of $S_{Mod}(z)$; equations (2.8) and (2.9), respectively. For the case in which $G_x(z) = k_r(G_o(z))^{-1}$, $\sigma = -1$, $W(z) = z^{-\frac{N}{2}}$ and $H(z) = 1$, the poles of $S_{Mod}(z)$ result

[3] Note that, as there is no pole in $z = 1$, there is no infinite gain in dc-frequency, i.e. no integrator.

$$z = \sqrt[N/2]{|1-k_r|}e^{\frac{2(2k-1)\pi j}{N}},\ k = 1,\ldots,\frac{N}{2}. \tag{5.6}$$

These poles are uniformly distributed over a circle of radius $\sqrt[N/2]{|1-k_r|}$. To accomplish stability these poles should be within the unit circle, namely $k_r \in (0,2)$. Although the introduction of $H(z) \neq 1$ and designs that involve nonminimum-phase plants affect the location of the closed-loop poles and also the convergence speed of the system as a function of k_r, this analysis gives a simple and intuitive approximation of the distribution of the poles [23].

5.3.2 Odd-harmonic HORC internal model

All previous works in HORC have been formulated for generic internal models which provide full harmonic actuation. However, using the generic model (2.4), they can be transformed into odd-harmonic internal models changing $\sigma = 1$ by $\sigma = -1$, N by $N/2$ and reformulating w_l in equation (5.1). Thus, the high order odd-harmonic internal model results:

$$I_{hodd}(z) = \frac{-W(z)H(z)}{1+W(z)H(z)}, \tag{5.7}$$

with

$$W(z) = \sum_{l=1}^{M}(-1)^{l-1}w_l z^{-lN/2}. \tag{5.8}$$

Then, the computation of w_l based on the procedure presented in [19] can be done by forcing $W(e^{j\omega}) = -1$ at odd-harmonic frequencies, thus providing of perfect asymptotic tracking at those frequencies, and forcing the $M-1$ first derivatives of $W(e^{j\omega})$ with respect to ω to be zero at odd-harmonic frequencies.

Similarly to [19], the procedure described here use the maximally flat concept to calculate the weightings of the function $W(z)$ in order to improve the performance robustness of the system.

It can be seen that the transfer function (5.7), with $H(z) = 1$, provides infinite gain when $W(z) = -1$. In the frequency domain that means

$$W(e^{j\omega}) = \sum_{l=1}^{M}(-1)^{l-1}w_l e^{-j\omega lN/2} = -1. \tag{5.9}$$

Since it is desirable to obtain infinite gain at odd-harmonic frequencies, it is required to set $\omega = 2\pi(2k-1)/N$ with $k = 1,2,3,\ldots$ in (5.9), which yields the following condition

$$\sum_{l=1}^{M} w_l = 1. \tag{5.10}$$

This condition allows for the achievement of perfect asymptotic tracking or disturbance rejection and guarantees that if the external signal is N-periodic with odd-harmonic content, the resulting weighted sum in (5.8) is the same as that obtained using just one delay element.

To show how the derivatives of $W(e^{j\omega})$ and $I_{hodd}(e^{j\omega})$ with respect to ω are related, the chain rule can be used, thus for the first derivative

$$\frac{\partial I_{hodd}(e^{j\omega})}{\partial \omega} = \frac{\partial I_{hodd}(e^{j\omega})}{\partial W(e^{j\omega})}\frac{\partial W(e^{j\omega})}{\partial \omega} = \frac{-1}{(1+W(e^{j\omega}))^2}\frac{\partial W(e^{j\omega})}{\partial \omega}$$

and for the second derivative

$$\begin{aligned}\frac{\partial^2 I_{hodd}(e^{j\omega})}{\partial \omega^2} &= \frac{\partial^2 I_{hodd}(e^{j\omega})}{\partial W^2(e^{j\omega})}\left(\frac{\partial W(e^{j\omega})}{\partial \omega}\right)^2 + \frac{\partial I_{hodd}(e^{j\omega})}{\partial W(e^{j\omega})}\frac{\partial^2 W(e^{j\omega})}{\partial \omega^2} \\ &= \frac{2}{(1+W(e^{j\omega}))^3}\left(\frac{\partial W(e^{j\omega})}{\partial \omega}\right)^2 + \frac{-1}{(1+W(e^{j\omega}))^2}\frac{\partial^2 W(e^{j\omega})}{\partial \omega^2}.\end{aligned}$$

The expressions to obtain higher order terms can be found using the Faà di Bruno's formula [3]. This result is useful to conclude that setting to zero the derivatives of $W(e^{j\omega})$ with respect to ω also sets to zero the derivatives of $I_{hodd}(e^{j\omega})$ with respect to ω.

Remark 5.2. It can be noticed that making $W(e^{j\omega})$ maximally flat at odd-harmonic frequencies also makes $I_{hodd}(e^{j\omega})$ maximally flat at those frequencies, therefore, increasing the frequency interval for which the internal model (5.7) provides the desired high gain.

Hence, to define the delay function $W(z)$, the weightings w_l can be calculated using (5.10) and making the first $M-1$ derivatives of $W(e^{j\omega})$ equal to 0 at odd-harmonic frequencies.

Thus, the first derivative is

$$\frac{\partial W(e^{j\omega})}{\partial \omega} = \sum_{l=1}^{M}(-1)^{l-1}w_l(-jl\frac{N}{2})e^{-j\omega lN/2}. \tag{5.11}$$

The condition states

$$\left.\frac{\partial W(e^{j\omega})}{\partial \omega}\right|_{\omega=\frac{2(2k-1)\pi}{N}} = 0,$$

which gives

$$\sum_{l=1}^{M} w_l l = 0. \tag{5.12}$$

Also, the $n-$th derivative results:

$$\frac{\partial W(e^{j\omega})}{\partial \omega} = \sum_{l=1}^{M}(-1)^{l-1}w_l l^n(-j\frac{N}{2})^n e^{-j\omega lN/2}. \tag{5.13}$$

Thus, making the $M-1$ derivatives equal to 0 at $\omega = 2\pi(2k-1)/N$, the following compact condition is obtained:

$$\sum_{l=1}^{M} w_l l^p = 0. \tag{5.14}$$

with $p = 1,2,\ldots,M-1$.

Thus, for $M=3$, (5.10) yields $w_1+w_2+w_3=1$ and (5.14) yields $w_1+2w_2+3w_3=0$, $w_1+4w_2+9w_3=0$, which renders $w_1=3$, $w_2=-3$, and $w_3=1$. In the same way, one gets $w_1=2$ and $w_2=-1$ for $M=2$.

The procedure described here attains the same conditions as those found in [19]. Also, the weightings derived for HORC in [1, 15, 20] can be used directly for odd-harmonic HORC using definition (5.8). At the same time, the properties obtained from each method are preserved.

Equations (5.10) and (5.14) can be put together in the following compact form:

$$\sum_{l=1}^{M} l^p w_l = \begin{cases} 1 \text{ if } p = 0 \\ 0 \text{ if } p = 1,\ldots,M-1. \end{cases} \tag{5.15}$$

Proposition 5.2. *The weights obtained from (5.15) yield*

$$W(z) = -1 + \left(1 + z^{-\frac{N}{2}}\right)^M \tag{5.16}$$

and, as a consequence, the internal model resulting from (2.4) with $\sigma = -1$ *and* $H(z) = 1$ *is*

$$I_{hodd}(z) = \frac{1 - \left(1 + z^{-\frac{N}{2}}\right)^M}{\left(1 + z^{-\frac{N}{2}}\right)^M}, \tag{5.17}$$

its poles being $z = \sqrt[N/2]{-1}$ *with multiplicity M.*

Proof. By straightforward calculation. □

In the light of Propositions 5.2 and 5.1 and using the same reasoning as before, it is immediate that the odd-harmonic internal models that can be obtained adapting the procedures [19] and [15] would yield the same (open loop) stability issues of those in the original version.

Finally, it is worth to notice that although odd-harmonic internal models only introduces high gain at odd-harmonic frequencies, they do not improve the interharmonic behavior. In Figure 5.6 a comparison of the sensitivity function $S_{Mod}(z)$, for the generic [19] and the odd-harmonic internal models is presented using $H(z) = 1$ and $M = 3$. It can be seen that the maximum resulting gain at interharmonic frequencies is equal in both cases, however robustness improvement against frequency variations/uncertainty at odd-harmonic frequencies is larger in the case of the odd-harmonic internal model presented here.

5.3.3 Selection of the gain k_r

Beside the repetitive controller speed convergence, the parameter k_r affects the magnitude response of the system sensitivity function at the inter-harmonic frequency intervals. This is an important fact since HORC increases the gain at those intervals and some alleviation of that problem can be attained by a proper selection of k_r.

The modifying sensitivity function for the odd-harmonic HORC system is:

$$S_{Mod}(z) = \frac{1 + W(z)H(z)}{1 - W(z)H(z)(G_x(z)G_o(z) - 1)}. \tag{5.18}$$

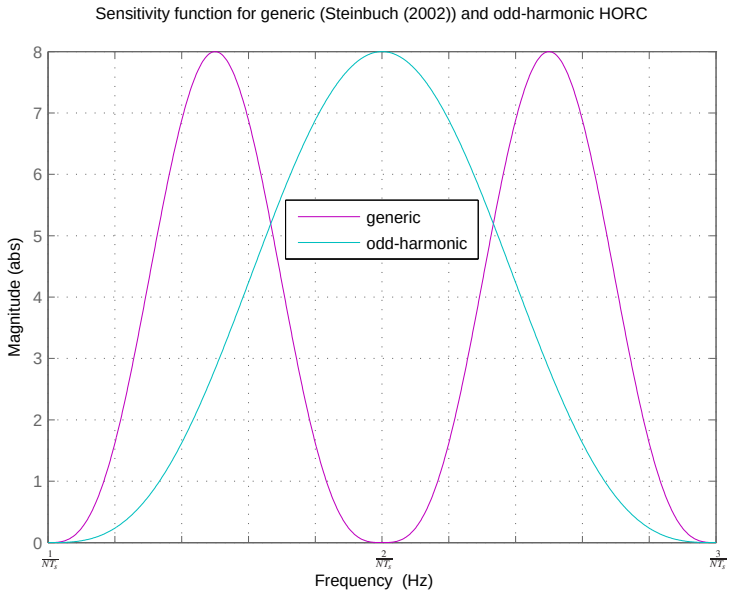

Fig. 5.6 Sensitivity functions of generic and odd-harmonic high-order repetitive controllers with $M = 3$ and $H(z) = 1$.

The transfer function $S_{Mod}(e^{j\omega})$ is periodic in the frequency domain with period $4\pi/N$ under the assumption that $H(z) = 1$, $G_x(z) = k_r G_o^{-1}(z)$ and $W(z)$ as defined in (5.16). Thus, the magnitude response between two harmonics can be described from $S_{Mod}(e^{j\omega})$ using the normalized frequency $\bar{\omega} = \omega N/2$ with $\bar{\omega} \in [\pi, 3\pi]$:

$$\left|S_{Mod}(e^{2j\bar{\omega}/N})\right| = \left|\frac{1 + W(e^{2j\bar{\omega}/N})}{1 - (k_r - 1)W(e^{2j\bar{\omega}/N})}\right|. \tag{5.19}$$

Figure 5.7, shows the magnitude of $S_{Mod}(z)$ for $M = 2$, $M = 3$ and for several values of k_r. It can be seen that $k_r < 1$ can be used to alleviate the over-amplification of frequencies between odd-harmonics while $k_r > 1$ causes an amplification of those frequencies.

Another important criterion used to select k_r is the closed loop poles distance to the origin. The main idea around this criterion is to analyse the modulus of the closed loop poles in order to obtain some insight about the convergence speed of the RC. As stated before, the closed loop poles are the poles of the sensitivity function $S(z)$ in equation (2.7) which in turn are the poles of $S_o(z)$ and $S_{Mod}(z)$. Thus, to analyse the speed convergence of the RC we are interested in the poles of $S_{Mod}(z)$. With $\sigma = -1$, $H(z) = 1$ and $G_x(z) = k_r/G_o(z)$, the closed loop poles can be calculated using:

$$1 - W(z)(k_r - 1) = 0,$$

$W(z) = z^{-N/2}$ and $W(z) = -1 + \left(1 + z^{-N/2}\right)^M$ being the delay function for odd-harmonic RC and HORC respectively.

In Figure 5.8, a comparison of the closed loop poles modulus vs k_r is presented for odd-harmonic RC ($M = 1$), second order ($M = 2$) and third order ($M = 3$) HORC

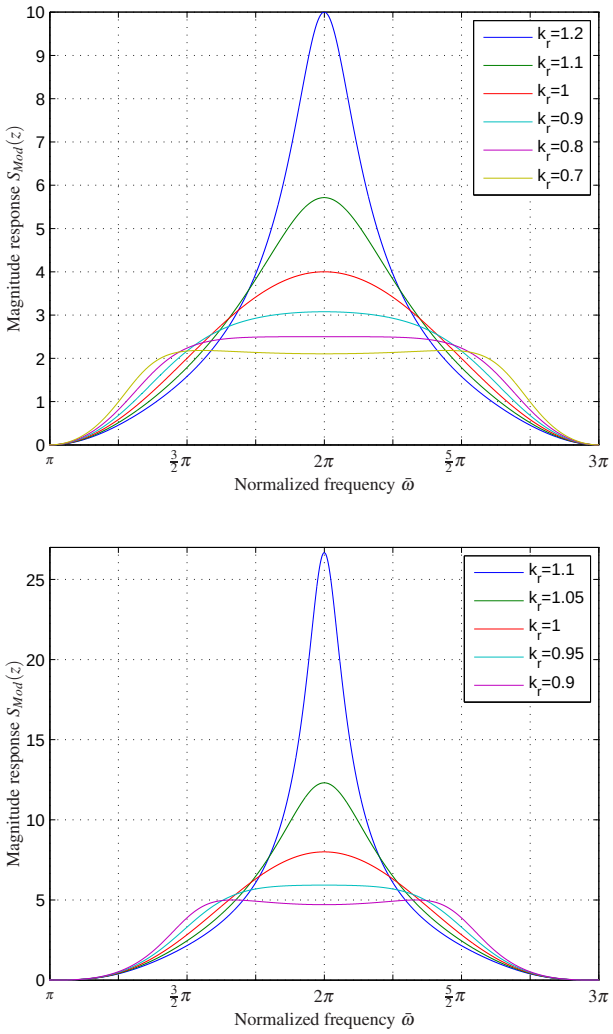

Fig. 5.7 $S_{Mod}(z)$ magnitude response for several values of k_r. Top $M = 2$, bottom $M = 3$

and using $N = 100$. It can be concluded that the system speed convergence increases as k_r approaches to 1 and also that the increment in the RC order reduces the speed convergence.

5.3.4 Performance under varying frequency conditions

Standard repetitive control, including the odd-harmonic version, is designed assuming the period T_p constant. Therefore, if T_p varies the control algorithm performance may drastically decay. In order to illustrate the performance robustness of the odd-harmonic HORC proposed here, Figure 5.9 compares the magnitude response of the internal models used in odd-harmonic RC and odd-harmonic HORC.

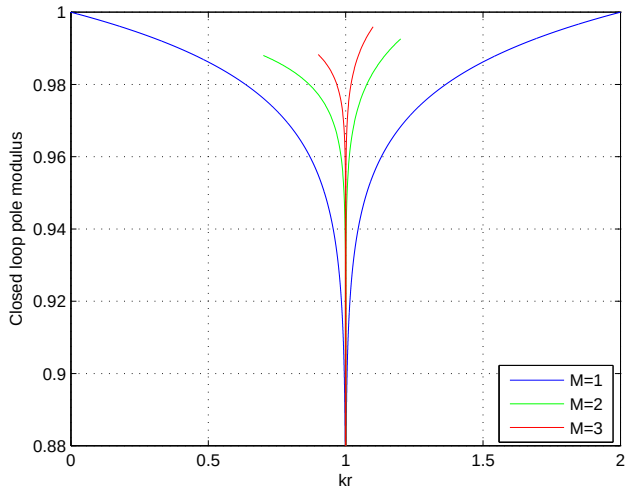

Fig. 5.8 Closed loop poles modulus vs k_r for odd-harmonic RC ($M = 1$), second order ($M = 2$) and third order ($M = 3$) HORC, using $N = 100$.

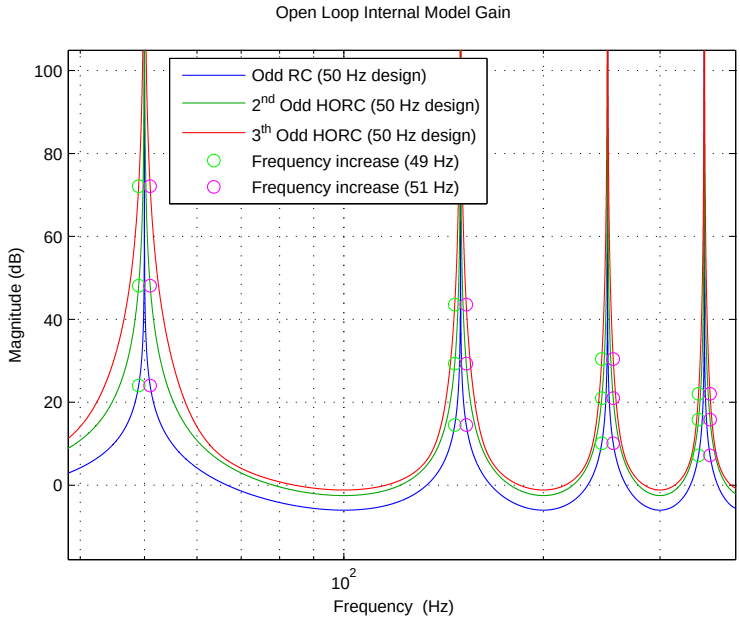

Fig. 5.9 Odd-harmonic RC and odd-harmonic HORC internal models gain diagram.

Thus, Figure 5.9 highlights the gain of the internal models (5.5) and (5.7), designed for a nominal frequency of 50 Hz, for 49 Hz, 50 Hz and 51 Hz (and some of their harmonics). First, the magnitude of the odd-harmonic function (5.5) is depicted in blue. Note that while for the 50 Hz signal the gain is important, it strongly decays for the other frequencies. On the other hand, the magnitude of the odd-harmonic HORC (5.7) for $M = 2$ and $M = 3$ is shown. It can be seen that the gain is higher for

a wider frequency region around the harmonics and this feature increases with the order of the internal model. This improves the robustness for variations in the period T_p. As a consequence, the gain decrease is much smaller for frequency variations around the nominal frequency in case of odd-harmonic HORC and the performance degradation is minor.

5.3.5 Second-order odd-harmonic Internal Model

Two aspects make the second-order odd-harmonic Internal Model an interesting case of HORC: first, the order of the IM and thus the need of memory in practical implementations is very similar to the standard RC with the additional benefit of providing robust performance and second, the traditional design of the filter $H(z)$ renders an open loop stable second order IM.

In this section, sufficient conditions for the internal model stability of the second order odd-harmonic repetitive controllers are established. With this purpose, lets set $\sigma = -1$ and $M = 2$ in (5.16). Then, the internal model obtained from (2.4) results:

$$I_{hodd}(z) = -\frac{\left(2z^{-\frac{N}{2}} + z^{-N}\right) H(z)}{1 + \left(2z^{-\frac{N}{2}} + z^{-N}\right) H(z)}. \tag{5.20}$$

Proposition 5.3. *The second-order, odd-harmonic internal model (5.20), $H(z)$ being a null-phase filter with $\|H(z)\|_\infty < 1$, contains no pole outside the unit circle.*

Proof. Let us first show that (5.20) with $H(z) = 1$ has no poles outside the unit circle using a Nyquist-based argument. For this, notice that the Nyquist plot of $W(z)$ crosses the negative real axis at $\bar{\omega} = \frac{2(2\cdot k+1)\pi}{N}$, $k = 0, \ldots, N/2-1$ and at $\bar{\omega} = \pi$ if N is multiple of 4. In all these frequencies the modulus of $W\left(e^{j\omega}\right)$ is equal to 1. Hence, no encirclements are produced around $z = -1$, so the internal model does not contain poles outside the unit circle.

Finally, the addition of a null-phase filter with $\|H(z)\|_\infty < 1$ does not modify the frequencies at which the negative real axis is crossed, since for all these frequencies:

$$|W(e^{j\bar{\omega}})H(e^{j\bar{\omega}})| \leq |W(e^{j\bar{\omega}})| \|H(z)\|_\infty < 1.$$

Thus, no encirclements around or crosses by $z = -1$ are produced and (5.20) is stable. □

Furthermore, assume that for the "plug-in" configuration of Figure 5.1:
(i) $G_x(z) = k_r \left(G_o(z)\right)^{-1}$, this yielding the modifying sensitivity function obtained from (5.18) to be:

$$S_{Mod}^{hodd}(z) = \frac{1 + \left(2z^{-\frac{N}{2}} + z^{-N}\right) H(z)}{1 + \left(2z^{-\frac{N}{2}} + z^{-N}\right) H(z)(1 - k_r)}. \tag{5.21}$$

(ii) The poles of the closed-loop system without the repetitive controller, i.e. the poles of $S_o(z)$, are stable.

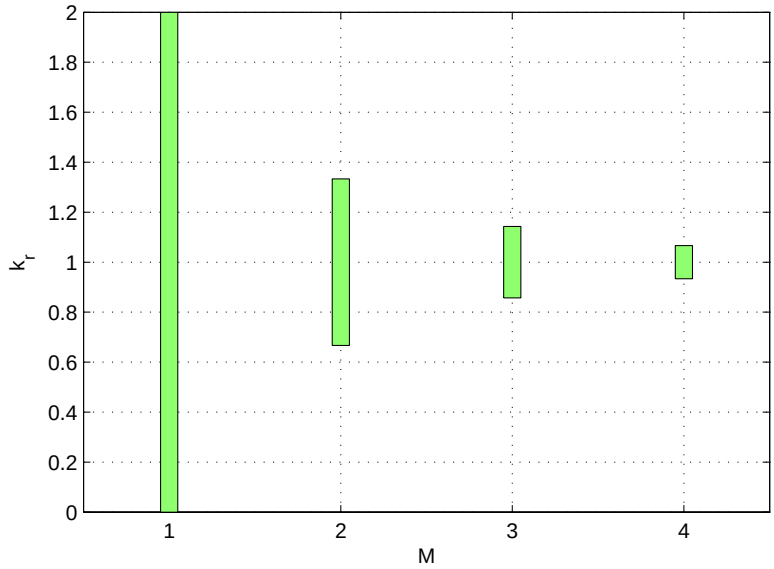

Fig. 5.10 Values of k_r vs. M for which the system is stable. $H(z)$ is a null-phase filter with $\|H(z)\|_\infty < 1$, $|H(e^{j\bar{\omega}})|_{\omega=0} = 1$ and $G_p(z)$ is a minimum phase plant.

Proposition 5.4. *When $H(z) = 1$, the closed-loop system corresponding to the "plug-in" configuration of Figure 5.1 is stable for $k_r \in \left(0, \frac{4}{3}\right)$.*

Proof. According to the discussion in Section 5.3.1, the poles of the closed-loop system are given by those of $S_o(z)$ and $S_{Mod}^{hodd}(z)$. The poles of $S_o(z)$ are stable by hypothesis, while the poles of $S_{Mod}^{hodd}(z)$ obtained from (5.21) are

$$\bar{z} = \sqrt[2/N]{k_r - 1 \pm \sqrt{k_r^2 - k_r}}.$$

Then, the analysis of the modulus of the poles reveals that $|\bar{z}| \leq 1, \forall k_r \in \left[0, \frac{4}{3}\right]$. □

Remark 5.3. For a given $k_r \neq 1$, the closed-loop poles obtained with the standard repetitive controller are two times faster than the ones obtained with the second-order odd-harmonic repetitive controller. When $k_r = 1$ all poles are in $z = 0$ for the first ($M = 1$) and second-order ($M = 2$) odd-harmonics internal models.

Proposition 5.5. *When $H(z)$ is a null-phase filter with $\|H(z)\|_\infty < 1$ and $|H(e^{j\bar{\omega}})|_{\omega=0} = 1$, the closed-loop system corresponding to the "plug-in" configuration of Figure 5.1 is stable for $k_r \in (2/3, 4/3)$.*

Proof. As it is immediate that $\|W(z)\|_\infty = 3$, the result follows straightforward from the stability of $G_o(z)$ and sufficient stability condition 2 in Proposition 2.1. □

In the light of proposition 5.5 and taking different values for M, Figure 5.10 shows a comparison of the values of k_r for which the system is stable. It is worth to note that for higher values of M the k_r interval that assures system stability is highly reduced yielding a small margin for a successful practical implementation design.

5.4 Anti-Windup synthesis for repetitive control

5.4.1 Introduction

5.4.1.1 Motivation

As discussed in previous chapters, the IM of the RC provides infinite or very high gain at a given frequency an its harmonics. It is well known that, in systems with actuator saturation, a controller with these characteristics may produce a wind-up effect in which the states of the controller can grow unbounded [10]. Even if the gain is not infinite but high, the states can overgrow significantly, making it harder to recover the system to the linear ideal one. Some conditions related to the boundedness of the state of the RC with actuator saturation are stated in [17].

Also it is known that marginally stable or unstable controllers are prone to originate the unbounded growing of the controller state. Thus, using the pole analysis presented in Section 5.2, it can be noted that the IM used in standard RC is marginally stable and those used in High Order Repetitive Control [11, 19] have poles over the unit circle with multiplicity equal or greater than two which can yield Bounded Input Bounded Output unstable IM. Additionally, the time response of the IM generally imposes a slow transient response for the closed loop which worsens the conditions in face of actuator saturation. Therefore, since the linear design of the repetitive control does not take into account the saturation in the actuator, it is needed to include an Anti-Windup compensator.

5.4.1.2 The general anti-windup designs

A recent review of standard AW techniques can be found in [22, 5]. In [5], modern anti-windup proposals have been classified in two groups: Direct Linear Anti-Windup (DLAW) and Model Recovery Anti-Windup (MRAW). The DLAW approach seeks to find an anti-windup compensator that assures specific performance and stability properties for the closed loop system. The MRAW approach selects the anti-windup filter in such a way that it is a dynamical system containing the model of the plant. However, due to the characteristics of the RC, most of the standard AW designs should not be applied straightforward since some difficulties can appear during design or implementation, as will be explained below. As a result, it would be necessary to adapt the generic anti-windup strategies in order to be applied in RC.

In the DLAW scheme, some strategies are based on solving an LMI problem; however, complications usually arise since the size of this LMI depends mostly on the internal model order which is usually large. Thus, for the RC case, the implementation of this scheme depends on whether the LMI is computationally solvable or not. Although the DLAW scheme allows us to obtain an anti-windup compensator of order 0, the solution includes elements that yield a large number of on-line calculations, thus increasing the computational burden.

The MRAW scheme uses the model of the plant in its structure. Although the order of the plant could be large, it is usually significantly smaller than the internal model order. Furthermore, the procedure to find the feedback gains does not depend on the controller dynamics, therefore the related LMI is always solvable.

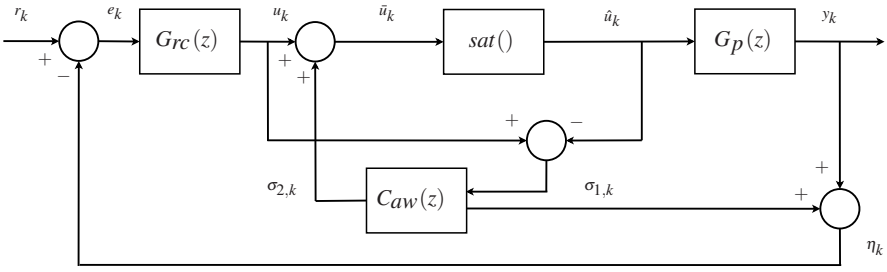

Fig. 5.11 The MRAW scheme in RC.

The computational load of the MRAW scheme implementation is the lowest one in comparison with the other strategies.

5.4.1.3 Anti-windup designs for RC - state of the art

The proposals in [4, 16, 17] are three examples of anti-windup design for repetitive control. In [16], an anti-windup law is derived for Iterative Learning Control (ILC) and also a extension to RC is briefly described. However, the anti-windup strategy is derived for a specific plant and the described repetitive controller does not correspond to the standard architecture since the filters for stability and robustness are not included. In [17], the anti-windup scheme cancels out the dynamics of the internal model during saturation and adds a structure to shape the transients when the system saturates and gets back from saturation. However, the internal model cancellation implies that, in addition to the repetitive controller order, it is necessary to implement an anti-windup filter which has at least the order of the internal model. Therefore, this scheme will be cost restrictive since it depends on a suitable implementation platform. The work in [4], can be categorized as a DLAW design. The strategy is derived in continuous time domain. It is an extension to RC of the general anti-windup design in [2], where the case of delayed systems is described. Also in this approach, unlike the RC design that will be described here, the filters for robustness and stability are designed together with the DLAW synthesis.

5.4.1.4 Contribution

In view of the analysis above, the MRAW appears as a good strategy when taken into account the computational solvability and load in the design and implementation of RC. Thus, in this work a MRAW scheme is presented in which the recovery of the system is achieved using the approximation to a deadbeat transition [13]. The advantage of selecting a deadbeat over other designs is shown as well as the design method.

5.4.2 The general MRAW scheme

Figure 5.11 shows the MRAW structure, where $G_p(z)$ is the plant, $G_{rc}(z)$ is the controller, $sat(\cdot)$ is the saturation function and $C_{aw}(z)$ is the anti-windup compensator. In the MRAW strategy, the mismatch between the saturated control action and the non-saturated one is fed back to the controller by means of the anti-windup compensator which is designed to be the model of the plant, $\sigma_{1,k}$ being the output that is used with this purpose. Additionally, another feedback signal, $\sigma_{2,k}$, is added with the aim of improving the behaviour of the system when it gets out from saturation. Thus, the design of this feedback involves different approaches. The Internal Model Control (IMC) anti-windup strategy [25], turns out to be the particular case where $\sigma_{2,k} = 0$. This causes that, when getting out of saturation, the system recovery relies on the plant poles, which can yield a non appropriated performance. A strategy based on Predictive Control which seeks an l_2 performance criterion can be found in [7], an optimization procedure using the Linear Quadratic (LQ) approach is proposed in [24] and a fully nonlinear strategy is described in [6].

In this Section, the signal $\sigma_{2,k}$ is designed to be a linear feedback of the anti-windup compensator state. This is aimed at finding a simple linear solution to the AW problem in case of RC, also avoiding the algebraic loop that can be created using the feedback of the control action mismatch, as in [24]. Furthermore, we analyse the benefits of designing a deadbeat behaviour in the AW filter in case of repetitive control. Also, as previously mentioned, the advantage of using the MRAW scheme for the repetitive control case is that the design does not depend on the internal model order. Additionally, as will be described later on, the error and control signals are the ideal ones (as if the system had no saturation in the actuator), which isolates the controller from the saturation effects.

5.4.2.1 Selected MRAW scheme

Consider the MRAW scheme depicted in Figure 5.11. Let the discrete-time and asymptotically stable linear plant $G_p(z)$ be

$$\begin{aligned} x_{k+1} &= Ax_k + Bsat(\bar{u}_k) \\ y_k &= Cx_k, \end{aligned} \tag{5.22}$$

where

$$sat(\bar{u}_k) = \begin{cases} u_{min} & \bar{u}_k < u_{min}, \\ \bar{u}_k & u_{min} \leq \bar{u}_k \leq u_{max}, \\ u_{max} & \bar{u}_k > u_{max} \end{cases} \tag{5.23}$$

with $u_{min} < 0$ and $u_{max} > 0$.

The state-space representation of the repetitive controller $G_{rc}(z)$ is:

$$\begin{aligned} \bar{x}_{k+1} &= A_{rc}\bar{x}_k + B_{rc}e_k \\ u_k &= C_{rc}\bar{x}_k + D_{rc}e_k. \end{aligned} \tag{5.24}$$

The AW filter $C_{aw}(z)$ is defined from the plant model (5.22) as:

$$\begin{aligned} \chi_{k+1} &= A\chi_k + B(u_k - sat(u_k + \sigma_{2,k})) \\ \sigma_{1,k} &= C\chi_k \end{aligned} \tag{5.25}$$

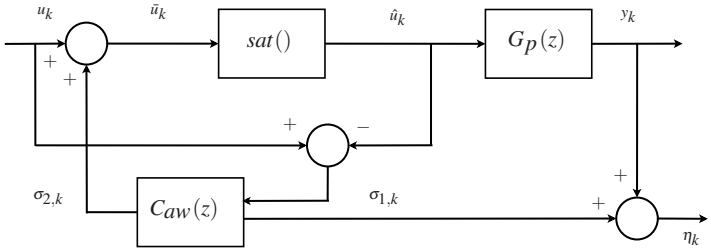

Fig. 5.12 The invariant part of the MRAW scheme.

and

$$\sigma_{2,k} = K\chi_k, \tag{5.26}$$

where K is the design parameter of the AW filter.

It can be noticed that while the input in system (5.22) is the saturated control action, the input in system (5.25) is the difference between the saturated and non-saturated control action. This fact, together with

$$\eta_k = y_k + \sigma_{1,k}, \tag{5.27}$$

helps to determine the system invariance. Thus, defining $\xi_k = x_k + \chi_k$, noticing that $\bar{u}_k = u_k + \sigma_{2,k}$ and adding equations (5.22) with (5.25) we have:

$$\begin{aligned} \xi_{k+1} &= A\xi_k + Bu_k \\ \eta_k &= C\xi_k. \end{aligned} \tag{5.28}$$

In this way, from the input u_k to the output η_k, the system in Figure 5.12 can be seen as a Linear Time Invariant (LTI) one with the dynamics of the plant.

This means that η_k is the ideal plant output in the sense that it would be the plant output in a system without actuator saturation. Furthermore, in the closed loop of Figure 5.11, the control action action u_k is the ideal control action, i.e. u_k is the same control signal as the one in a system without actuator saturation. This fact isolates the controller from the saturation effects, allowing us to reduce the analysis to the behaviour of the invariant part shown in Figure 5.12, including its internal stability.

Remark 5.4. In this scheme the deviation from the ideal performance can be measured through $\sigma_{1,k}$, since $\sigma_{1,k}$ is the difference between the ideal behaviour and the plant output $\sigma_{1,k} = \eta_k - y_k$.

Proposal 1 *Given a RC design, the smallest possible $\sigma_{1,k}$ corresponds to the best possible performance in case of saturation (the smallest deviation from the ideal behaviour). Therefore, the problem formulation is to find K such that $\sigma_{1,k}$ is small enough to obtain a good tracking performance.*

It is important that the AW design aims at achieving good tracking performance since RC is a technique which is intended to obtain null steady-state tracking error. Also due to this RC feature, we are interested in the saturation effect produced in steady state even though it also can occur in transient state.

5.4.3 MRAW proposal: the deadbeat anti-windup controller for RC

This section analyses the selection of the design parameter K in the context of repetitive control. The analysis is carried out in steady state, therefore, in the RC frame we can consider that all the signals present in the system are periodic (assuming that non periodic disturbance signals do not cause saturation we can neglect their effect on the system in this analysis). Furthermore, the actuator saturation depends on the signal to be tracked or rejected, i.e. the command signal or the disturbances.

In steady state, we can assume as standard scenario a control action that saturates only in specific parts of each period of the signal. Thus, at that moment the plant output deviates from the ideal behaviour and in the other part of the period the system can recover.

The system saturates when $u_k + \sigma_{2,k} > u_{max}$, moment at which the input of the anti-windup filter, the difference $u_{max} - u_k \neq 0$ and its dynamics corresponds with the plant dynamics thus establishing the invariance from u_k to η_k. Notice that $\sigma_{2,k}$ only has influence in the saturation function condition $u_k + \sigma_{2,k} > u_{max}$, helping to determine when the system can go out from saturation. Thus, the design of K affects the amount of time the system remains saturated. Also, notice that K does not affect the magnitude of $\sigma_{1,k}$ nor the AW state dynamics χ_k at this stage.

Getting out of saturation, this is when $u_k + \sigma_{2,k} < u_{max}$, the vanishing of the AW filter state χ_k, and so $\sigma_{1,k}$, will lie in the dynamics imposed by the state feedback loop created by $\sigma_{2,k}$. In this way, we can obtain the IMC anti-windup strategy with $K = 0$ and also other dynamics can be obtained using different pole placement designs. In general we are interested in values of K that provide $C_{aw}(z)$ with faster dynamics than the plant one.

Proposal 2 *The feedback gain K can be designed to be a deadbeat solution, thus locating the poles of $C_{aw}(z)$ in the origin and providing the fastest vanishing of the states and outputs of $C_{aw}(z)$.*

For more details about the deadbeat design and behaviour see [13].

As an example[4], let us assume that the signal to be tracked is a sine waveform signal, and that the saturation occurs due to the amplitude of the sinusoidal control signal for $u \geq 75$. Figure 5.13, shows the ideal linear behaviour and the response when there is saturation in the actuator and three different values of K: $K = 0$ i.e. IMC AW strategy, K for a deadbeat (DB) AW filter and K obtained from a LQR design with a faster dynamics than the plant one.

In the first case, with $K = 0$ i.e. the IMC strategy where $\sigma_{2,k} = 0$, the saturated control action is simply the result of limiting the ideal control action to its maximum, namely the system only saturates when $u_k > u_{max}$. Thus, once the system returns to the linear zone, $u_{max} - u_k = 0$, the state of the AW filter, and so $\sigma_{1,k}$, will vanish with the plant model dynamics, whereupon the output of the plant will be the ideal one. Is it also worth to notice that this is an asymptotic behaviour.

In the deadbeat case, once $u_k + \sigma_{2,k} < u_{max}$, the state of $C_{aw}(z)$ and its outputs, $\sigma_{1,k}$ and $\sigma_{2,k}$, will vanish in n sampling steps, where n is the relative degree of the plant model. At that moment $y_k = \eta_k$ (and $\psi = 0$). This means that, based on the system invariance, the system will remain saturated until the output plant y_k, with input u_{max}, can equal the ideal output η_k. Therefore, we are applying the maximum

[4] The simulation has been performed using the scheme of Figure 5.12 with $u_k = 120sin(100\pi t_k)$, sampling time $T_s = 50\ \mu$s and the discrete time model of the active power filter in Chapter 7

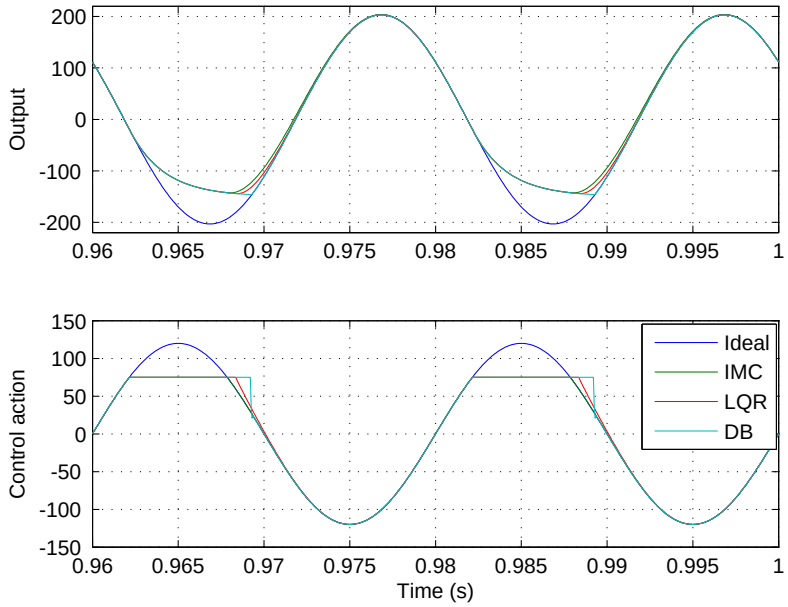

Fig. 5.13 AW compensator comparison: Ideal response for the system without saturation, IMC for $K = 0$, DB for a deadbeat behaviour and LQR for an intermediate behaviour.

possible effort by means of u_{max}, until the moment the ideal input can be reached again.

For other values of K, the AW filter will exhibit an intermediate behaviour with asymptotic response when getting out of saturation.

Comparing the response for different values of K we have that during saturation all the systems have similar behaviour since K does not modify the value of $\sigma_{1,k}$; however, the amount of time the system saturates is different, being the longest the deadbeat design. Also, it can be seen that the system which remains saturated longer has a smaller $\sigma_{1,k}$.

5.4.4 MRAW proposal: design and stability

The proposal is based on the idea of having a deadbeat recovery once the system gets back from saturation. The goal is to obtain a $C_{aw}(z)$ AW filter such that during saturation it takes the form of the plant model, and additionally, when the control action gets back from saturation, the outputs of $C_{aw}(z)$ vanish in a finite number of samples.

To obtain a deadbeat behaviour during recovery it is needed that the feedback loop created by $\sigma_{k,2}$ relocates all the poles of $C_{aw}(z)$ to $z = 0$, which can be done using the pole placement procedure, thus obtaining the gains vector K. However, the internal stability of the system must be verified.

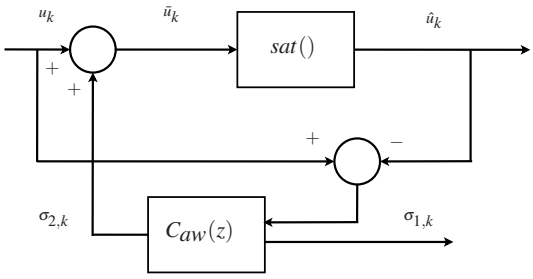

Fig. 5.14 The connection between the AW compensator $C_{aw}(z)$ and the saturation block.

5.4.5 Stability

Remark 5.5. The closed loop stability of the system in Figure 5.11 is established by the design of the RC and additionally by the internal stability of the system in Figure 5.12.

Moreover, from the facts that: 1) we are assuming an asymptotically stable plant and 2) from input u_k to output η_k the system in Figure 5.12 can be seen as a LTI one with the dynamics of the plant, we have that the internal stability of this system can be established analysing only the stability of the interconnection between the saturation block and $C_{aw}(z)$ (see Figure 5.14).

Proposition 5.6. *Given an open loop stable AW compensator $C_{aw}(z)$, as defined in (5.25), the closed loop system in Figure 5.14 is $\mathscr{L}_2$ stable from input u_k to the state χ_k of $C_{aw}(z)$ if there exist $P = P^T > 0$ and $W = W^T > 0$ such that:*

$$\begin{bmatrix} A^T PA - P & -A^T PB + K^T W \\ -B^T PA + WK & -2W + B^T PB \end{bmatrix} < 0. \tag{5.29}$$

Proof. In a first step, it can be easily shown that the function $sat()$ satisfies the following inequality:

$$\Psi = 2(\bar{u}_k - sat(\bar{u}_k))W(sat(\bar{u}_k)) \geq 0, \tag{5.30}$$

with W obtained from (5.29). Noticing that $\bar{u}_k = u_k + K\chi_k$, equation (5.30) can be rewritten as:

$$\Psi = \bar{\Psi} + \tilde{\Psi},$$

where

$$\bar{\Psi} = sat(\bar{u}_k)WK\chi_k + \chi_k^T K^T W sat(\bar{u}_k) - 2sat(\bar{u}_k)W sat(\bar{u}_k)$$

and

$$\tilde{\Psi} = 2u_k W sat(\bar{u}_k).$$

In a second step, based on equation (5.25) and system interconnection in Figure 5.14 we propose the candidate Lyapunov function $V(\chi_k) = \chi_k^T P\chi_k$, where P is obtained from (5.29). Thus we find that:

$$\Delta V = V(\chi_{k+1}) - V(\chi_k) = (A\chi_k + Bu_k - Bsat(\bar{u}_k))^T P(A\chi_k + Bu_k - Bsat(\bar{u}_k)) - \chi_k^T P\chi_k,$$

which can be expressed as:

$$\Delta V = \Delta\bar{V} + \Delta\tilde{V},$$

where

$$\begin{aligned}\Delta\bar{V} = {} & \chi_k^T (A^T PA - P)\chi_k - sat(\bar{u}_k)B^T PA\chi_k - \chi_k^T A^T PBsat(\bar{u}_k) \\ & + sat(\bar{u}_k)B^T PBsat(\bar{u}_k)\end{aligned}$$

and

$$\begin{aligned}\Delta\tilde{V} = {} & u_k B^T PA\chi_k + \chi_k^T A^T PBu_k \\ & - u_k^T B^T PBsat(\bar{u}_k) - sat(\bar{u}_k)B^T PBu_k + u_k^T B^T PBu_k.\end{aligned}$$

Thus, based on (5.30), $V(\chi_{k+1}) - V(\chi_k)$ satisfies the following inequality:

$$\Delta V \leq \Delta\bar{V} + \Delta\tilde{V} + \bar{\Psi} + \tilde{\Psi}.$$

It can be easily seen that (5.29) corresponds to:

$$\Delta\bar{V} + \bar{\Psi} < 0.$$

Since this is a strict inequality then there is a small enough scalar $\varepsilon > 0$ such that

$$\Delta\bar{V} + \bar{\Psi} \leq -\varepsilon \left(\chi_k^T \chi_k + sat(\bar{u}_k)^2\right).$$

Therefore, it results that

$$\Delta V + \varepsilon \left(\chi_k^T \chi_k + sat(\bar{u}_k)^2\right) - \Delta\tilde{V} - \tilde{\Psi} \leq 0$$

Then, using completion of squares, we obtain:

$$\begin{aligned}\Delta V + \frac{\varepsilon}{2}\chi_k^T \chi_k + \frac{\varepsilon}{2}\left(\chi_k - \frac{2}{\varepsilon}A^T PBu_k\right)^T \left(\chi_k - \frac{2}{\varepsilon}A^T PBu_k\right) - u_k^T Q_1 u_k \\ + \varepsilon\left(sat(\bar{u}_k) + \frac{1}{\varepsilon}\left(B^T PB - W\right)u_k\right)^2 - u_k^T Q_2 u_k - u_k^T B^T PBu_k \leq 0,\end{aligned}$$

with $Q_1 = \frac{2}{\varepsilon}B^T PAA^T PB$ and $Q_2 = \frac{1}{\varepsilon}\left(B^T PB - W\right)^2$. With this, the following holds

$$\Delta V + \frac{\varepsilon}{2}\chi_k^T \chi_k - u_k^T Q_T u_k \leq 0,$$

with $Q_T = \frac{2}{\varepsilon}B^T PAA^T PB + \frac{1}{\varepsilon}\left(B^T PB - W\right)^2 + B^T PB$. Therefore, there exists sufficiently large $\gamma > 0$ such that:

$$\Delta V + \frac{\varepsilon}{2}\chi_k^T \chi_k \leq \gamma u_k^T u_k,$$

Summing both sides of previous equation from 0 to ∞ we have

$$(V(\chi_\infty) - V(\chi_0)) + \frac{\varepsilon}{2}\sum_{k=0}^{\infty}\chi_k^T \chi_k \leq \gamma\sum_{k=0}^{\infty}u_k^T u_k$$

then, assuming that the candidate Lyapunov function $V(\chi_\infty) = 0$ we have

$$\frac{\varepsilon}{2}\sum_{k=0}^{\infty}\chi_k^T\chi_k \leq \gamma\sum_{k=0}^{\infty}u_k^T u_k + \chi_0^T P\chi_0$$

from this $\mathscr{L}_2$ stability from u_k to χ_k follows. □

Inequality (5.30) is referred in the literature as the sector condition (see [12]). Thus, the memoryless function $sat()$ is said to belong to the sector $[0,1]$ since $sat(t,u)\,[u - sat(t,u)] \geq 0$.

Finally, it is important to note that (5.29) is a nonlinear inequality, therefore to make it linearly solvable we can apply the Schur−complement and a congruence transformation [9]. Thus, (5.29) can be expanded as:

$$\begin{bmatrix} -P & K^TW \\ WK & -2W \end{bmatrix} - \begin{bmatrix} A^T \\ -B^T \end{bmatrix}[-P]\,[\,A \;\; -B\,] < 0,$$

then, applying the Schur−complement we obtain

$$\begin{bmatrix} -P^{-1} & A & -B \\ A^T & -P & K^TW \\ -B^T & WK & -2W \end{bmatrix} < 0.$$

We can perform the following congruence transformation

$$\begin{bmatrix} I & 0 & 0 \\ 0 & P^{-1} & 0 \\ 0 & 0 & W^{-1} \end{bmatrix}\begin{bmatrix} -P^{-1} & A & -B \\ A^T & -P & K^TW \\ -B^T & WK & -2W \end{bmatrix}\begin{bmatrix} I & 0 & 0 \\ 0 & P^{-1} & 0 \\ 0 & 0 & W^{-1} \end{bmatrix} < 0,$$

resulting

$$\begin{bmatrix} -P^{-1} & AP^{-1} & -BW^{-1} \\ P^{-1}A^T & -P^{-1} & -P^{-1}K^T \\ -W^{-1}B^T & KP^{-1} & -2W^{-1} \end{bmatrix} < 0,$$

then, using $Q = P^{-1}$, $U = W^{-1}$, $X_1 = KQ$ the following LMI is obtained

$$\begin{bmatrix} -Q & AQ & -BU \\ QA^T & -Q & X_1^T \\ -UB^T & X_1 & -2U \end{bmatrix} < 0. \tag{5.31}$$

Hence, if LMI (5.31) is feasible with $Q = Q^T > 0$ and $U = U^T > 0$ we can stablish the system stability for the previously designed deadbeat gain K.

5.4.6 Optimal design

In the previous design a deadbeat feedback gain K is synthesized using for example a pole placement strategy, nevertheless it was shown that after that procedure it is needed to check for the system internal stability. In this section, following a different idea, we propose a design which looks for obtaining the deadbeat behaviour explained previously and at the same time assures global asymptotic stability. In this way we propose to put together condition (5.31) with an optimal LQ design in LMI form.

Remark 5.6. In this case the LQ design is used to find the deadbeat gain K which is shown to be optimal when the weight matrix $Q_p = T^T T$, T being the linear transformation of the system (5.25) into the controllable canonical form (see [14]).

Other results related with the deadbeat design as an optimal LQ solution can be found in [21]. Thus, the problem formulation is to find K such that the stability of the interconnection between $C_{aw}(z)$, equations (5.25) and (5.26), and the saturation block is preserved and additionally, solve the constrained LQ problem:

$$\min_K \sum_{k=0}^{\infty} \chi_k^T Q_p \chi_k$$

subject to:

$$\begin{aligned} \chi_{k+1} &= A\chi_k - B\sigma_{2,k} \\ \sigma_{2,k} &= K\chi_k, \end{aligned}$$

The complete problem can be formulated as an LMI minimization problem:

$\min \gamma$

s.t.

$$\begin{bmatrix} -Q & AQ & -BU \\ QA^T & -Q & X_1^T \\ -UB^T & X_1 & -2U \end{bmatrix} < 0,$$

$$\begin{bmatrix} \gamma I & I \\ I & -Q \end{bmatrix} > 0,$$

$$\begin{bmatrix} -Q & QA^T - X_1^T B^T & QQ_p \\ AQ - BX_1 & -Q & 0 \\ Q_p Q & 0 & -Q_p \end{bmatrix} < 0,$$

where $Q = Q^T > 0$, $U = U^T > 0$, $\gamma > 0$ and $X_1 = KQ$. It is worth to note that the first LMI corresponds to the stability condition (5.31) and the later two LMIs are the optimal LQ design in LMI form (see appendix C for derivation of this LMI).

Also, it is worth saying that there exists some conservativeness in the sector condition Ψ which is applied to non-linearities belonging to the sector $[0, 1]$. In general, this fact may yield a gain K that is an approximation to the deadbeat solution.

5.5 Conclusions

As the main contribution, this Chapter propounds an odd-harmonic high order repetitive controller. It has been shown that this controller provides robust performance in case of signals with uncertain or varying frequency. As a consequence, the proposed controller allows the system to operate in a wider frequency range without reducing its performance and without the need of a frequency observer or adaptive mechanisms. A comparison with an odd-harmonic repetitive controller reveals a better efficiency of the proposed controller working under varying frequency conditions. The stability of the internal models used in HORC has been analysed and a stable second order internal model for repetitive controllers has been proposed and studied. Additionally, the implementation complexity turns out to be the same when com-

paring the order and computational cost of the standard (full-harmonic) repetitive controller and the second order odd-harmonic repetitive controller proposed here. Finally in the last Section, the Model Recovery Anti-Windup scheme is studied and adapted to the Repetitive Control case. An optimal LQ design has been proposed aimed at finding a deadbeat recover behaviour and assuring the global asymptotic stability of the closed loop system. The future research includes the inclusion of less-restrictive sector conditions for the nonlinear saturation function in order to better approximate the deadbeat design.

References

1. W. S. Chang, I. H. Suh, and T. W. Kim. Analysis and design of two types of digital repetitive control systems. *Automatica*, 31(5):741–746, 1995.
2. J. G. da Silva, Jr., and S. Tarbouriech. Antiwindup design with guaranteed regions of stability: an LMI-based approach. *IEEE Transactions on Automatic Control*, 50(1):106 – 111, jan. 2005.
3. F. F. di Bruno. Note sur une nouvelle formule de calcul differentiel. *The Quarterly Journal of Pure and Applied Mathematics*, 1:359360, 1857.
4. J. Flores, J. Gomes da Silva, L. Pereira, and D. Sbarbaro. Robust repetitive control with saturating actuators: a lmi approach. In *Proceedings of the American Control Conference (ACC), 2010*, pages 4259 –4264, 302010-july2 2010.
5. S. Galeani, S. Tarbouriech, M. Turner, and L. Zaccarian. A tutorial on modern anti-windup design. *European Journal of Control*, 15:418 440, 2009.
6. S. Galeani, A. R. Teel, and L. Zaccarian. Constructive nonlinear anti-windup design for exponentially unstable linear plants. *Systems & Control Letters*, 56(5):357 – 365, 2007.
7. G. Grimm, A. R. Teel, and L. Zaccarian. The l2 anti-windup problem for discrete-time linear systems: Definition and solutions. *Systems & Control Letters*, 57(4):356 – 364, 2008.
8. R. Griñó and R. Costa-Castelló. Digital repetitive plug-in controller for odd-harmonic periodic references and disturbances. *Automatica*, 41(1):153–157, January 2005.
9. G. Herrmann, M. Turner, and I. Postlethwaite. Linear matrix inequalities in control. In M. Turner and D. Bates, editors, *Mathematical Methods for Robust and Nonlinear Control*, volume 367 of *Lecture Notes in Control and Information Sciences*, pages 123–142. Springer Berlin / Heidelberg, 2007.
10. P. Hippe. *Windup in Control: Its Effects and Their Prevention*. Advances in Industrial Control. Springer, 2010.
11. T. Inoue. Practical repetitive control system design. In *Proceedings of the 29th IEEE Conference on Decision and Control*, pages 1673–1678, 1990.
12. H. K. Khalil. *Nonlinear Systems*. Prentice Hall, Upper Saddle River, New Jersey, 3. edition edition, 2002.
13. V. Kucera. *Analysis and Design of Discrete Linear Control Systems*. Prentice Hall, 1991.
14. V. Kucera. Deadbeat response is l2 optimal. In *Proceedings of the 3rd International Symposium on Communications, Control and Signal Processing, 2008. ISCCSP 2008.*, pages 154 –157, 2008.
15. G. Pipeleers, B. Demeulenaere, and S. Sewers. Robust high order repetitive control: Optimal performance trade offs. *Automatica*, 44:2628–2634, 2008.
16. Y. S. Ryu and R. Longman. Use of anti-reset windup in integral control based learning and repetitive control. In *Proceedings of the IEEE International Conference on Systems, Man, and Cybernetics, 1994. 'Humans, Information and Technology'*, volume 3, pages 2617 –2622 vol. 3, oct 1994.
17. D. Sbarbaro, M. Tomizuka, and B. L. de la Barra. Repetitive control system under actuator saturation and windup prevention. *Journal of Dynamic Systems, Measurement, and Control*, 131(4):044505, 2009.
18. M. Seron, G. C. Goodwin, and J. Braslavsky. *Fundamental limitations in filtering and control*. Springer, London; New York, 1997.
19. M. Steinbuch. Repetitive control for systems with uncertain period-time. *Automatica*, 38(12):2103–2109, 2002.

20. M. Steinbuch, S. Weiland, and T. Singh. Design of noise and period-time robust high order repetitive control, with application to optical storage. *Automatica*, 43:2086–2095, 2007.
21. K. Sugimoto, A. Inoue, and S. Masuda. A direct computation of state deadbeat feedback gains. *IEEE Transactions on Automatic Control*, 38(8):1283 –1284, Aug. 1993.
22. S. Tarbouriech and M. Turner. Anti-windup design: an overview of some recent advances and open problems. *Control Theory Applications, IET*, 3(1):1 –19, january 2009.
23. J. W. Yeol, R. W. Longman, and Y. S. Ryu. On the settling time in repetitive control systems. In *Proceedings of 17th International Federation of Automatic Control (IFAC) World Congress*, July 2008.
24. L. Zaccarian and A. R. Teel. A common framework for anti-windup, bumpless transfer and reliable designs. *Automatica*, 38(10):1735 – 1744, 2002.
25. A. Zheng, M. V. Kothare, and M. Morari. Anti-windup design for internal model control. *International Journal of Control*, 60:1015–1024, 1993.

Part III
Experimental validation

Chapter 6
Roto-magnet

6.1 Introduction

Systems with rotary elements are usually affected by periodic disturbances due to the movement of these parts (e.g. electrical machines, CD players). This kind of system is supposed to be moving, in some cases, at a fixed angular speed. Under these operating conditions any friction, unbalance or asymmetry appearing on the system generates a periodic disturbance that affects its dynamical behaviour. In this context, repetitive control has been shown to be one of the most effective control strategies used in these applications. Different test beds can be found in the literature which may be used to emulate pulsating periodic load or disturbance torques aimed at reproducing some particular real applications [5, 11]. In this chapter, an experimental didactic plant intended for the educational purpose of analysing and understanding the nature of the periodic disturbances as well as studying the different control techniques used to tackle this problem has been adopted as experimental test bench for rotational machines. Thus, the Roto-magnet" plant has been successfully used as a laboratory control plant for educational purposes [2]. In Appendix D, the use of the Roto-magnet plant in the context of an educational remote laboratory is presented.

The main goal of this chapter is to experimentally validate the proposals presented in previous chapters regarding RC working under time varying frequency conditions. In practice, varying period disturbances can be found in applications where the rotational speed may vary with time [3, 6]. Thus, aimed at providing varying frequency disturbances different reference profiles involving speed variations are employed.

The chapter is organized as follows, Section 6.2 presents the Roto-magnet plant, its concept, components and dynamic model, Section 6.3 describes the design of the standard RC for this plant. In Section 6.4 some implementation issues and two stability analysis for the RC working under varying sampling period are included. Section 6.5 and 6.6 are devoted to the implementation of the Robust design method and the adaptive pre-compensation strategy, respectively. Finally, the optimal AW strategy is experimentally validated for HORC in Section 6.7.

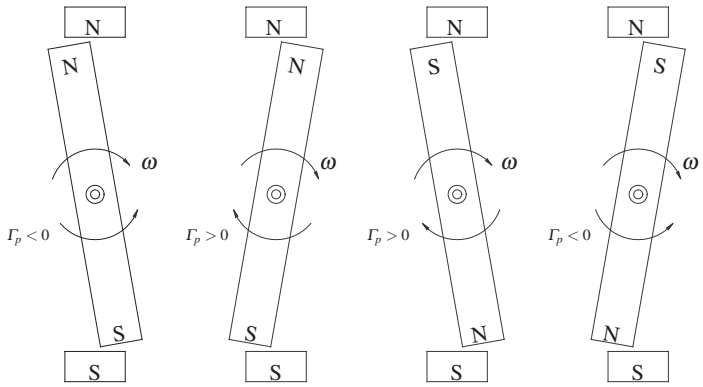

Fig. 6.1 Mechanical load: fixed and moving permanent magnets sketch (ω and Γ_p stand for the angular speed and the disturbance torque, respectively).

Fig. 6.2 Picture of the main part of the Roto-magnet plant: DC motor, optical encoder, magnetic system (load), and supporting structure.

6.2 Plant description

With the objective to perform an experimental validation of the techniques presented in the previous chapters, a device intended to reproduce the working conditions described above has been designed [2]. A picture of that device can be seen in Figure 6.2. It is composed of a bar holding a permanent magnet in each end, with each magnet magnetically oriented in the opposite way, and attached to a DC motor and two fixed electromagnets (see a sketch in Figure 6.1). The rotation of the DC motor causes a pulsating load torque (Γ_p) that depends on the mechanical angle θ of the motor axis. When the motor axis angular speed $\omega = \dot{\theta}$ is constant, i.e. $\dot{\omega} = 0$, the pulsating torque is a periodic signal with a fundamental period directly related to the axis speed: $T_p = \omega^{-1}$, with ω expressed in rev/s. The control goal for this plant is keeping the motor axis angular speed constant at a desired value.

The plant system consists of the DC motor arranged with a power driver in current control loop configuration. Due to the high gain in open loop of this configuration the identification procedure is carried out in closed-loop using a proportional gain controller [7]. In the present case a proportional gain equal to 1 was used. Thus, Figure 6.3 shows the closed-loop time response of the system without the electromagnets under a square input signal. The model used to approximate this closed-loop scheme is as follows:

$$G_{os}(s) = \frac{0.9417}{0.02665s+1}\frac{\text{rev/s}}{\text{V}}.$$

In this way the plant model can be inferred based on the knowledge of the controller [9]. The following plant model has been derived:

$$G_p(s) = \frac{K}{\tau s+1} = \frac{16.152}{0.457s+1}\frac{\text{rev/s}}{\text{V}}. \tag{6.1}$$

This is a first order parametrization with characteristic time response $\tau = 0.457$ s and stationary state gain $K = 16.152$ rev$/(\text{V}\cdot\text{s})$.

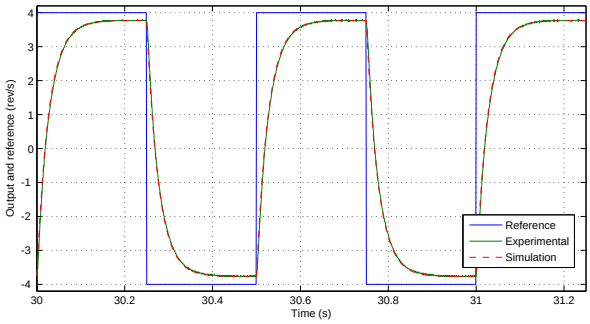

Fig. 6.3 Closed-loop time response of the system without the electromagnets.

6.3 Standard repetitive controller

The controller is constructed from (6.1), for a nominal speed of $\omega = 4$ rev$/$s and obtaining 250 samples per period, i.e. $N = 250$. These conditions imply a nominal sampling period of $\bar{T} = T_p/N = 1/(\omega N) = 1$ ms. Under these assumptions the nominal discrete time plant is:

$$G_p(z) = G_p(z,\bar{T}) = \frac{K(1-e^{-\bar{T}/\tau})}{z-e^{-\bar{T}/\tau}} = \frac{0.0353}{z-0.9978}. \tag{6.2}$$

The standard full-harmonic internal model will be used:

$$I_{st}(z) = \frac{H(z)}{z^N - H(z)}. \tag{6.3}$$

According to Proposition 2.1 and Remark 2.1, the following design issues have been taken into account:

- $G_c(z) = (1.8z - 1.796)/(z-1)$ provides a very robust inner loop.
- The first order null-phase FIR filter $H(z) = 0.25z + 0.5 + 0.25z^{-1}$ provides good performance in the present case.
- The fact that $G_p(z)$ is minimum-phase allows $G_x(z) = k_r G_o^{-1}(z)$, with $k_r = 0.7$.

These settings yield the control law:

$$\begin{aligned} u_k = {} & 1.8e_k - 3.592e_{k-1} + 1.792e_{k-2} + 4.958e_{k-248} - 5.071e_{k-249} \\ & -9.916e_{k-250} + 10.14e_{k-251} + 4.958e_{k-252} - 5.07e_{k-253} \\ & +1.998u_{k-1} - 0.9978u_{k-2} + 0.25u_{k-249} + 0.0005556u_{k-250} \\ & -0.4994u_{k-251} - 0.0005556u_{k-252} + 0.2494u_{k-253}, \end{aligned} \tag{6.4}$$

with $e_k = r_k - y_k$, where y_k is the system output (speed) and r_k is the reference.

Also, it is useful to define the open loop function $G_l(z) = (1 + I_{st}(z))G_c(z)G_p(z)$.

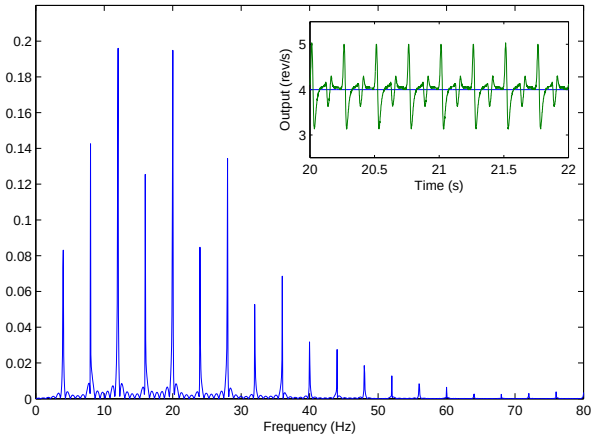

Fig. 6.4 Close loop time response and harmonic content without repetitive controller and with the electromagnets.

Figure 6.4 shows the closed-loop time response and the harmonic content[1] of the plant operating with the electromagnets, the controller $G_c(z)$ and without the repetitive controller, i.e. the steady state response of $G_o(z)$ with the disturbances. It is important to note that the speed describes an almost periodic signal. It can be seen that this type of disturbance may not be rejected by the controller $G_c(z)$.

The next experiment is performed with the repetitive controller. Figure 6.5 and 6.6 show the frequency response of the open loop function $G_l(z)$ and closed loop sensitivity function of the designed repetitive controller. These figures depict the action of the controller at the fundamental and harmonic frequencies. Figure 6.7

[1] Along this chapter the calculation of the harmonic content is carried out eliminating the constant component of the signals.

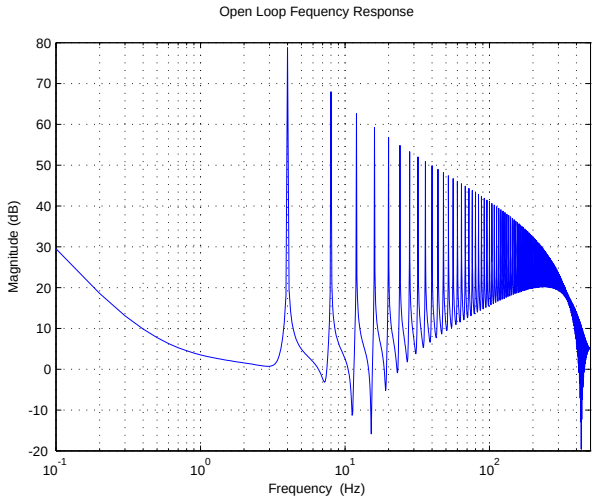

Fig. 6.5 Frequency response of the open-loop function $G_l(z)$.

shows the experimental steady state output response at nominal frequency and its corresponding harmonic content. It can be seen that the system can successfully reject the periodic disturbances. Figure 6.8 depicts the transient response of the system after a step signal is applied as reference. It is shown that the RC reject the disturbances after a small transient.

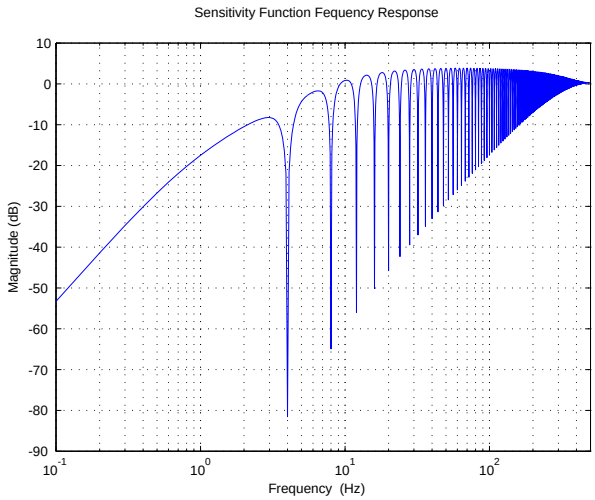

Fig. 6.6 Frequency response of the sensitivity function $S(z)$.

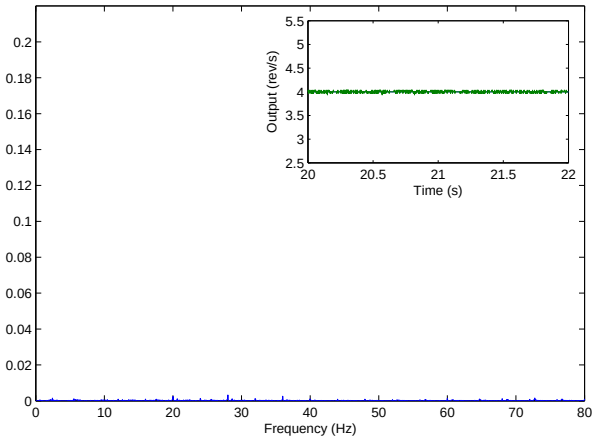

Fig. 6.7 Steady state response and output signal harmonic content of the repetitive control. system.

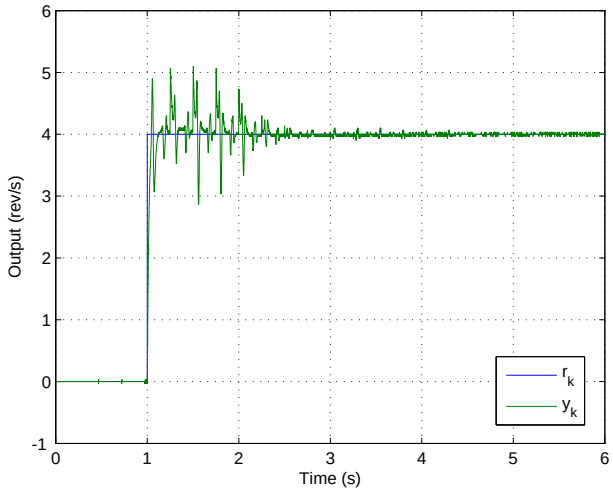

Fig. 6.8 Step response of the designed repetitive control system.

6.4 The varying sampling period strategy

6.4.1 Implementation issues

The first issue to deal with in the implementation of the control action is the measurement of the uncertain or time-varying period T_p of the signal to be tracked or rejected. In the general case an adaptive scheme similar to those in [1, 12, 6] is used for this task; the complete controller architecture is depicted in Figure 3.1. The frequency values, $T_p^{-1}(t)$, are obtained by means of a frequency observer us-

ing information from different sources, namely, reference profile, output signal and control action. Then, the sampling rate is calculated as

$$T_s = \frac{T_p}{N}. \tag{6.5}$$

Nevertheless, as it has been previously stated, in mechanical turning systems the frequency to be tracked/rejected is directly related to the turning speed. Hence, for the analysed mechatronic plant the disturbance frequency is straightforward computed from the turning speed reference. This allows us to study the effect of the adaptive approach on the closed-loop system decoupled from the frequency observer dynamics.

For the general case, the study of the effect of the frequency observer dynamics on the global system stability is out of the scope of this work. However, it is also worth recalling that any fault in the estimation and/or implementation of T_s causes a difference between the experimental ratio T_p/T_s and the implemented value for N which, in turn, may yield a performance degradation. As an example, Figure 6.9 shows the first harmonic gain factor evolution of the internal model against a relative deviation of the sampling period T_s with respect to the nominal $\bar{T} = 1$ *ms*, namely

$$\frac{\left|I_{st}\left(\exp\left[j\frac{2\pi}{N(1+Q(T_s))\bar{T}}\bar{T}\right]\right)\right|}{\left|I_{st}\left(\exp\left[j\frac{2\pi}{N\bar{T}}\bar{T}\right]\right)\right|} = \frac{\left|I_{st}\left(e^{\frac{2\pi j}{N(1+Q(T_s))}}\right)\right|}{\left|I_{st}\left(e^{\frac{2\pi j}{N}}\right)\right|},$$

where $I_{st}(\cdot)$ is defined in (6.3) and

$$Q(T_s) = \frac{T_s - \bar{T}}{\bar{T}}.$$

Notice that even small deviations of T_s entail important gain reductions. However, as stated in Remark 3.2.iv, closed-loop stability is not threatened unless $T_s \notin \mathscr{T}$.

Finally, and also in accordance with Remark 3.2.iv, the frequency observer output has to be saturated so as to guarantee that $T_s \in \mathscr{T}$.

6.4.1.1 Quantification error effect

It is well known that in a real setup T_s cannot be fixed with infinite precision but within the limitations imposed by the timer quantification. In the following, it will be shown that even small quantification errors entail important gain reductions.

The proposed implementation uses a digital counter as a time source, which offers a resolution of 1.6 μs. For a nominal sampling time of $\bar{T} = 1$ ms this implies a relative error of $1.6 \cdot 10^{-3}$, that may yield a gain reduction factor of 0.016 in the worst case, i.e. when approximating by truncation. Although the gain reduction is important, the sampling time adaptation scheme allows to maintain the gain of (6.3) above 40 dB, which is good enough for most applications.

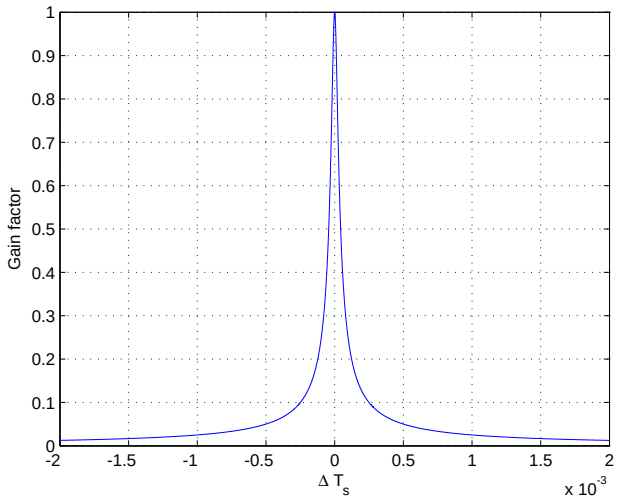

Fig. 6.9 First harmonic gain factor evolution at harmonic frequencies.

6.4.2 LMI gridding approach

This Section is devoted to the stability analysis of the repetitive controller that employs the sampling adaptation mechanism in order to preserve the performance under varying frequency conditions.

The stability analysis of RC working with varying sampling period using the LMI gridding approach has been described in Section 3.3. It is important to recall that, as mentioned in Remark 3.2, the high order involving the internal model of the RC imposes a restriction in the applicability of the LMI approach. In this way, with the order of the controller obtained in the previous Section the resulting LMI problem is not computationally solvable. For that reason, in this Section a special setup of the RC for the mechatronic plant has been designed. Thus, the new setup is based on a nominal sampling period $\bar{T} = 5$ ms and nominal speed $\omega = 8$ rev/s which results in $N = 25$. This value of N is now appropriate to carry out the analysis. Also the following has been set:

- $G_p(z) = G_p(z, \bar{T}) = (0.1757)/(z - 0.9891)$.
- $G_c(z) = (1.8z - 1.78)/(z - 1)$.
- $H(z) = 0.02z + 0.96 + 0.02z^{-1}$.
- $G_x(z) = k_r G_o^{-1}(z)$, with $k_r = 0.7$.

Although the controller is designed to regulate the speed at 8 rev/s, in practice it will be necessary to move from this design point. Let us assume that we are interested in varying the speed reference in the interval $[6, 13]$ rev/s: this entails a sampling period variation in the interval $\mathscr{T} = [3.077, 6.667]$ ms.

To start the analysis procedure it is needed to write the closed-loop system in the form presented in Section 3.2, namely equation (3.2). We need especially to find matrix $\Phi(T_k)$ to derive the subsequent LMI problem.

The stability analysis that stems from Proposition 3.3 includes the solution of the LMI (3.6), which is known to be feasible, and the checking of the negative-definite

character of $L_{T_k}(P_N)$. Figure 6.10 shows the evolution of the maximum eigenvalue of $L_{T_k}(P_N)$ when solving for $\alpha = 100$, and also for 50000 uniformly distributed values of T_k. Therefore, it can be presumed that the closed-loop system may operate in a speed range of $[7.32, 8.94]$ rev/s with dynamically preserved stability. This speed interval is obviously very narrow and operation conditions are limited to a sampling period interval $\mathscr{I}_N$ such that $\mathscr{T} \not\subseteq \mathscr{I}_N$. Once at this point, it is important to recall that this test comes not from a necessary condition but from a sufficient condition, so moving out of this interval does not necessarily imply instability[2].

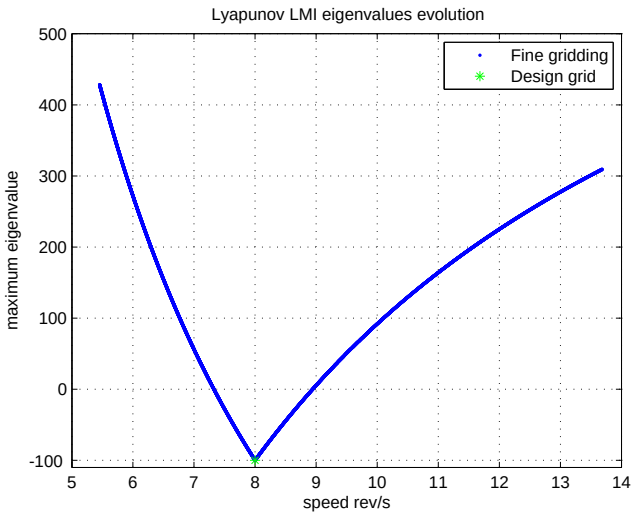

Fig. 6.10 Maximum eigenvalue of $L_{T_k}(P_N)$ with $\alpha = 4645$ and $\bar{T} = 0.005$s.

In order to guarantee a broader stability interval, the second method described in Section 3.3 may be applied. Therefore, 40 uniformly distributed points are selected in $\mathscr{T} = [0.00307, 0.00667]$ s. These points are used to construct the set of LMIs (3.7), and a feasible solution $P = P_G$ with $\alpha = 100$ is obtained. Figure 6.11 depicts the maximum modulus eigenvalue of $L_{T_k}(P_G)$, detailing with a star the 40 points leading to the LMI formulation. The maximum modulus eigenvalue of $L_{T_k}(P_G)$ corresponding to a finer grid consisting of 55121 uniformly distributed points is also drawn in Figure 6.11. These points are used to check the sign of $L_{T_k}(P_G)$ in the intervals between the points defining the LMI set. It can be seen that $L_{T_k}(P_G) < 0$ for every point in this finer grid of the interval $\mathscr{T}$; hence, stability is dynamically preserved therein. This method extends the previously obtained stability interval $[7.32, 8.94]$ rev/s, thus providing less conservative results. Further extensions of the new interval could also be feasible. It is also worth to say that the finer grid contains the points that correspond to the system clock resolution, therefore the stability of the digital implementation can be guaranteed in the obtained internal.

[2] Although this step can be avoidable in most cases, its results are very useful to tune the LMI solver regarding next step.

However, according to Remark 3.2, this LMI approach does not provide sufficient stability conditions and may entail numerical problems. Hence, the robust control approach results are given in next section.

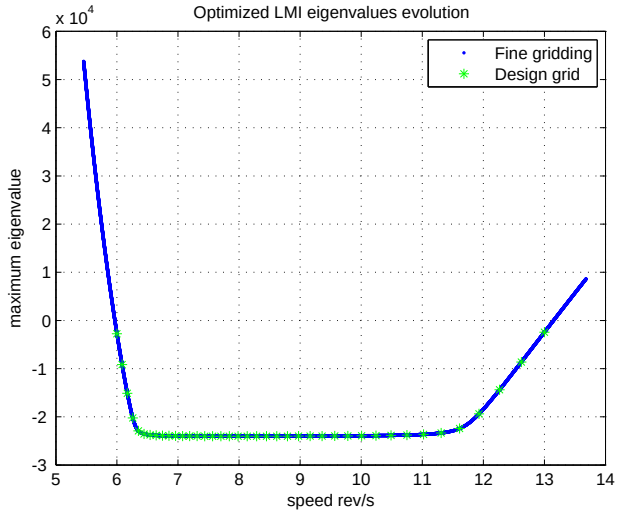

Fig. 6.11 Maximum eigenvalue of $L_{T_k}(P_G)$ with 40 points for the design grid and 55121 points to check stability.

6.4.3 Robust control theory approach

The stability analysis method used in this section is based on robust control theory. The approach was previously described in Section 3.4 and the procedure renders sufficient conditions for the closed-loop stability of the repetitive control system.

Firstly, it is needed to find matrix $\Phi(T_k)$ (equation (3.2)) and its representation in the form of Proposition 3.4 (equation (3.8)), then re-write the system as in the system definition (3.15) and Figure 3.4.

Based on Theorem 3.1, to calculate the sampling period variation interval for which the system preserves the stability it is needed to calculate the H_∞-norm of system $G_{\bar{T}}(z)$.

Following Subsection 3.4, the settings for the plant and the repetitive controller in Section 6.3, i.e. $N = 250$ and $T_s = 1$ ms, yield $\|G_{\bar{T}}(z)\|_\infty = 1302.2$. In order to define $\gamma_{\bar{T}}$ (see (3.16)), $\varepsilon = 0.0001$ has been selected. Furthermore, the plant being first order yields a scalar value for its continuous-time system matrix: $A = -2.1876$; hence, an exact bounding of $\|\Delta(T_k - \bar{T})\|$ is possible. Straightforward calculation [4] shows that (3.17) is fulfilled with (see also Appendix B)

$$\mathscr{T} = \left[\bar{T} + \frac{1}{A}\log\left(1 - \frac{A}{\gamma_{\bar{T}}}\right), \bar{T} + \frac{1}{A}\log\left(1 + \frac{A}{\gamma_{\bar{T}}}\right)\right].$$

The specific numerical values are $\mathscr{T} = [0.2327, 1.7686]$ ms, which indicates that the performance of the device is ensured in the range $\omega \in [2.2617, 17.1906]$ rev/s.

With the settings specially applied for the LMI gridding approach (Section 6.4.2, i.e. $N = 50$ and $T_s = 5$ ms) the following has been found: $\|G_{\bar{T}}(z)\|_\infty = 273.5081$, $\mathscr{T} = [1.3583, 8.6709]$ ms and $\omega \in [4.6131, 29.4476]$ rev/s. These results show that the robust approach yields a wider stability interval compared with the LMI gridding approach.

6.4.4 Experimental results

In order to illustrate the control system stability and performance, two different speed reference profiles have been used in the experimentation. Each profile corresponds with one of the two different settings described in the preceding section. The profile $\omega_{4ref}(t)$ and $\omega_{8ref}(t)$ for the $T_s = 1$ ms and $T_s = 5$ ms setup respectively:

$$\omega_{4ref}(t) = \begin{cases} 4 \text{ rev/s} & \text{if } t \in [0,15) \text{ s}, \\ -\frac{7}{32}t + \frac{233}{32} \text{ rev/s} & \text{if } t \in [15,19) \text{ s}, \\ 3.125 \text{ rev/s} & \text{if } t \in [19,28) \text{ s}, \\ \frac{25}{96}t - \frac{25}{6} \text{ rev/s} & \text{if } t \in [28,40) \text{ s}, \\ 6.25 \text{ rev/s} & \text{if } t \geq 45 \text{ s}. \end{cases}$$

$$\omega_{8ref}(t) = \begin{cases} 8 \text{ rev/s} & \text{if } t \in [0,15) \text{ s}, \\ -\frac{7}{16}t + \frac{233}{16} \text{ rev/s} & \text{if } t \in [15,19) \text{ s}, \\ 6.25 \text{ rev/s} & \text{if } t \in [19,28) \text{ s}, \\ \frac{25}{48}t - \frac{25}{3} \text{ rev/s} & \text{if } t \in [28,40) \text{ s}, \\ 12.5 \text{ rev/s} & \text{if } t \geq 45 \text{ s}. \end{cases}$$

During the time interval $[0, 15]$ s, the reference is maintained constant at the nominal value $\bar{\omega}$. At $t = 15$ s a ramp reference change, from $\bar{\omega}$ to $0.7812\bar{\omega}$, is introduced in the system; then, the speed is kept constant for 9 s and finally at $t = 28$ s the speed is gradually augmented at a constant acceleration until it reaches the value $1.5625\bar{\omega}$ at $t = 40$ s.

Additionally, the experiment has been carried out for three different settings of the sampling time: keeping constant the sampling period at nominal value $\bar{T}$, assuming a 2nd order frequency observer for T_p and using an exact estimation of T_p. The following continuous model has been used to simulate the second order dynamics of the observer:

$$G_{obs}(s) = \frac{6.25}{s^2 + 2.5s + 6.25}.$$

This model has been implemented in discrete time according to the selected sampling time.

In Figures 6.12.a and 6.13.a the sampling period is kept constant at the nominal value $\bar{T}$, for all t; it is important to realize that disturbances are almost rejected in $[0, 15]$, that is, when both reference and sampling are at the nominal values. However, for $t > 15$ s disturbances cannot be properly compensated and performance is strongly degraded. Figures 6.12.b and 6.13.b depict the output behavior when the sampling period is varied adaptively assuming that the estimation of T_p uses a 2nd order frequency observer; the profile of the actually used T_s are in Figures 6.14 and 6.15 respectively. Notice that the performance gets worse in the regions where there

is estimation error. Finally, Figures 6.12.c and 6.13.c portray the response under adaptive variation of T_s from an exact estimation of T_p. According to Sections 3 and 6.4.1, stability is preserved in the three situations because T_s always belongs to $\mathscr{T}$. Performance in the steady-state depends on the accuracy of the estimation of T_p, while performance during transients, although not guaranteed by repetitive control theory, follows here the same pattern as that observed for the steady state, i.e. it improves with better estimations of T_p.

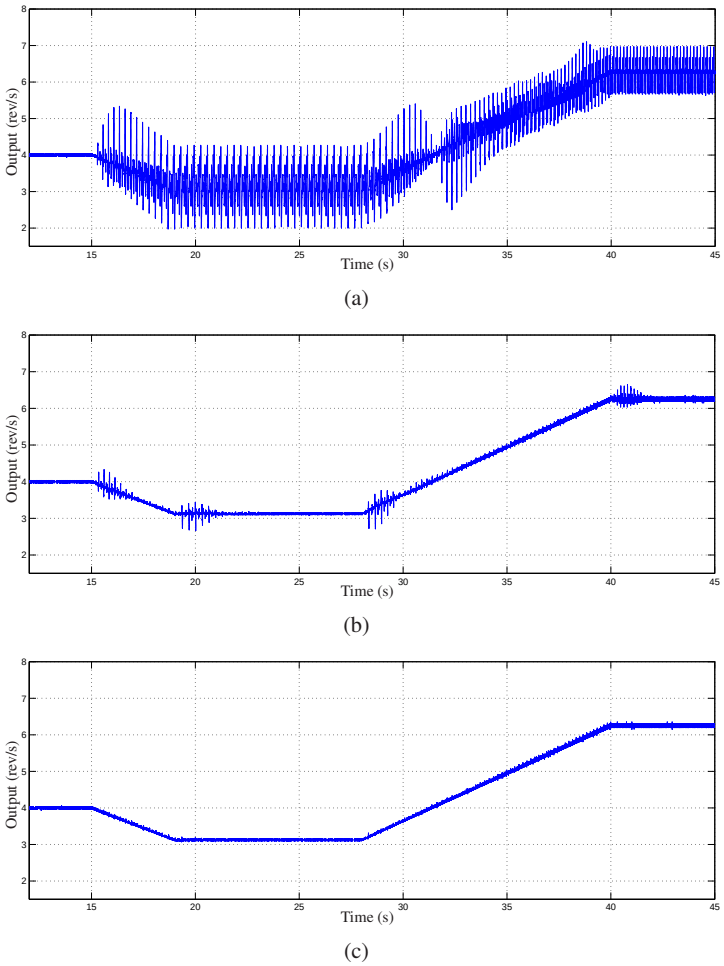

Fig. 6.12 Closed-loop system behavior using a repetitive controller and with sampling period T_s: (a) Fixed at the nominal value ($\bar{T} = 1$ ms); (b) Obtained from a 2nd order frequency observer for T_p; (c) Obtained from an exact estimation of T_p.

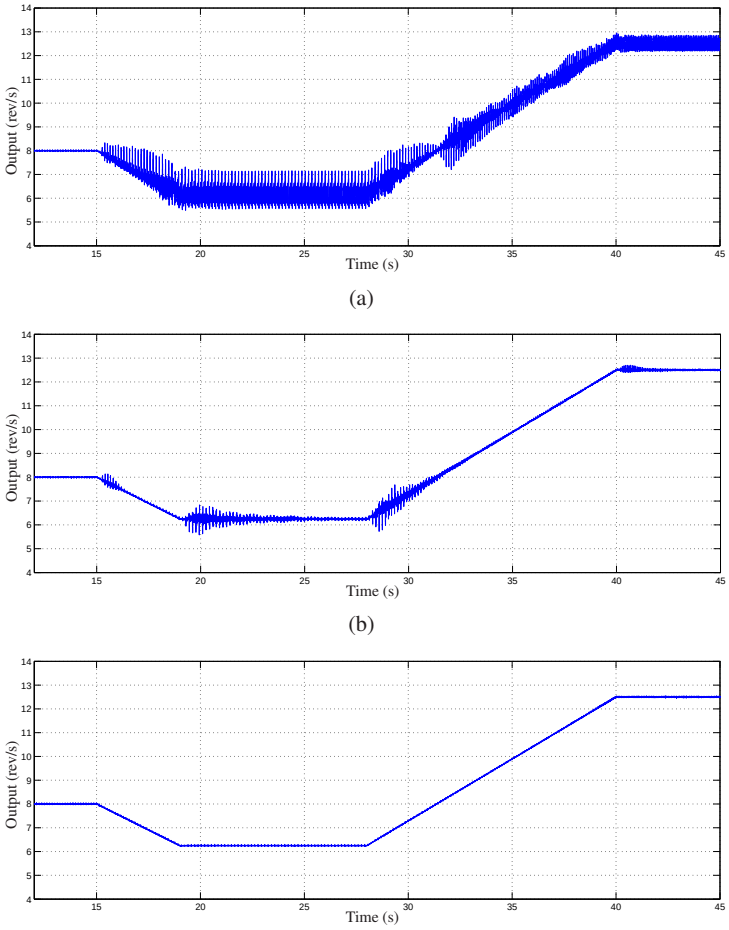

Fig. 6.13 Closed-loop system behavior using a repetitive controller and with sampling period T_s: (a) Fixed at the nominal value ($\bar{T} = 5$ ms); (b) Obtained from a 2nd order frequency observer for T_p; (c) Obtained from an exact estimation of T_p.

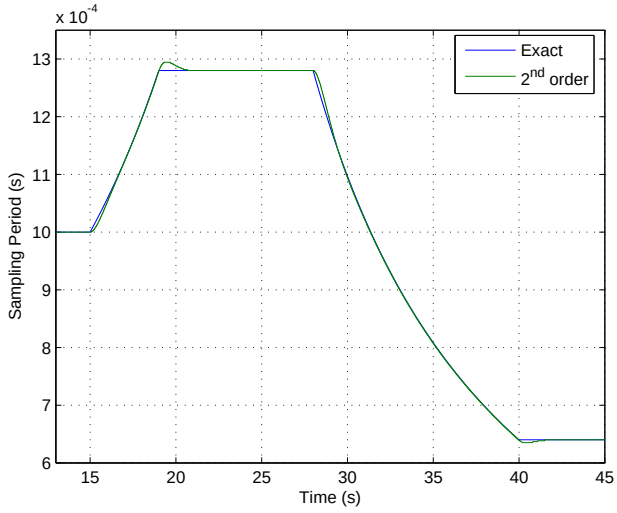

Fig. 6.14 Sampling period T_s corresponding to an exact (blue) and a 2nd order (green) observer for T_p. Design for $\bar{T} = 1$ms.

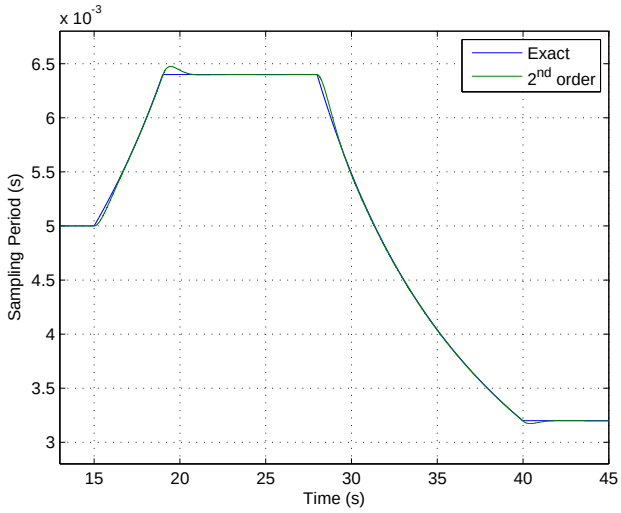

Fig. 6.15 Sampling period T_s corresponding to an exact (blue) and a 2nd order (green) observer for T_p. Design for $\bar{T} = 5$ms

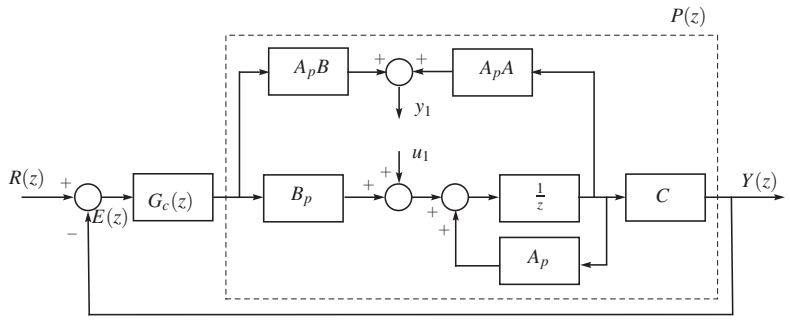

Fig. 6.16 Adaptation of the $G_o(z)$ control loop to the H_∞ formulation.

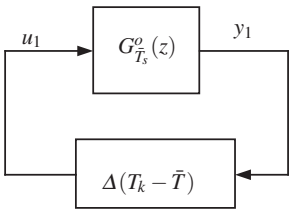

Fig. 6.17 The resulting feedback system with the uncertainty.

6.5 Robust design

The robust design proposal is a repetitive control system design that takes into account the effect of the sampling period variations and yields a controller which assures stability for a given sampling period interval. In order to do that, the variation of the sampling period is rendered into a norm bounded uncertainty. The strategy is described in detail in Section 4.2.

Thus, following Section 4.2, the design may be performed in two stages: first, verify the design of $G_c(z)$ and second, re-design the stabilizing filter $G_x(z)$. To check that the controller $G_c(z)$ provides robust stability for the given sampling period variation interval it is needed to accomplish the following condition (see Figures 6.16 and 6.17):

$$\|G^o_{\bar{T}_s}(z)\|_\infty < (1+\varepsilon)^{-1}\|\Delta\,(T_s-\bar{T})\,\|^{-1}_\infty,$$

which permits to calculate the sampling period interval $\mathscr{T}$ for which the system remains stable. For the experimental validation the design is based on an interval of $\omega \in [2.5, 8]$ rev/s. Thus, for the settings in Section 6.3, the following is obtained: $\|G^o_{\bar{T}}(z)\|_\infty = 1024.95$ and with this, the variation intervals result $\mathscr{T} = [0.0253, 1.9766]$ ms and $\omega \in [2.0235, 157.5851]$ rev/s. This means that with the selected $G_c(z)$ it is possible to perform a design for the speed variation interval of $\omega \in [2.5, 8]$ rev/s.

In the second stage, a μ-synthesis approach is used to take advantage from the problem structure. Figures 4.1 and 4.2 depict the scheme of the problem formulation

and equation (4.2) show the generalized plant needed to set-up the problem. For the interval $T_s \in \mathscr{T} = \left[(2.5N)^{-1}, (8N)^{-1}\right]$, with $N = 250$, the uncertainty due to the sampling time variation can be estimated as: $\Delta_{T_s} \in [5.002, 5.996] \cdot 10^{-4}$. Thus, the procedure seeks a controller that, from the point of view of the delay block, provides a closed loop system with H_∞ norm less than 1. With this information the μ-synthesis can be carried out and the following controller is obtained:

$$\begin{aligned}\tilde{G}_x(z) = {} & (2.908z^{16} - 26.6z^{15} + 104z^{14} - 218.3z^{13} + 236z^{12} - 36.29z^{11} \\ & -254.1z^{10} + 350.6z^9 - 187.7z^8 - 15.82z^7 + 84.18z^6 - 51.93z^5 \\ & +14.7z^4 - 1.683z^3 - 0.0006212z^2 + 2.565 \cdot 10^{-10}z + 9.445 \cdot 10^{-14}) \\ & /(z^{16} - 8.27z^{15} + 28.79z^{14} - 52.55z^{13} + 47.03z^{12} - 1.468z^{11} \\ & -40.55z^{10} + 36.96z^9 - 6.567z^8 - 9.728z^7 + 6.573z^6 - 0.9262z^5 \\ & -0.3955z^4 + 0.1141z^3 + 4.215 \cdot 10^{-15}z^2 + 1.294 \cdot 10^{-11}z + 4.761 \cdot 10^{-15}),\end{aligned}$$

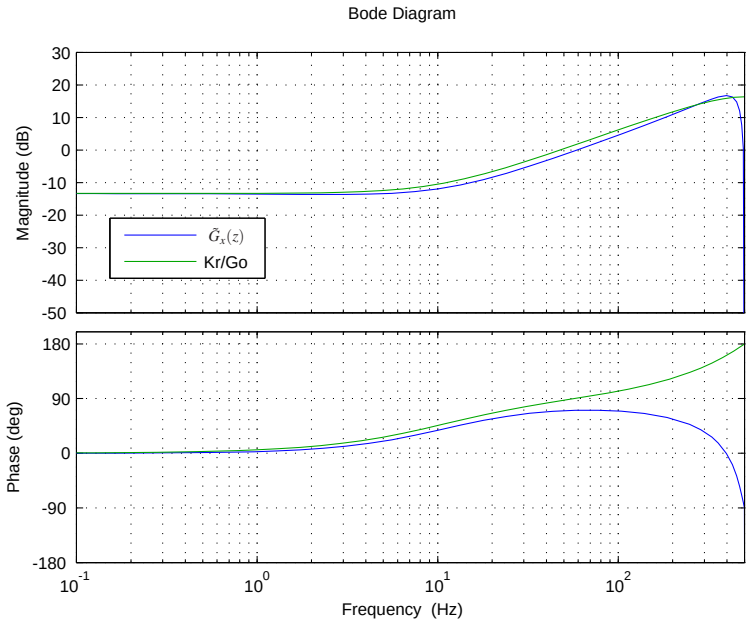

Fig. 6.18 Frequency response comparison between $\tilde{G}_x(z)$ and of the original controller $G_x(z) = k_r G_o^{-1}(z)$, with $k_r = 0.21$.

Remark 6.1. The frequency response of $\tilde{G}_x(z)$ and the original controller $G_x(z) = k_r G_o^{-1}(z)$, with a new value of $k_r = 0.21$, is shown in Figure 6.18. It can be observed that the responses are very similar in the low and medium range. Therefore, for the purpose of keeping low the order of the controller, the structure $G_x(z) = k_r G_o^{-1}(z)$ with $k_r = 0.21$ has been implemented in the experimental setup.

An important difference to be taken into consideration is that the standard design uses a stabilizing filter $G_x = k_r / G_o(z)$ which is a non causal transfer function while

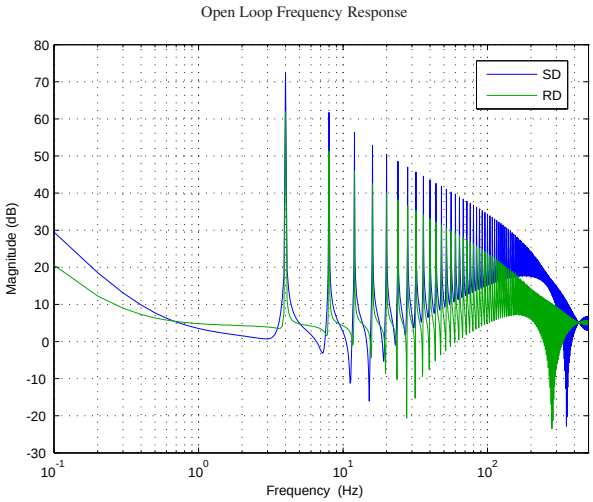

Fig. 6.19 Open loop magnitude response of function $G_l(z)$. Standard design (SD) and robust design (RD) comparison.

the μ-synthesis design seeks a causal filter $\tilde{G}_x(z)$ to obtain a stable system for a given frequency variation interval.

Also it is valuable to note that, based on the Internal Model Principle, the performance in steady state can be preserved if T_n, and in the same way T_s, stays constant for sufficiently large time intervals.

The open loop and sensitivity function frequency response of the RC designed in Section 6.3 and the robust design presented in this section using $\tilde{G}_x(z)$ are compared in Figures 6.19 and 6.20 respectively. It is shown that the tracking/rejection action is lower when using $\tilde{G}_x(z)$ since it corresponds to a smaller gain k_r. Additionally, in the sensitivity function comparison figure, it can be seen that the system using $\tilde{G}_x(z)$ exhibit better behaviour at inter-harmonic frequencies.

6.5.1 Experimental results

Figure 6.21 shows the steady state time response and harmonic content of the RC robust design described in this section. Also, Figure 6.22 shows the system evolution using the speed profile of Section 6.4.4 with $\bar{T} = 5$ ms and $N = 250$, both, speed output and control action are depicted. In these figures can be noticed that a small performance degradation appears due to the use of a smaller gain k_r; however the harmonic rejection is kept at a very acceptable level.

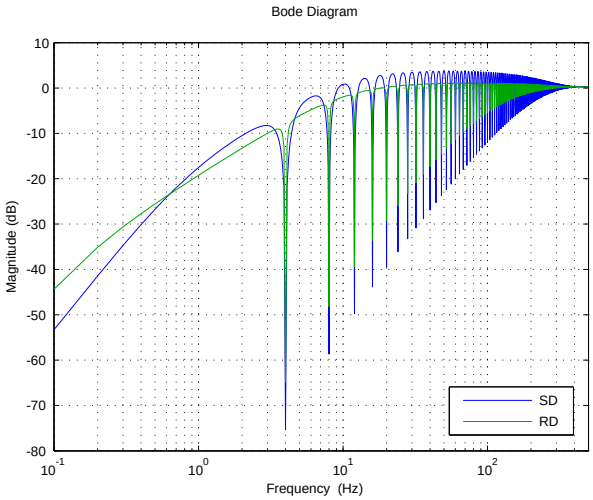

Fig. 6.20 Sensitivity function magnitude response. Standard design (SD) and robust design (RD) comparison.

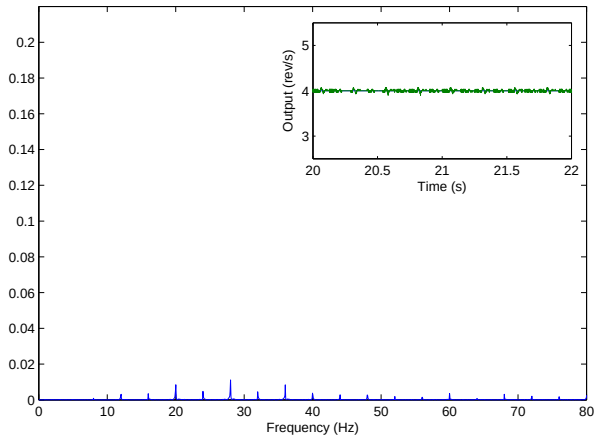

Fig. 6.21 Steady state time response and harmonic content using the RC robust design for nominal speed $\omega = 4$ rev/s.

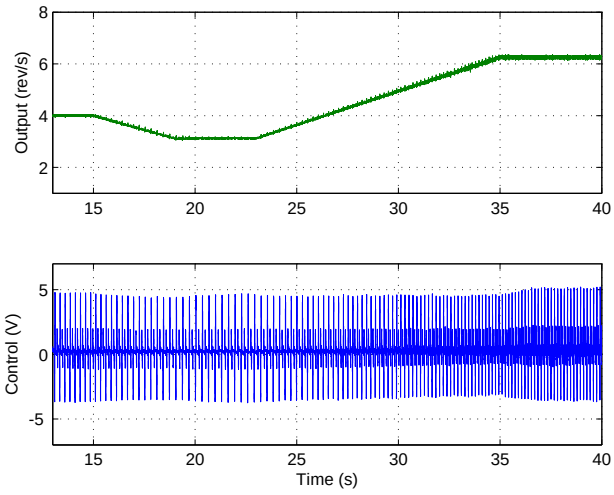

Fig. 6.22 Closed-loop system behaviour using the RC robust design with varying sampling rate T_s obtained from an exact estimation of T_p.

6.6 Adaptive pre-compensation

6.6.1 Controller design

The aim of adaptive pre-compensation design is to compensate for the structural variation effect encountered when using the sampling period adaptation mechanism. The proposal has been detailed in Section 4.3. According to that section, to force the system to behave as the one designed for the nominal sampling time the following pre-compensator needs to be included (see Figure 4.3):

$$C(z,T_s) = G_p(z,\bar{T})G_p^{-1}(z,T_s),$$

with

$$G_p(z,\bar{T}) \triangleq \frac{Num(z,\bar{T})}{Den(z,\bar{T})} = \mathscr{Z}\left\{G_p(s)\right\}$$

the LTI model of the plant at nominal sampling time, and

$$G_p(z,T_s) = \frac{Num(z,T_s)}{Den(z,T_s)}$$

the plant LTV model, i.e. working at varying sampling period.

For the Roto-magnet plant we have the following:

$$G_p(z,\bar{T}) = \frac{Num(z,\bar{T})}{Den(z,\bar{T})} = \frac{0.0353}{z-0.9978} \tag{6.6}$$

and

$$G_p(z,T_s) = \frac{Num(z,T_s)}{Den(z,T_s)} = \frac{K(1-e^{-T_s/\tau})}{z-e^{-T_s/\tau}}, \tag{6.7}$$

with K and τ set as in (6.1). Model (6.7) is first order, stable and minimum phase; hence, its inversion is possible and one can define:

$$\frac{Den(z,T_s)}{Num(z,T_s)} = \frac{z-e^{-T_s/\tau}}{K(1-e^{-T_s/\tau})}. \tag{6.8}$$

Therefore, (6.6) and (6.8) yield

$$C(z,T_s) = \frac{0.0353\left(z-e^{-T_s/\tau}\right)}{K(1-e^{-T_s/\tau})(z-0.9978)}, \tag{6.9}$$

which is a time-varying model that depends on the sampling period T_s and this, in turn, depends on the disturbance period variation T_p.

It is important to emphasize that, in this case, the function $P(z)$ introduced in (4.6) is composed of the series connection of:

1. The system $C(z,T_s)$ described in (6.9), which admits a LTV state-space representation $(A_c(k),B_c(k),C_c(k),D_c(k))$ with $A_c(k) = 0.9978$, $B_c(k) = 1$,

$$C_c(k) = \frac{0.0353(0.9978-e^{-T_k/\tau})}{K(1-e^{-T_k/\tau})},$$

$$D_c(k) = \frac{0.0353}{K(1 - e^{-T_k/\tau})},$$

the sampling period being $T_k = T_s(k) = t_{k+1} - t_k$.
Its internal stability is guaranteed by the fact that the state equation is time-invariant, A_c being a 1×1 real matrix with modulus less than 1, which yields uniform exponential stability [8]. Moreover, as $B_c(k)$ is constant and $C_c(k)$, $D_c(k)$ are bounded for all T_k belonging to any compact interval $\mathscr{T} \subset \mathbb{R}^+$, uniform Bounded-Input Bounded-Output (BIBO) stability is also ensured [8].

2. The system $G_p(z, T_s)$ described in (6.7), which is internally and uniformly BIBO stable because it corresponds to the sampled version of the LTI, continuous-time stable plant, $G_p(s)$.

As the series connection of internally and BIBO stable systems is also internally and BIBO stable, in the case under study $P(z)$ fulfils the hypothesis of Proposition 4.1, so the overall closed-loop system will be stable.

In order to derive the control action applied to the plant, i.e. the signal $\bar{U}(z)$ (see Figure 3.1), it has to be taken into account that the compensator makes the system time-invariant. Therefore, $\bar{u}_k$ is the invariant control law obtained from the nominal repetitive control, that is:

$$\begin{aligned}\bar{u}_k = {} & 1.8e_k - 3.592e_{k-1} + 1.792e_{k-2} + 4.958e_{k-248} - 5.071e_{k-249} \\ & -9.916e_{k-250} + 10.14e_{k-251} + 4.958e_{k-252} - 5.07e_{k-253} \\ & +1.998\bar{u}_{k-1} - 0.9978\bar{u}_{k-2} + 0.25\bar{u}_{k-249} + 0.0005556\bar{u}_{k-250} \\ & -0.4994\bar{u}_{k-251} - 0.0005556\bar{u}_{k-252} + 0.2494\bar{u}_{k-253},\end{aligned}$$

with $e_k = r_k - y_k$, r_k, y_k being, respectively, the system output and the reference velocities.

The derivation of u_k according to Figure 4.4 yields:

$$u_k = \frac{0.0353}{K(T_s)}\bar{u}_k - 0.0353\frac{1 - K(T_s)}{K(T_s)}\bar{u}_{k-1} + 0.9978u_{k-1},$$

with $K(T_s) = 1 - e^{-T_s/\tau}$. It can be easily seen by straightforward calculation than when the sampling interval remains constant at nominal the sampling time, i.e. $T_s = \bar{T}$, then $u_k = \bar{u}_k$.

6.6.2 Experimental results

Figure 6.23 shows the experimental results using the adaptive pre-compensation scheme with varying sampling rate T_s, which is calculated using (6.5). One may observe that the controller can preserve the system performance. The control action, also shown in Figure 6.23, has a periodic behaviour and it can be seen how this period is changing so the controller can reject the varying frequency disturbances.

Additionally, Table 6.1 shows the error comparison for the three proposed designs that work with sampling time adaptation: Standard, which corresponds with the conventional design, Robust, that uses the robust control strategy and Pre-compensation which lies in the pre-compensation technique. The results obtained in Figures 6.12, 6.22 and 6.23 with an exact estimation of T_p were used to calculate

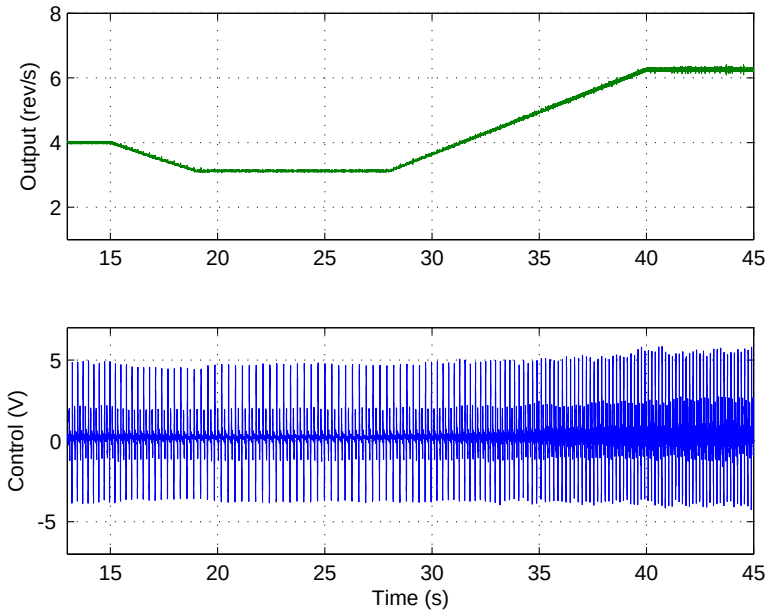

Fig. 6.23 Closed-loop system behaviour using a repetitive controller with adaptive pre-compensation with varying sampling rate T_s obtained from an exact estimation of T_p.

the 2-norm and infinite norm of the resulting error. It can be noticed that the Standard design yields the smaller errors followed by the Pre-compensation strategy and finally the Robust technique.

Error / RC Design	Standard	Robust	Pre-compensation
$\|e_k\|$	11.1996	12.2048	17.2289
$\|e_k\|_\infty$	0.1164	0.1562	0.2088

Table 6.1 Normed error for the three proposed designs with time varying sample time: Standard, Robust and Pre-compensation

6.7 Anti-windup optimal design for HORC

In this section, a HORC is implemented in the Roto-magnet plant. The strategy is intended to provide robust performance against small speed variations which causes that the frequency of the disturbances varies in time. However, as mentioned in Section 5.2, the characteristics of the internal models used in HORC make the systems prone to the wind-up effect when there exists saturation in the control signal. For that reason it is necessary to include an anti-windup compensator in the design. Thus, this section is aimed at experimentally validating the anti-windup strategy described in Section 5.4 using the Roto-magnet plant. Two different tests have been developed, a disturbances rejection example at constant speed using the electromagnets of the plant and a periodic reference tracking example without the effect of the electromagnets.

6.7.1 Experimental setup

The settings are the same used in Section 6.3 but changing the standard internal model by a second order internal model:

$$I_{ho2}(z) = \frac{\left(2z^{-N} - z^{-2N}\right) H(z)}{1 - \left(2z^{-N} - z^{-2N}\right) H(z)}$$

and defining

$$H(z) = 0.003297z^{-3} + 0.05897z^{-2} + 0.2492z^{-1} + 0.377 + 0.2492z + 0.05897z^2 + 0.003297z^3.$$

Figures 6.24 and 6.25 show the open loop and sensitivity function magnitude response obtained with these settings. A comparison with the standard RC design of Section 6.3 has also been included. As it can be seen, the HORC offers a wider action around the harmonics compared with the standard RC. As discussed in previous chapters this effect provides the robustness against frequency variations. Figure 6.25 shows that HORC presents higher gain at inter-harmonic frequencies which in turn causes larger amplification at the high frequency zone. For that reason the bandwidth of the low pas filter $H(z)$ has been reduced thus providing the system with the appropriated stability robustness and additionally the gain $k_r = 0.7$ has been selected to reduce the inter-harmonic amplification (see Section 5.3.3).

The design of the AW compensator follows the procedure described in Section 5.4.6 and uses the structure of Figure 5.11. In this way, a compensator that has the dynamics of the plant during saturation and a deadbeat behaviour going out of saturation is designed.

Given the state space discrete-time model of the plant: (A,B,C,D), and its reachability matrix $W_A = \left[B\ AB\ \cdots\ A^{n-1}B\right]$, then the matrix $T = \left[v_n^T\ v_n^T A\ \cdots\ v_n^T A^{n-1}\right]$ with v_n^T the last row of W_A^{-1}. Thus, for this example:

$$A = 0.9978, B = 0.15, C = 0.1412, D = 0, T = 4.$$

Using the optimal MRAW approach described in Section 5.4.6, the parameters that have been found to be a feasible solution are: $K_{db} = -3.991391$, using $Q_p = T^T T$ for a deadbeat approximation .

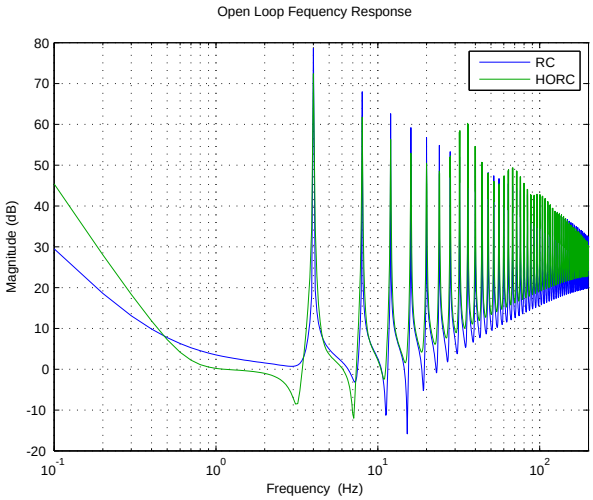

Fig. 6.24 Magnitude response of open-loop function $G_l(z)$. RC design and HORC design comparison

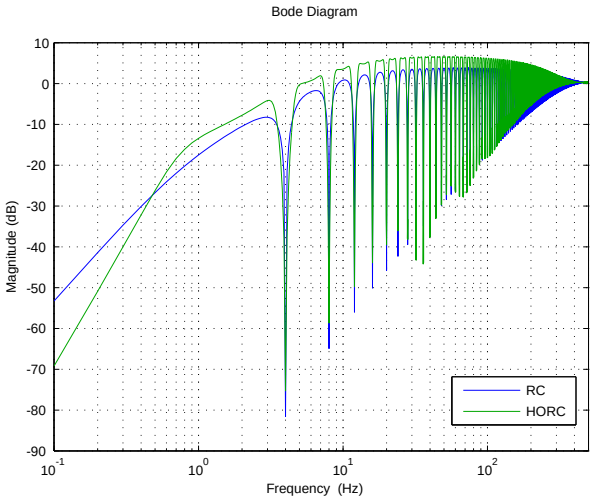

Fig. 6.25 Sensitivity function magnitude response. RC design and HORC design comparison.

6.7.2 Experimental results

The first experiment is aimed at showing the benefit of having a HORC to preserve the performance in case of small variation/uncertainty of the disturbance period. Figures 6.26 and 6.27 depict the steady state time response and harmonic content of the RC and HORC for a 0.5% deviation of the nominal speed $\omega = 4$ rev/s. It can be noticed that HORC obtains a lower degradation due to the speed variation.

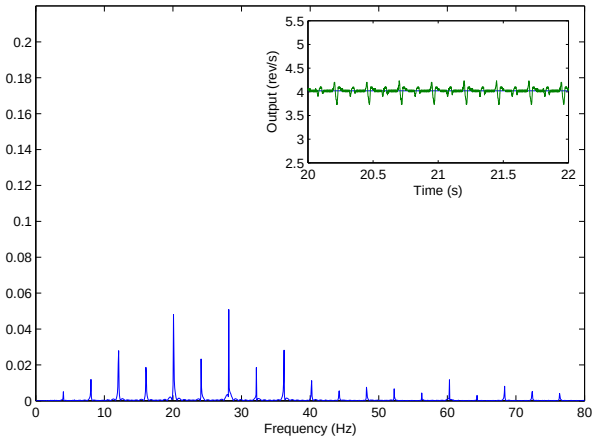

Fig. 6.26 Steady state time response and harmonic content of the RC for a 0.5% speed deviation.

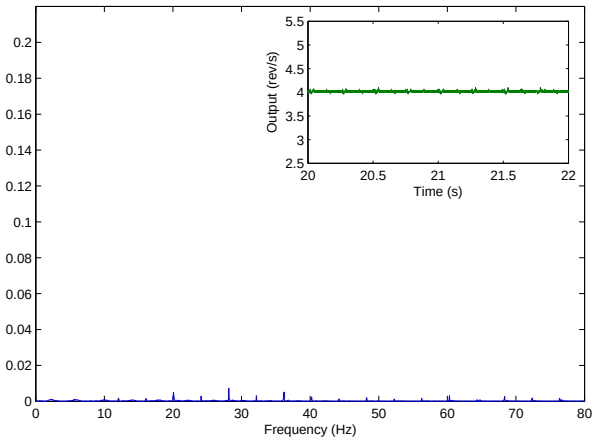

Fig. 6.27 Steady state time response and harmonic content of the HORC for a 0.5% speed deviation.

6.7.2.1 Anti-windup experiments

The first experiment regarding the AW design problem is carried out in steady state for nominal speed $\omega = 4$ rev/s and with the disturbances generated by the electromagnets. The actuator saturation has been simulated limiting the control action at the output of the controller. Initially, the system has reached the steady state without saturation and at $t = 30$ s a limitation in the control action has been set at the value $u_{max} = 3$ V. Figures 6.28, 6.30 and 6.31 show the output signal and control action under three different cases: without any AW strategy, using the IMC AW technique and with the deadbeat optimal AW compensator proposed in this work, respectively.

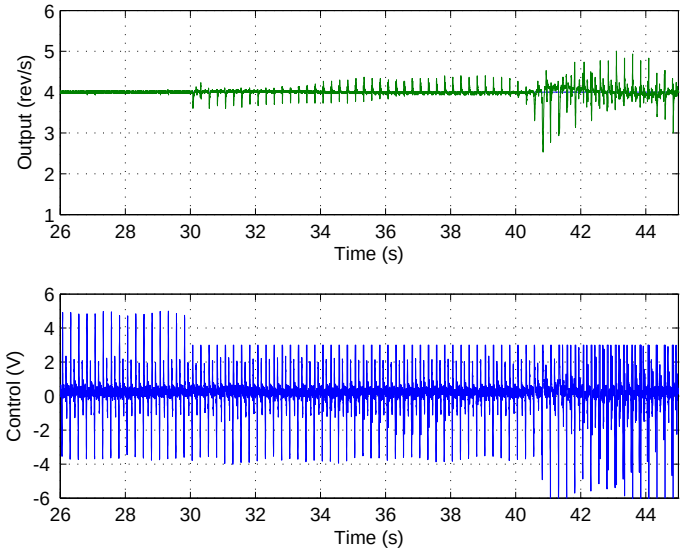

Fig. 6.28 Steady state time response of the system without AW compensator.

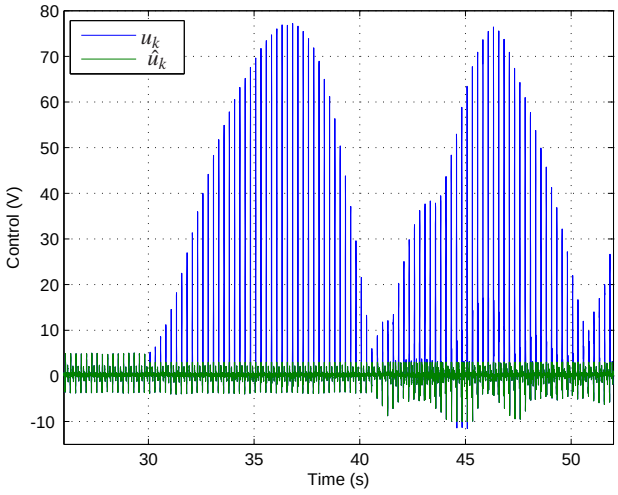

Fig. 6.29 Detailed control action of the system without AW compensator.

As it can be noticed, until $t = 30$ s, i.e. without saturation, the HORC can effectively reject the periodic disturbances generated by the electromagnets. However, without any AW strategy, Figure 6.28 shows that the system lose completely the performance and Figure 6.29 makes explicit the control action degradation after $t = 30$ s, where u_k starts growing, making it hard or impossible the recovery of the system. In the second case, using the IMC AW design, Figure 6.30 shows that even though the control action is not growing unbounded the system performance is very pour

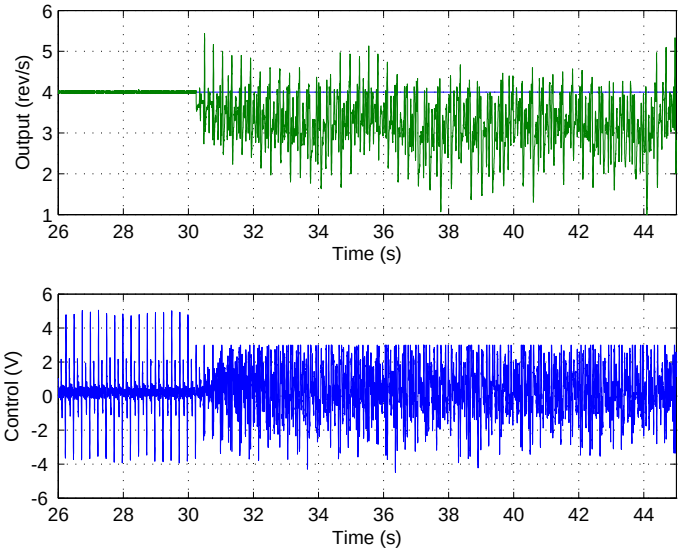

Fig. 6.30 Steady state time response of the system with IMC AW compensator.

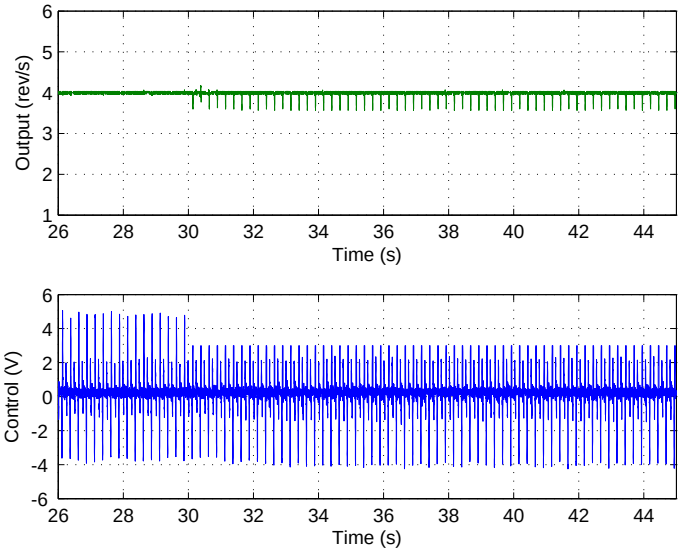

Fig. 6.31 Steady state time response of the system with deadbeat optimal AW compensator.

and is in continuous degradation. In the third case, using the deadbeat AW optimal design, Figure 6.31 shows that although the system can not reject completely the disturbance due to the saturated control signal, the performance is practically completely recovered in the zones where the control action does not reach the saturation limit (see also Figure 6.32). Figure 6.32 shows the control action in detail, it can be

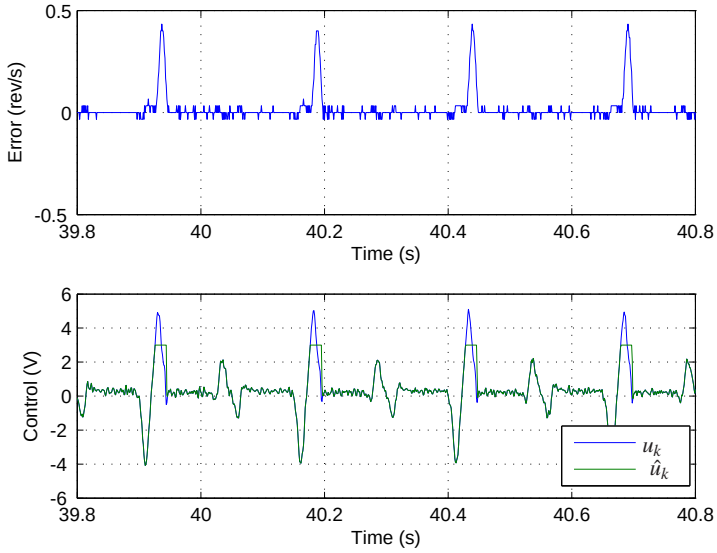

Fig. 6.32 Detailed error $e_k = r_k - y_k$ and control signal of the system with deadbeat optimal AW compensator.

noticed that the repetitive controller is providing the ideal control action and it is not affected by the saturation action while the plant receives the saturated version of this signal. Additionally, looking at the error signal, it is possible to see that the error signal grows only at time intervals when the control signal saturates.

The second experiment has been performed without the electromagnets and in this case it is a reference tracking example. Thus, the reference is a sinusoidal signal, and the saturation occurs limiting the control signal at $u_{max} = 3$. The same three cases analysed in the previous experiment have been implemented. Figure 6.33, shows the output an control signal in steady state when there is no compensation for the saturation effect. It can be seen that the tracking performance can not be longer preserved and there is an important steady state error. Figure 6.34 shows the detailed control action evolution and it is noticed that the controller output is reaching very high values making evident the windup effect. Figure 6.35 depicts the system response in case the IMC AW design. It is shown that although the control action is bounded and the only difference with the ideal control signal is the truncation at the saturation limit, the tracking error is even larger than in the previous case since a constant deviation has been added. Figure 6.36 presents the system response when the deadbeat optimal design is applied. It is noticeable that the tracking error only appears when the system gets into saturation and it vanishes as soon as the system can reach the reference signal again. The control signal is similar to the previous one but in this case the system remains saturated longer allowing a faster recovery of the tracking performance for the rest of the period. The error signal $e_k = r_k - y_k$ of the three strategies is shown in Figure 6.37. It is evident that the optimal AW design exhibit the smallest error for this repetitive control system.

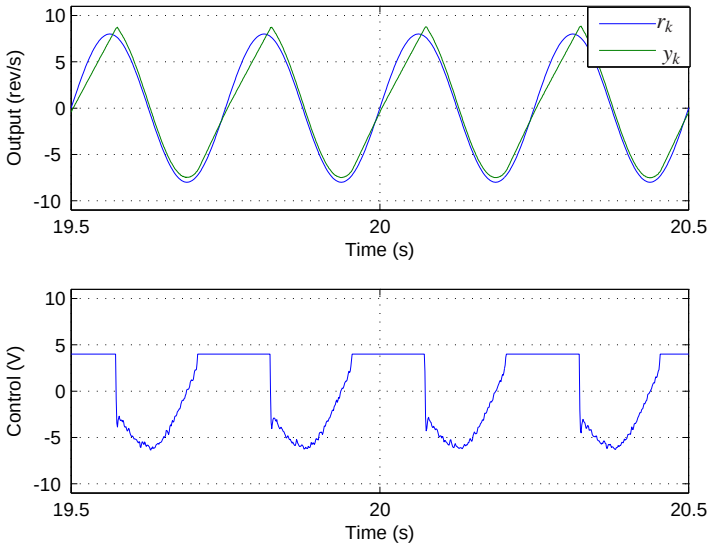

Fig. 6.33 Steady state time response of the system without AW compensator.

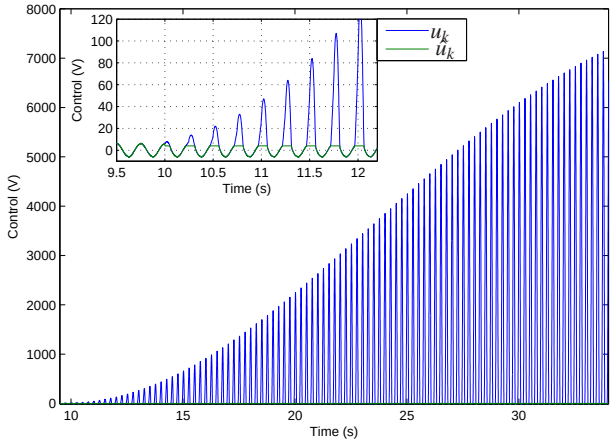

Fig. 6.34 Detailed control action of the system without AW compensator.

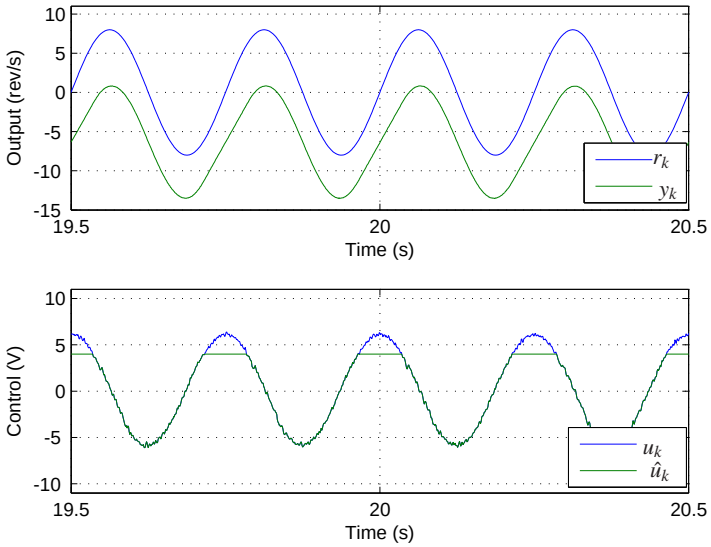

Fig. 6.35 Steady state time response of the system with IMC AW compensator.

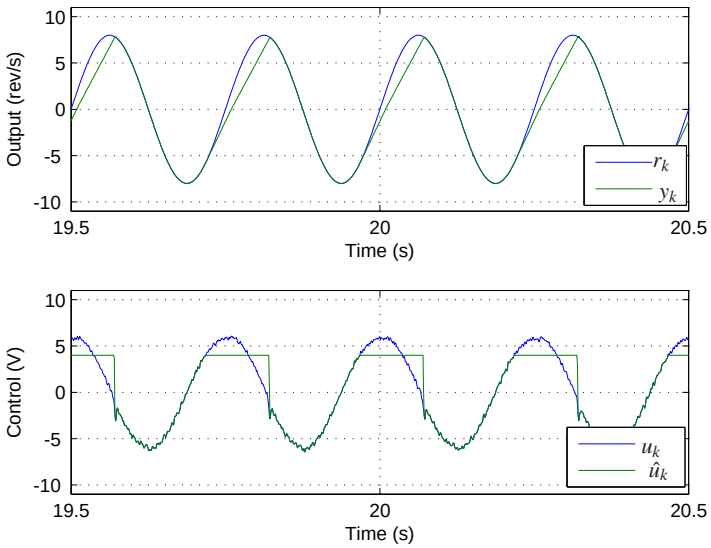

Fig. 6.36 Steady state time response of the system with DB optimal AW compensator.

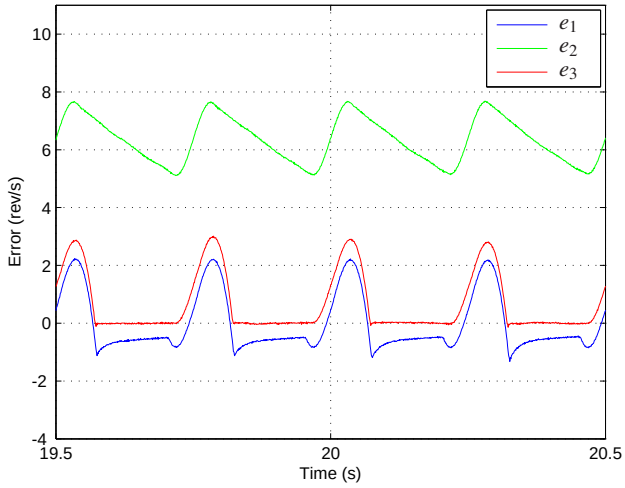

Fig. 6.37 Steady state error comparison of the three AW strategies. e_1 stands for no AW compensation, e_2 for IMC AW strategy and e_3 for the optimal AW proposal

6.8 Conclusions

Section 6.4 analyses the BIBO stability of a closed loop system containing a digital repetitive controller working under time-varying sampling period. The analysis was carried out using LMI gridding and robust control theory approaches that allow a stability assessment in a known, bounded interval where the reference/disturbance period is assumed to vary. The theoretically predicted results have been experimentally validated through the Roto-magnet plant in which rejection of periodic disturbances with time-varying period is successfully achieved. A detailed description of fundamental issues related to the implementation procedure have been provided.

The pre-compensation scheme proposed in Section 4.3 is implemented in Section 6.6. Thus, additionally to the sampling period adaptation mechanism a precompensator is added to the system in order to eliminate the structural changes due to the varying sampling period. As a consequence the closed loop stability can be assured despite the sampling period adaptation and the frequency observer dynamics.

Section 6.5 uses the robust control theory to synthesise a controller that ensures system stability for a predefined sampling period variation interval. As a result, it is found that the original controller $G_x(z)$ designed using the traditional methods is very closely related to the controller calculated using this strategy. This is consistent with the idea that the traditional design may be close to the optimum [10].

In Section 6.7, the optimal LQ design of Section 5.4 has been synthesized for the Roto-magnet plant aimed at finding a deadbeat recovery behaviour and assuring the global asymptotic stability of the closed loop system. Through experimental results it is shown that the proposed AW scheme gets better performance when compared with other designs with the same structure, thus providing the smallest deviation from the ideal plant output and isolating the repetitive controller from the saturation effect. The future research includes the inclusion of less-restrictive sector conditions for the nonlinear saturation function in order to better approximate the deadbeat design.

References

1. Z. Cao and G. F. Ledwich. Adaptive repetitive control to track variable periodic signals with fixed sampling rate. *IEEE/ASME Transactions on Mechatronics*, 7(3):374–384, September 2002.
2. R. Costa-Castelló, J. Nebot, and R. Griñó. Demonstration of the internal model principle by digital repetitive control of an educational laboratory plant. *IEEE Transactions on Education*, 48(1):73–80, 2005.
3. H. Dotsch, H. Smakman, P. Van den Hof, and M. Steinbuch. Adaptive repetitive control of a compact disc mechanism. *Decision and Control, 1995., Proceedings of the 34th IEEE Conference on*, 2:1720–1725 vol.2, Dec 1995.
4. H. Fujioka. A discrete-time approach to stability analysis of systems with aperiodic sample-and-hold devices. *IEEE Transactions on Automatic Control*, 54(10):2440–2445, 2009.
5. B. Grcar, P. Cafuta, G. Stumberger, and A. Stankovic. Control-based reduction of pulsating torque for pmac machines. *IEEE Transactions on Energy Conversion*, 17(2):169 –175, jun 2002.
6. R. D. Hanson and T.-C. Tsao. Periodic sampling interval repetitive control and its application to variable spindle speed noncircular turning process. *Journal of Dynamic Systems, Measurement, and Control*, 122(3):560–566, 2000.

7. I. D. Landau and G. Zito. *Digital Control Systems Design, Identification and Implementation*. Springer, 2006.
8. W. Rugh. *Linear system theory, 2nd Ed.* Prentice-Hall, Inc., Upper Saddle River, NJ, 1996.
9. T. Söderström and P. Stoica. *System identification*. Prentice-Hall, Inc., Upper Saddle River, NJ, USA, 1988.
10. S. Songschonc and R. W. Longman. Comparison of the stability boundary and the frequency response stability condition in learning and repetitive control. *International Journal of Applied Mathematics and Computer Science*, 13(2):169–177, 2003.
11. T. Su, S. Hattori, M. Ishida, and T. Hori. Suppression control method for torque vibration of ac motor utilizing repetitive controller with fourier transform. *IEEE Transactions on Industry Applications*, 38(5):1316 – 1325, sep/oct 2002.
12. T.-C. Tsao, Y.-X. Qian, and M. Nemani. Repetitive control for asymptotic tracking of periodic signals with an unknown period. *Journal of Dynamic Systems, Measurement, and Control*, 122(2):364–369, 2000.

Chapter 7
Shunt active power filter

7.1 Introduction

Shunt active power filters have been introduced as a way to overcome the power quality problems caused by nonlinear and reactive loads [9, 14, 23]. These power electronics devices are designed with the goal of obtaining a power factor close to 1 and achieving current harmonics and reactive power compensation [5, 6, 15]. The usual approaches [5, 15] for the control of shunt active filters are based on two hierarchical control loops: an inner one that assures the desired current and an outer one in charge of determining its required shape and the appropriate power balance as well. The control structure followed in this Chapter is the one in [7], in which the current controller is composed of a feedforward action that provides very fast transient response, and also of a feedback loop which includes an odd-harmonic repetitive control that yields closed-loop stability and a very good harmonic correction performance. In turn, the outer control law is based on the appropriated computation of the amplitude of the sinusoidal current network and, aiming at a robustness improvement, this is combined with a feedback control law including an analytically tuned PI controller.

However, although the control system performance is very good, it shows a dramatic performance decay when the network frequency value is not accurately known or changes in time. For a better assessment of this issue this Chapter shows the experimental behaviours under constant and varying network frequency. Also this performance degradation is presented and analysed in terms of the Total Harmonic Distortion[1] (THD), Power Factor[2] (PF) and $cos\phi$.

The Chapter organization is as follows. Section 7.2 introduces the plant, the control objectives and the two hierarchical control loops. Section 7.3 shows the odd harmonic controller designed for constant network frequency, also analysing the

[1] THD is calculated using $THD = \sqrt{\sum_{l=2}^{p} u_l^2}/u_1$, where u and l stand for the signal magnitude and harmonic order respectively.

[2] The PF calculation can be done with $PF = cos\phi/\sqrt{1+THD^2}$, where $\cos\phi$ is the difference in phase between the voltage signal and the fundamental component of the current signal at the source.

performance degradation through the THD, PF and $cos\phi$. Section 7.4 details the results for the varying sampling time repetitive controller including the stability analysis by means of robust control theory. It is worth to say that the stability analysis using the LMI approach introduced in Section 3.3 can not be applied in this implementation since the size of the resulting matrices makes the problem computationally unsolvable. Section 7.5 and Section 7.6 present the implementation of the adaptive pre-compensation scheme and the robust design respectively and finally a second order HORC is applied in Section 7.7.

7.2 Plant description

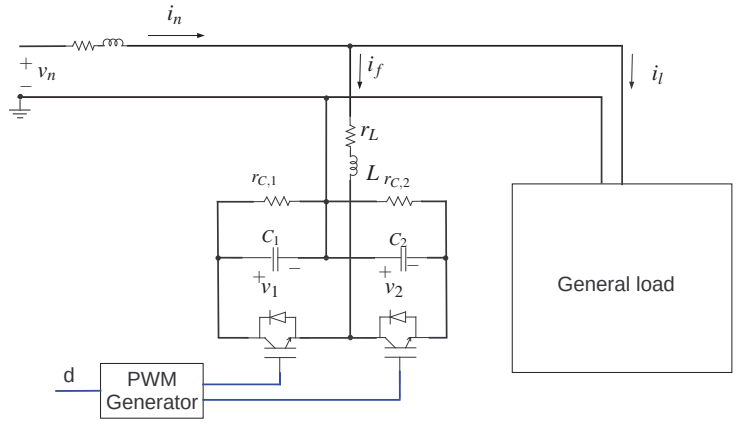

Fig. 7.1 Single-phase shunt active filter connected to the network-load system.

Figure 7.1 shows the system configuration. The active filter is connected in parallel between the power source and the load with the aim of guaranteeing unity Power Factor (PF) at the network side. The active filter is composed of a boost converter with the ac neutral line connected directly to the middle point of the dc bus. The dynamical behaviour of the boost converter can be expressed using the model averaged at the switching frequency as follows:

$$L\frac{di_f}{dt} = -r_L i_f - v_1\frac{d+1}{2} - v_2\frac{d-1}{2} + v_n, \tag{7.1}$$

$$C_1\frac{dv_1}{dt} = -\frac{v_1}{r_{C,1}} + i_f\frac{d+1}{2}, \tag{7.2}$$

$$C_2\frac{dv_2}{dt} = -\frac{v_2}{r_{C,2}} + i_f\frac{d-1}{2}, \tag{7.3}$$

where d is the control variable; i_f is the inductor current; v_1, v_2 are the dc capacitor voltages, respectively; $v_n = V_n\sqrt{2}\sin(\omega_n t)$ is the voltage source, with $\omega_n = 2\pi/T_n$, T_n being the network period; L is the converter inductor; r_L is the inductor parasitic resistance; C_1, C_2 are the converter capacitors and $r_{C,1}$, $r_{C,2}$ are the parasitic resistances of the capacitors. The control variable, d, takes its value in the closed

real interval $[-1,1]$ and it is directly related to the Pulse-Width Modulation (PWM) control signal injected to the actual system.

Because of the nature of the voltage source, the steady-state load current is usually an odd symmetric periodic signal. Hence, its Fourier series expansion can be written as

$$i_l(t) = \sum_{n=0}^{\infty} a_n \sin\left[(2n+1)\,\omega_n t\right] + b_n \cos\left[(2n+1)\,\omega_n t\right].$$

Let us consider the partial state feedback $\alpha = \frac{d+1}{2} v_1 + \frac{d-1}{2} v_2$ and the variables

$$E_C = \frac{1}{2}\left(C_1 v_1^2 + C_2 v_2^2\right), \quad D = C_1 v_1 - C_2 v_2,$$

where E_C is the energy stored in the converter capacitors and D is the charge unbalance between them. Let us also assume that the two dc bus capacitors are equal ($C = C_1 = C_2$, $r_C = r_{C,1} = r_{C,2}$). Then, the system dynamics using the new variables is

$$L\frac{di_f}{dt} = -r_L i_f + v_n - \alpha \tag{7.4}$$

$$\frac{dE_C}{dt} = -\frac{2E_C}{r_C C} + i_f \alpha \tag{7.5}$$

$$\frac{dD}{dt} = -\frac{1}{r_C C} D + i_f. \tag{7.6}$$

7.2.1 Control objectives

The objective of the active filter is to assure that the current at the source, $i_n(t)$, has a sinusoidal shape in phase with the network voltage signal. This can be stated as[3] $i_n^* = I_d^* \sin(\omega_n t)$. In this way, it is needed that the control system tracks a sinusoidal shape signal with suitable magnitude and rejects the harmonics introduced by the load and any existing phase difference.

Additionally, for the correct operation of the boost converter, it is necessary to assure constant average value of the dc bus voltage[4], namely, $< v_1 + v_2 >_0^* = v_d$, where v_d must fulfil the boost condition ($v_d > 2\sqrt{2} v_n$). It is also desirable for this voltage to be almost equally distributed among both capacitors ($v_1 \approx v_2$). This can be reached as a consequence of seeking the active power balance of the system which is achieved if the energy stored in the active filter capacitors, $E_C = v_1^2 + v_2^2$, is equal to a reference value, E_C^d.

7.2.2 Controller structure

The controller proposed in this work takes advantage of the hierarchical approach studied in [7] and shown in Figure 7.2. Firstly, an inner current controller is used to

[3] x^* represents the steady-state value of signal $x(t)$.

[4] $< x >_0$ means the dc value, or mean value, of the signal $x(t)$.

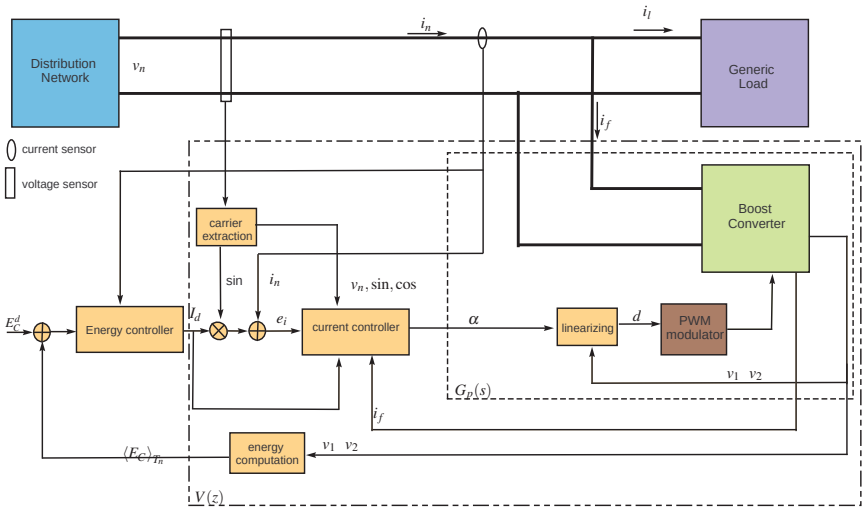

Fig. 7.2 Global architecture of the control system.

force the sine wave shape for the network current by fixing α and, and, consequently, d. Then, the appropriate active power balance for the whole system is achieved by an outer energy shaping control loop that fixes the amplitude of the sinusoidal reference, I_d, for the current control loop. It is also worth remarking that a carrier extraction filter (see Figure 7.2) cleans the source voltage from possible background harmonic distortion.

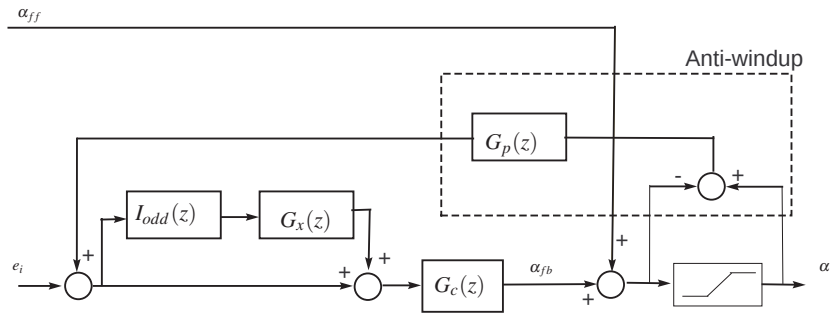

Fig. 7.3 Current control block diagram.

7.2.2.1 The current loop controller

The current control loop, pictured in Figure 7.3, aims at forcing a sinusoidal shape in i_n. Notice that its output signal, i.e. the control action α, is composed of a feedforward term, α_{ff}, and feedback term, α_{fb} [7].

The feedforward term is computed through the analysis of the control action required to obtain the desired steady state behaviour [7], and it is also in charge of providing fast transient response:

$$\alpha_{ff} = v_n + L\frac{di_l}{dt} + r_L i_l - I_d\left(r_L \sin\omega_n t + L\omega_n \cos\omega_n t\right). \tag{7.7}$$

The feedback term, introduced to overcome model uncertainties, disturbances and measurement noise, is designed taking advantage of the linearity of (7.4). This controller uses a repetitive control under a plug-in scheme. Thus, the implementation of the approaches proposed in previous Chapters will be described in the subsequent Sections.

As usual, the active filter control action is subject to saturation. This nonlinearity may introduce a windup effect [12] in the repetitive controller that should be avoided. However, the high order inherent to repetitive controllers limits the applicable anti-windup techniques [11]. Specific anti-windup schemes for repetitive control have been proposed in [18, 16], but most of them increase the necessary computational burden. This work uses a strategy which allows a simple implementation: it consists in placing the plant model in the anti-windup feedback chain as shown in Figure 7.3. This scheme coincides with the IMC AW approach described in Section 5.4.2 which may be seen as a particular case of the MRAW scheme [11]. Hence, the real plant sees the saturated control action while the plant model sees the difference between the saturated and the unsaturated control, which makes the system LTI from the controller point of view. Consequently, the anti-windup feedback loop stability is proved by construction. It is worth to say that we skip the optimal AW design proposed in Section 5.4.6 with the purpose of maintaining the active filter control design simpler.

The control action is the PWM duty cycle, d, which in practice belongs to the interval $[-0.975, 0.975]$. Hence, the anti-windup scheme, as shown in Figure 7.3, is applied over α in the dynamic interval $[0.025v_1 - 0.975v_2, 0.975v_1 - 0.025v_2]$.

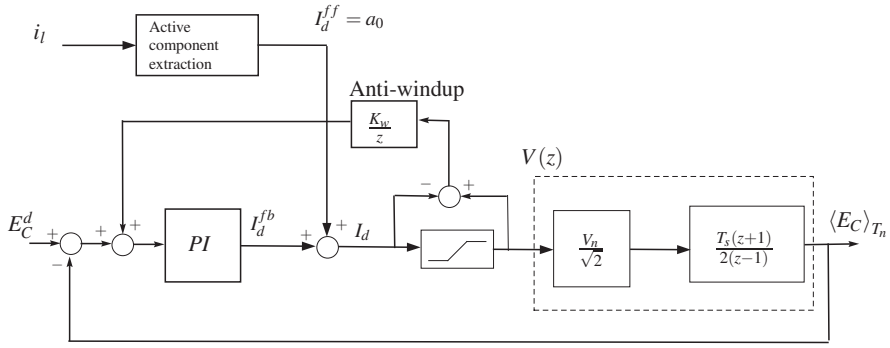

Fig. 7.4 Energy shaping controller block diagram.

7.2.2.2 The energy shaping controller

Following [7], once $i_n(t) \approx I_d(t)\sin(\omega_n t)$ is achieved, the outer plant can be modelled as:

$$\frac{d}{dt}\langle E_C(t)\rangle_{T_n} = \frac{-2}{Cr_C}\langle E_C(t)\rangle_{T_n} + \frac{\sqrt{2}V_n\pi}{\omega_n}\left(I_d - a_0\right). \tag{7.8}$$

The control of this plant is carried out through a two-action controller [7], as portrayed in Figure 7.4. The first action is a feedforward term, defined as $I_d^{ff} = a_0$, which assures the energy balance in the ideal case ($r_L = 0$, $r_C = 0$) and takes into account the characteristics and changes of i_l instantaneously. The second action is given by the PI controller:

$$I_d^{fb} = k_i \frac{T_s\,(z+1)}{2\,(z-1)} \Delta E + k_p \Delta E, \tag{7.9}$$

where $\Delta E = E_C^d - \langle E_C\,(t)\rangle_{T_n}$, which regulates $\langle E_C\,(t)\rangle_{T_n}$ to the set point E_C^d with null steady-state error.

The implementation of this controller needs the computation of the mean value of certain signals. In this work the digital notch filter [4]

$$F_N(z) = \frac{1}{N} \cdot \frac{1 - z^{-N}}{1 - z^{-1}} \tag{7.10}$$

has been used to compute $\langle \cdot \rangle_{T_n}$. It is important to emphasize that the notch filter takes advantage from the fact that $E_C(t)$ is a periodic signal and annihilates all its periodic components.

Finally, the PI controller is completed with a standard anti-windup mechanism that bounds the desired active power which the active filter may handle (see Figure 7.4). For the current setup it is $I_d \in [-40, 40]\,\mathrm{A}$.

7.3 Odd harmonic repetitive controller

The nominal period of the signal to be tracked/rejected is $T_p = 1/50$ s which corresponds with the nominal European network frequency of 50 Hz. The sampling period is selected to be $T_s = 5 \cdot 10^{-5}$s (the PWM switching period), then resulting $N = T_p/T_s = 400$.

The discrete-time plant model is obtained from (7.1) and the addition of an anti-aliasing filter with time constant τ:

$$G_p(z) = \left(1 - z^{-1}\right) \mathscr{Z}\left[\frac{-1}{Ls + r_L} \cdot \frac{1}{\tau s + 1} \cdot \frac{1 - e^{-T_s}}{s}\right]_{T_s}, \tag{7.11}$$

which gives a minimum-phase system. The inductor and the parasitic resistance values are $L = 1$ mH and $r_L = 0.5\ \Omega$ respectively. For the inner loop, the following lag controller is used

$$G_c(z) = -\frac{3.152z - 3.145}{z - 0.9985},$$

which provides a phase margin of 79.36^o. The odd-harmonic internal model (5.5) is used:

$$I_{odd}(z) = \frac{-H(z)}{z^{\frac{N}{2}} + H(z)}, \tag{7.12}$$

with

$$H(z) = \frac{1}{4}z + \frac{1}{2} + \frac{1}{4}z^{-1},$$

while

$$G_x(z) = k_r(G_o(z))^{-1}, \tag{7.13}$$

and $k_r = 0.7$ has been selected. The open loop function is defined as $G_l(z) = (1 + I(z))G_c(z)G_p(z)$, with $I(z)$ corresponding the IM.

The repetitive controller yields the feedback law

$$\alpha_{fb} = G_c(z)\left[1 + G_x(z)I_{odd}(z)\right]e_i$$

which, together with the feedforward action given in (7.7), yields the control action $\alpha = \alpha_{fb} + \alpha_{ff}$. Under its combined effect, one can assume that the network current is $i_n(t) \approx I_d(t)\sin\omega_n t$, which will be taken as a fact.

The frequency response of the open loop and sensitivity function are depicted in Figure 7.5 and 7.6, respectively. These Figures show the tracking and rejection action of the repetitive controller over the harmonic frequencies.

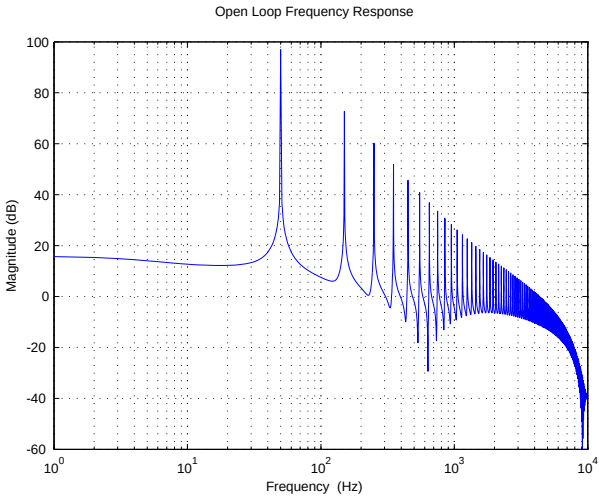

Fig. 7.5 Magnitude response of the open loop function $G_l(z)$ for the active filter RC design.

7.3.1 Performance at nominal frequency

Figure 7.7 shows the distribution network voltage, v_n, and the network current, i_n, when a rectifier (i.e. a nonlinear load) is connected to the network and no active filter is acting[5]. This current has a Total Harmonic Distortion[6] (THD) of 62.6% and a Root Mean Square (RMS) value of 19.56 A, while the Power Factor (PF) amounts to 0.76. The function of active filters is to inject the current needed to transform the network current i_n into a sinusoidal one with low THD in v_n and i_n.

[5] The scales in the Figures of this chapter are: v_n (230 V/div), i_n (48 A/div) and v_1, v_2 (74,5 V/div).

[6] In this work, the THD is calculated with respect to the RMS value of the signal.

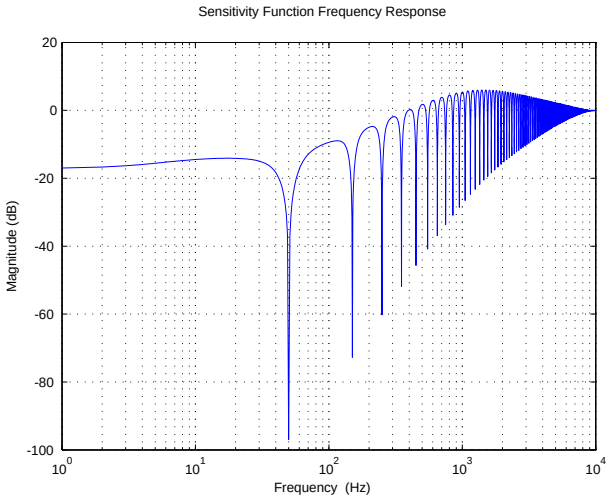

Fig. 7.6 Sensitivity function magnitude response for the active filter RC design.

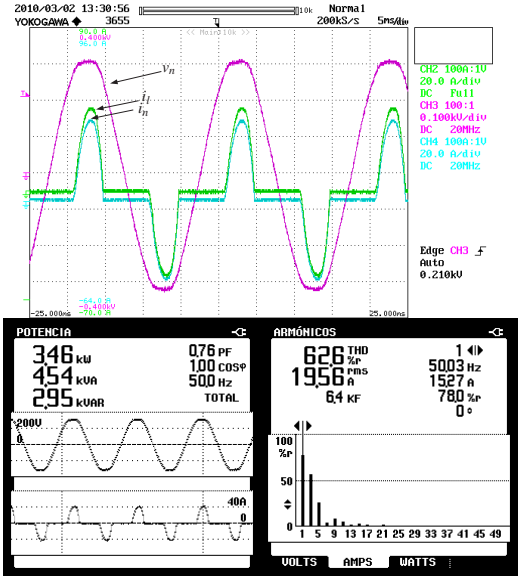

Fig. 7.7 Nonlinear load connected to the ac source working at 50 Hz. Top: v_n, v_1, i_l and i_n. Bottom: PF, $\cos\varphi$ and THD for i_n.

Figure 7.8 shows the experimental system response at nominal frequency. As can be seen, the control system can effectively reject the harmonic components present in the load current achieving a sinusoidal shape current at the source, i_n, with a THD of 0.3% with unitary PF and $cos\phi$. Additionally, Figure 7.9 depicts the transition registered in i_n when the load is switched on. As shown, the system reaches the steady state in 7 cycles approximately.

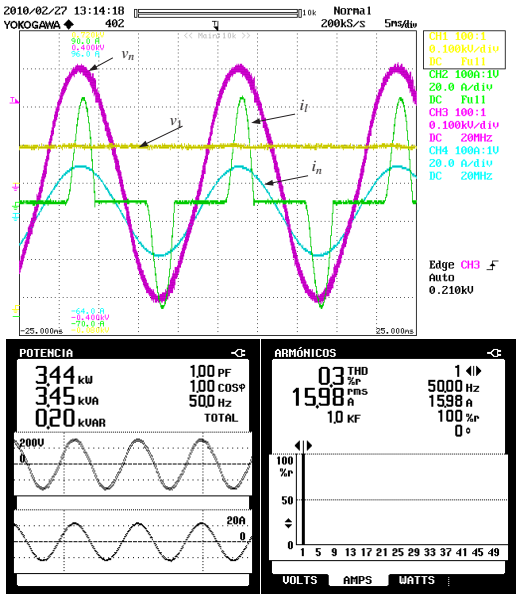

Fig. 7.8 Nonlinear load and the active filter connected to source (50 Hz). (top) v_n, i_n, i_l and v_1 *vs* time; (bottom) PF, $\cos\phi$ and THD for i_n.

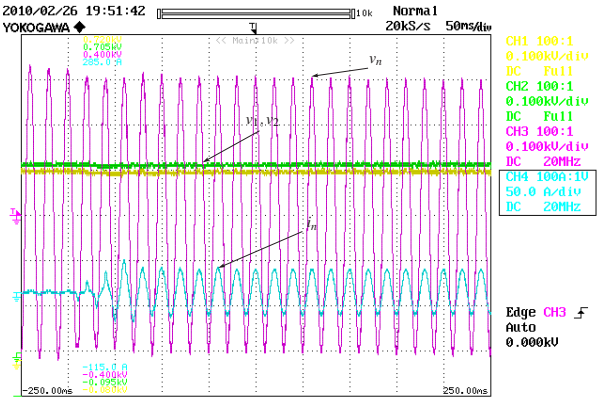

Fig. 7.9 An off-on transition of the nonlinear load with the active filter connected to source (50 Hz). v_n, i_n, v_1 and v_2 *vs* time.

The next experimental setup consists of a linear load composed of a capacitive-resistive array, the previously described single phase active filter and second order odd harmonic controller. Figure 7.10 shows the waveforms of v_n and i_n when the linear load is connected to the ac source. The system power factor (PF) and $cos\phi$ are 0.75.

As Figure 7.10 shows, when the frequency of the voltage source is fixed to 50 Hz and the active filter is connected in parallel with the linear load, the PF and $\cos\phi$ at the port are unitary.

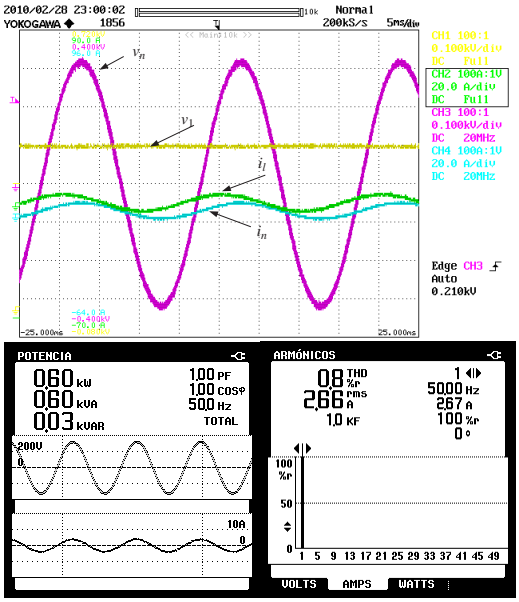

Fig. 7.10 Linear load and the active filter connected to source (50 Hz). (top) v_n, i_n, i_l and v_1 *vs* time; (bottom) PF, $\cos\phi$ and THD for i_n.

7.3.2 Performance under network frequency variations

Network frequency is prone to suffer slight variations around its nominal value. Since the standard design of repetitive controller uses a fixed network frequency, the system performance will be largely degraded at frequencies values diverging from the nominal one. For the active filter application, this is reflected in a shape degradation of the source current, which in turn can be seen as the THD, PF and $\cos\phi$ degradation of the system.

In order to show the performance degradation under frequency variations, the same controller and settings of the preceding section have been used.

Figure 7.11 shows the response when the frequency is deviated to 49.5 Hz. As it is shown, an important shape degradation occurs which can be noticed through the presence of the additional harmonic components. The THD is now 10% and the power factor and $cos\phi$ are 0.97 and 0.98 respectively.

7.3.2.1 THD, PF and $cos\phi$ degradation

Figures 7.12 and 7.13 show the simulated performance decay through the THD, PF and $cos\phi$ degradation with respect to the frequency variation. For this calculation, the current control loop and the energy control loop have been included in the simulation and the load current $i_l(t)$ shown in Figure 7.8 has been assumed. As can be seen from Figure 7.12, as the network frequency departs from the nominal one the system looses its tracking and rejection capacity allowing the increase of the harmonic components which is reflected directly in the THD value. It is worth to notice that the simulated THD degradation seems to be lower than the experimental one

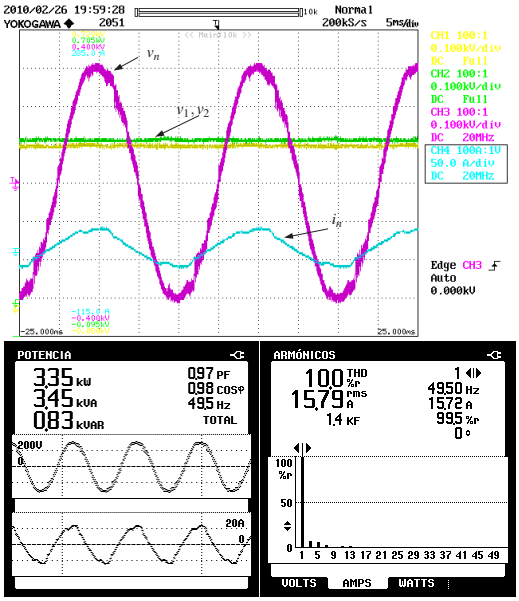

Fig. 7.11 Nonlinear load and the active filter connected to source (49.5 Hz). (top) v_n, i_n, v_1, and v_2 *vs* time; (bottom) PF, $\cos\phi$ and THD for i_n.

which can be explained through the additional degradation of the voltage source in practice, plant non-linearities and unmodeled dynamics. On the other hand, Figure 7.13 shows that although the load has a $cos\phi$ close to 1, the $cos\phi$ and PF exhibit some degradation due to the frequency variation. In case of capacitive or inductive loads, the AF control system will provide the $cos\phi$ and PF correction at nominal frequency, however this performance will be also compromised when the network frequency changes with the subsequent $cos\phi$ and PF degradation. Fig. 7.14 shows the PF behaviour using the settings of the previous section with a pure capacitive load. As can be seen, an important PF degradation occurs when the network frequency deviates from the nominal one.

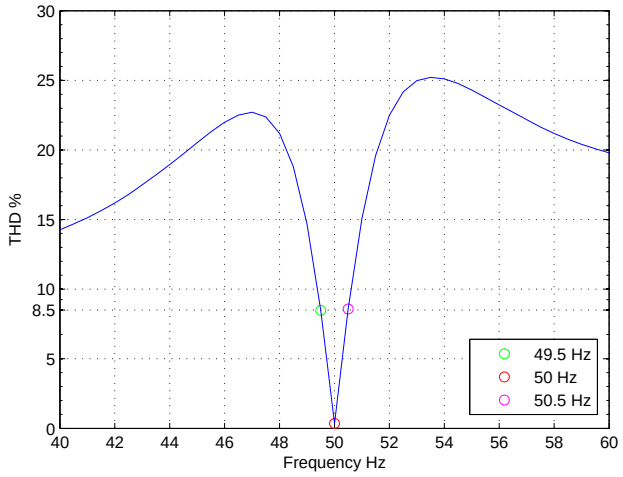

Fig. 7.12 THD degradation due to the frequency variation having a nonlinear load

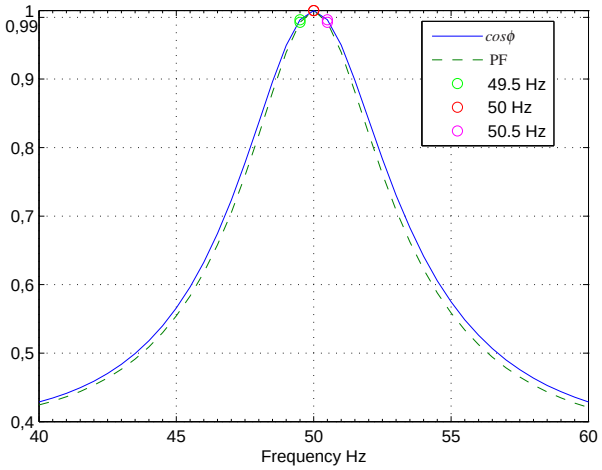

Fig. 7.13 $cos\phi$ and PF degradation due to the frequency variation having a nonlinear load

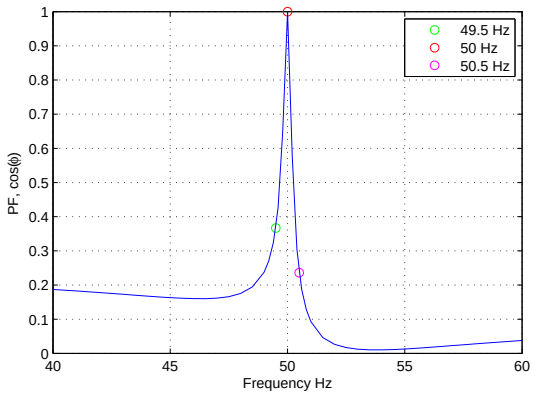

Fig. 7.14 Power factor variation as a function of the network frequency having a pure capacitive load.

7.4 Varying sampling results

7.4.1 Implementation issues

The experimental setup is composed of the ac power source PACIFIC Smartsource 140-AMX-UPC12 that acts as a variable frequency ac source, a nonlinear load consisting of a full-bridge diode rectifier and the previously described single-phase active filter which is connected in a shunt manner with the rectifier to compensate its nonlinear effects.

The active filter controller has been digitally implemented on a DSP based hardware consisting of an ADSP-21161 floating-point DSP processor with an ADSP-21990 fixedpoint mixed-signal DSP processor that acts as coprocessor, both from Analog Devices. The ADSP-21161 and the ADSP-21990 communicate with each other using a high-speed synchronous serial channel in Direct Memory Access (DMA) mode. The ADSP-21990 deals with the PWM generation and the A/D conversions with the provided 14 bits eight high-speed A/D channels. The PWM switching frequency is equal to the nominal sampling frequency of 20 kHz.

The network frequency is obtained through some additional hardware that runs in the DSP. Figure 7.15 shows the three main components of the frequency estimation: 1) the zero crossing detector module which comprises a low pass filter to remove noise from the voltage measure and a smith trigger comparator to detect the zero crossings; 2) the frequency calculation module which consists of two counters acting as a period estimation block and finally, 3) a low pass digital filter in charge of reducing noise in the digital estimation of the period. With this information the sampling frequency is updated to maintain the ratio $N = 400$.

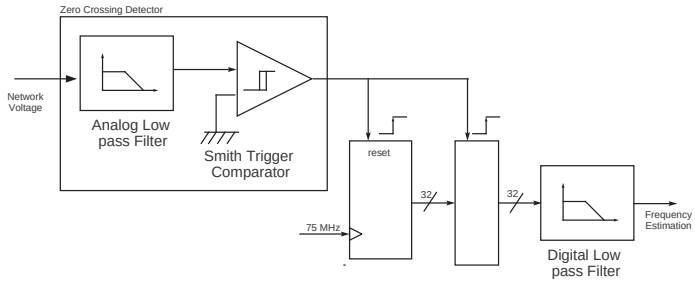

Fig. 7.15 Network frequency computation.

It is well known that in a real setup T_s cannot be fixed with infinite precision but within the limitations imposed by the timer quantification. Notice that even small quantification errors entail important gain reductions. In spite of the gain reduction, the sampling time adaptation scheme allows to maintain the gain of (7.12) above 52 dB, which is good enough for most applications.

7.4.2 Robust control theory approach

According to Section 3.4 and Remark 3.3, the above settings yield $\|G_{\bar{T}}(z)\|_\infty = 2.6530 \times 10^4$. In order to define $\gamma_{\bar{T}}$ (see (3.16)), $\varepsilon = 0.0001$ is selected. Furthermore, the continuous-time plant matrix is

$$A = \begin{pmatrix} -28651.9058 & -4276.5664 \\ 4096 & 0 \end{pmatrix}.$$

Table 7.1 contains the stability intervals obtained with the optimized Γ defined in (3.18) and also for $\Gamma = \mathbb{I}$ (i.e. the proposal in [10, 20]) using three different norm bounds for the matrix exponential Δ: a numerical calculation, the log norm of a matrix with respect to the 2-norm [10] and a Schur decomposition-derived bound [20] (see Appendix B for more details in the calculation of the stability intervals). Notice that the numerical bound and the log norm provide similar results, while the latter appears to be sharper than the Schur decomposition bound. The reduction in conservatism achieved with the assignment of Γ proposed in this article is between 300 % and 336 %, depending on the norm bound calculation method. It is worth mentioning that nominal line frequency is usually 50 Hz or 60 Hz depending on the geographical area, and may vary by not more than 10 % of its value. Therefore, line frequency variations in the interval $[45, 66]$ Hz can be expected.

7.4.3 Experimental results

Figure 7.16 shows, when the frequency of the voltage source is fixed to 48 Hz and the active filter is connected in parallel with the rectifier the shape of the current at the source port is nearly sinusoidal with a THD of 0.4%. It is also worth remarking that the power factor (PF) and $cos\phi$ at the port are unitary.

Figure 7.17 shows the system response when the network frequency is 52 Hz and the sampling time is adapted as described in this work. As it can be seen, the system behaviour is similar to the one obtained when working at nominal frequency (shown in Figure 7.8).

In the following experiment the network frequency is changed from 53 Hz to 48 Hz in a ramp manner (40 cycles); the nonlineal load has been used. Figure 7.18 depicts the responses of v_n and i_n. Notice that, after a transient, the system reaches the steady-state maintaining the performance.

For the next two experiments the linear load is used and the network frequency of the system is changed to 51 Hz and 49 Hz, and the sampling time is adapted as described previously. Figures 7.19 and 7.20 show that the system performance is

Bounds	$\Gamma = \text{col}([0,0]^\top, [0,\mathbb{I}]^\top)$	$\Gamma = \mathbb{I}$
Numerical	$[28.4944, 102.3305]$	$[42.4676, 59.3855]$
Log norm	$[28.5096, 102.2870]$	$[42.4680, 59.3850]$
Schur dec.	$[29.9672, 95.5837]$	$[42.6741, 59.0878]$

Table 7.1 Shunt active filter: stability intervals in frequency units (Hz).

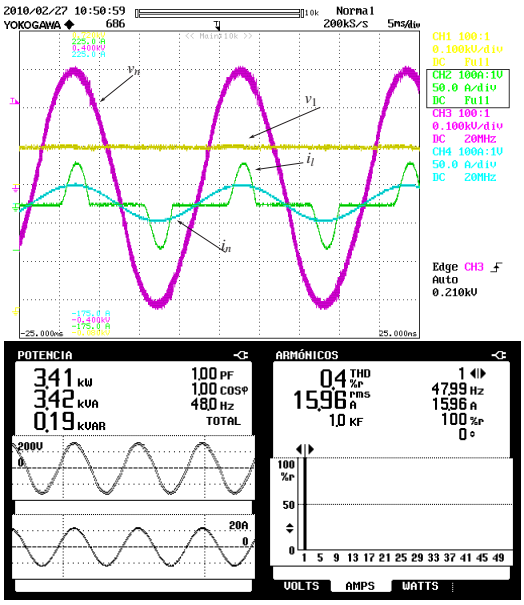

Fig. 7.16 Nonlinear load with active filter connected to the ac source working at 48 Hz with adaptive scheme. Top: v_n, v_1, i_l and i_n. Bottom: PF, cos φ and THD for i_n.

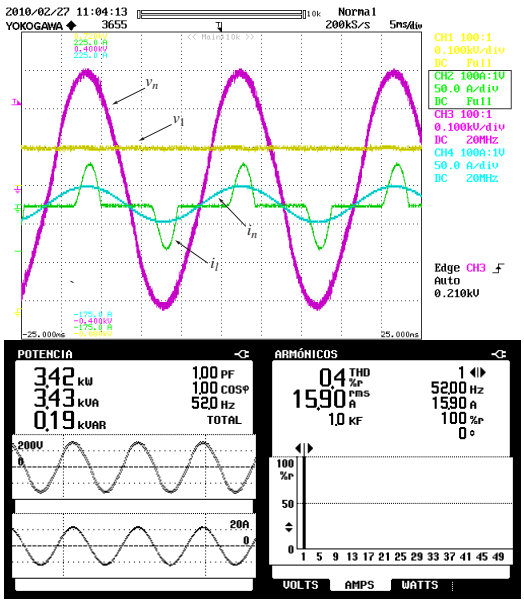

Fig. 7.17 Nonlinear load with active filter connected to the ac source working at 52 Hz with adaptive scheme. Top: v_n, v_1, i_l and i_n. Bottom: PF, cos φ and THD for i_n.

kept similar to the one obtained for the nominal frequency providing a unitary PF and $cos\phi$.

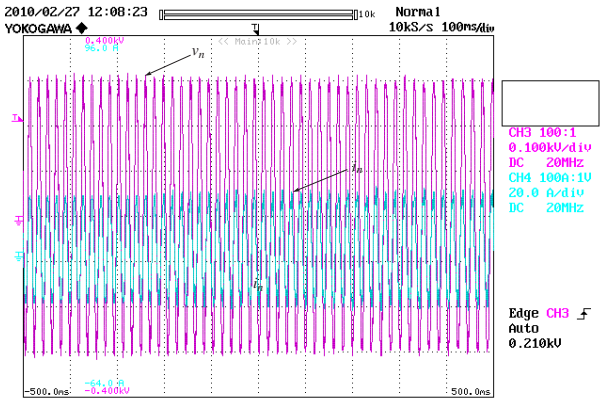

Fig. 7.18 Nonlinear load with active filter connected to the ac source with adaptive scheme. v_n and i_n when the network frequency changes from 53 Hz to 48 Hz in 49 cycles.

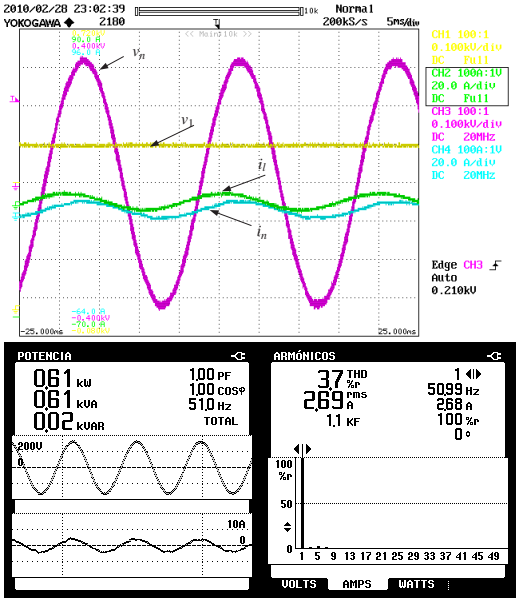

Fig. 7.19 Linear load and the active filter connected to source (51 Hz). (top) v_n, i_n, i_l and v_1 *vs* time; (bottom) PF, $\cos\phi$ and THD for i_n.

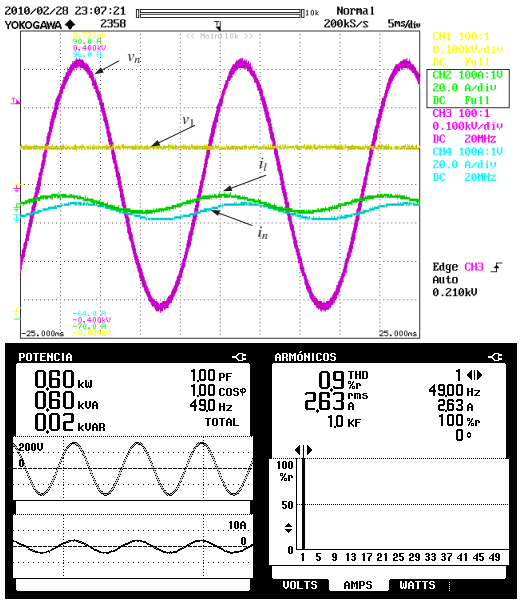

Fig. 7.20 Linear load and the active filter connected to source (49 Hz). (top) v_n, i_n, i_l and v_1 *vs* time; (bottom) PF, $\cos\phi$ and THD for i_n.

7.5 Adaptive pre-compensation

7.5.1 Controller design

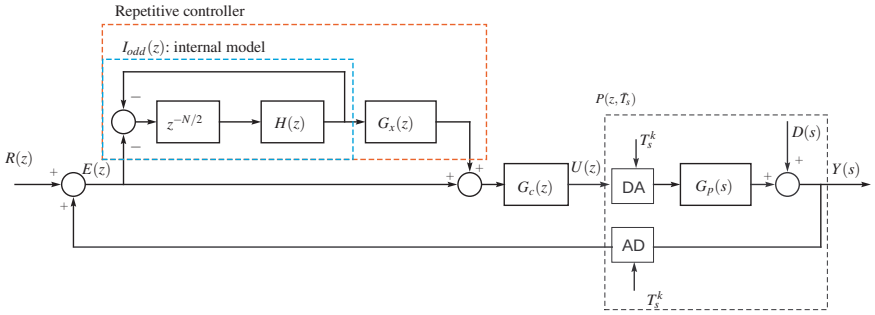

Fig. 7.21 Discrete-time block-diagram of the basic varying sampling repetitive control structure.

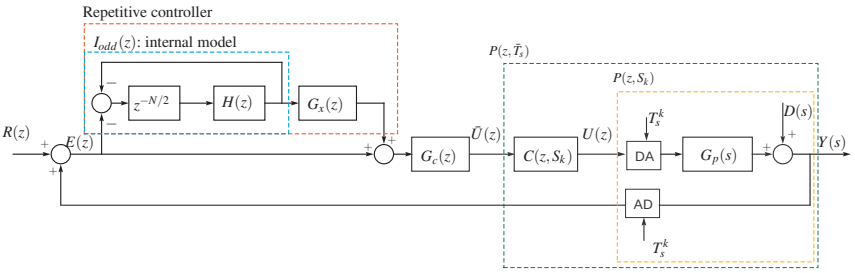

Fig. 7.22 Discrete-time block-diagram of the closed-loop system with the adaptation-compensation controller structure.

Aiming at annihilating the effect of the time-varying sampling and forcing an output behaviour corresponding to that of the nominal sampling period $\bar{T}$, a pre-compensator is introduced between the nominal controller $G_c(z)$ and the plant (see Section 4.3). Namely, let the repetitive controller be designed and implemented to provide closed-loop stability for an a priori selected nominal sampling period $\bar{T}$, using the LTI model

$$G_p(z,\bar{T}) \triangleq \frac{Num(z,\bar{T})}{Den(z,\bar{T})} = \mathscr{Z}\left\{G_p(s)\right\}$$

(see Figure 7.21), with

$$G_p(s) = \frac{i_f(s)}{\alpha(s)} = -\frac{\frac{1}{r_l}}{\left(\frac{L}{r_L}s+1\right)(\tau s+1)},$$

τ being the time constant of the antialiasing filter. When working at varying sampling period T_s, this model is a LTV system

$$G_p(z,T_s) = \frac{Num(z,T_s)}{Den(z,T_s)},$$

with $T_s = \{T_k, T_{k-1}, T_{k-2}\}$ (recall that the order of $G_p(s)$ is 2). In order to annihilate the effect of the sampling rate change, the pre-compensator

$$C(z,T_s) = G_p(z,\bar{T})G_p^{-1}(z,T_s) = \frac{Num(z,\bar{T})}{Den(z,\bar{T})}\frac{Den(z,T_s)}{Num(z,T_s)} \tag{7.14}$$

is connected in series with the LTV plant $G_p(z,T_s)$. Thence, the overall behaviour is that of the nominal LTI system: $C(z,T_s)G_p(z,T_s) = G_p(z,\bar{T})$. Figure 7.22 inner loop control scheme.

As the pre-compensator-plant subsystem is kept invariant and equal to the nominal plant, closed-loop system stability is preserved. Additionally, the inner loop transfer function is preserved invariant and, as a consequence, outer-loop stability is also preserved. The pre-compensator 7.14 can be equivalently implemented in input-output or state-space approaches, but the state-space formulation leads to a more efficient code. Finally, although this approach guarantees closed-loop stability, it is necessary to check the internal stability of the compensator-plant subsystem $P(z)$ (including possible forbidden cancellations). LMI gridding techniques (see Section 3.3) allow to prove that, for the active filter used in this paper, the pre-compensation scheme is internally stable for a wide range of values of T_s, in particular those covering the most relevant frequency interval from the practical point of view ([45,66] Hz).

7.5.2 Controller calculation

The active filter system together with the anti-aliasing filter can be seen as a second order continuous-time system with the following transfer function

$$G(s) = \frac{k_1}{\tau_1 s+1}\frac{k_2}{\tau_2 s+1}, \tag{7.15}$$

where $k_1 = -1/r_L$, $\tau_1 = L/r_L$, $k_2 = 1$, and τ_2 the time constant of the anti-aliasing filter. A state-space Jordan form can be found to be

$$\begin{aligned}\dot{x}(t) &= \begin{bmatrix} -\frac{1}{\tau_1} & 1 \\ 0 & -\frac{1}{\tau_2} \end{bmatrix} x(t) + \begin{bmatrix} 0 \\ 1 \end{bmatrix} u(t) \\ y(t) &= \begin{bmatrix} \frac{k_1 k_2}{\tau_1 \tau_2} & 0 \end{bmatrix} x(t). \end{aligned} \tag{7.16}$$

The discretization of the continuous model (7.16) for a given T_k is

$$x_{k+1} = A(T_k)x_k + B(T_k)u_k \tag{7.17}$$
$$y_k = Cx_k, \tag{7.18}$$

with

$$A(T_k) = \begin{bmatrix} e^{-\frac{T_k}{\tau_l}} & \frac{\left(-e^{-\frac{T_k}{\tau_2}} + e^{-\frac{T_k}{\tau_l}}\right)\tau_2\,\tau_l}{(\tau_l - \tau_2)} \\ 0 & e^{-\frac{T_k}{\tau_2}} \end{bmatrix},$$

$$B(T_k) = \begin{bmatrix} -\frac{\tau_2\,\tau_l\left(\tau_l\, e^{-\frac{T_k}{\tau_l}} - \tau_2\, e^{-\frac{T_k}{\tau_2}} - \tau_l + \tau_2\right)}{(\tau_l - \tau_2)} \\ -\tau_2\left(e^{-\frac{T_k}{\tau_2}} - 1\right) \end{bmatrix},$$

$$C = \begin{bmatrix} \frac{k_1 k_2}{\tau_1 \tau_2} & 0 \end{bmatrix}.$$

The model of the plant at a given nominal sampling period $\bar{T}$ results

$$\bar{x}_{k+1} = A(\bar{T})\bar{x}_k + B(\bar{T})\bar{u}_k \tag{7.19}$$
$$\bar{y}_k = C\bar{x}_k. \tag{7.20}$$

7.5.2.1 Control law

The goal is to find u_k such that $y_k = \bar{y}_k$ or, what is the same, $Cx_k = C\bar{x}_k$. With this, and the discrete LTV plant (7.17) the expression for $y_{k+1} = \bar{y}_{k+1}$ is obtained:

$$C \cdot A(\bar{T})\bar{x}_k + C \cdot B(\bar{T})\bar{u}_k = C \cdot A(T_k)x_k + C \cdot B(T_k)u_k. \tag{7.21}$$

Thus, the control law results

$$u_k = (C \cdot B(T_k))^{-1}(-C \cdot A(T_k)x_k + C \cdot A(\bar{T})\bar{x} + C \cdot B(\bar{T})\bar{u}_k). \tag{7.22}$$

Since the state of the plant is not available we can use the following LTV model to obtain a estimation $\tilde{x}_k$ of the state x_k:

$$\tilde{x}_{k+1} = A(T_k)\tilde{x}_k + B(T_k)u_k \tag{7.23}$$
$$y_k = C\tilde{x}_k. \tag{7.24}$$

Then the control law results:

$$u_k = (C \cdot B(T_k))^{-1}(-C \cdot A(T_k)\tilde{x}_k + C \cdot A(\bar{T})\bar{x} + C \cdot B(\bar{T})\bar{u}_k). \tag{7.25}$$

Figure 7.23 shows the block diagram of this control law. The dynamics of the system composed of the pre-compensator and the plant is:

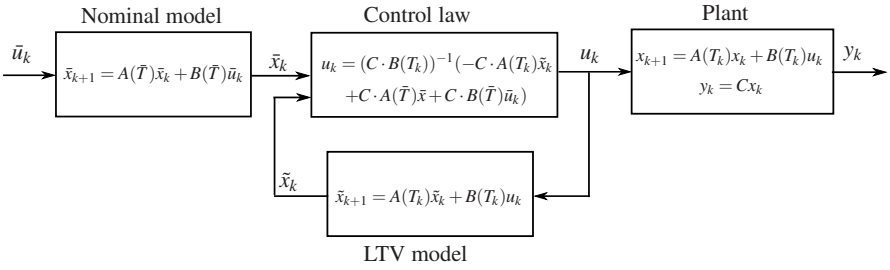

Fig. 7.23 Pre-filtering scheme.

$$\begin{aligned}
\begin{bmatrix} \bar{x} \\ \tilde{x} \\ x \end{bmatrix}_{k+1} &= \begin{bmatrix} A(\bar{T}) & 0 & 0 \\ B(T_k)(C \cdot B(T_k))^{-1}C \cdot A(\bar{T}) & -B(T_k)(C \cdot B(T_k))^{-1}C \cdot A(T_k) + A(T_k) & 0 \\ B(T_k)(C \cdot B(T_k))^{-1}C \cdot A(\bar{T}) & -B(T_k)(C \cdot B(T_k))^{-1}C \cdot A(T_k) & A(T_k) \end{bmatrix} \begin{bmatrix} \bar{x} \\ \tilde{x} \\ x \end{bmatrix}_k \\
&\quad + \begin{bmatrix} B(\bar{T}_k) \\ B(T_k)(C \cdot B(T_k))^{-1}C \cdot B(\bar{T}) \\ B(T_k)(C \cdot B(T_k))^{-1}C \cdot B(\bar{T}) \end{bmatrix} \bar{u}_k \\
y_k &= \begin{bmatrix} 0 & 0 & C \end{bmatrix} \begin{bmatrix} \bar{x} \\ \tilde{x} \\ x \end{bmatrix}_k .
\end{aligned} \tag{7.26}$$

7.5.2.2 Internal stability

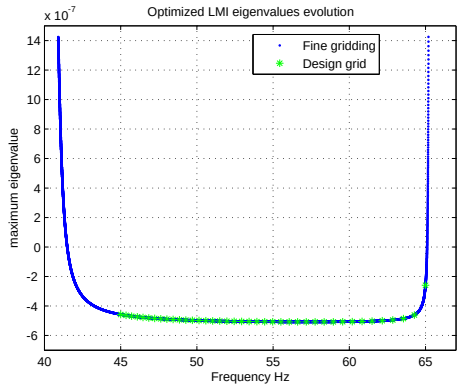

Fig. 7.24 Internal stability evaluation. Eigenvalues evolution of $L_{T_k}(P_G)$ using 40 in the design grid and 50000 points to check stability.

We are interested in analyzing the stability of (7.26) for all sampling periods $T_k \in \mathscr{T}$. The LMI gridding approach introduced in [2, 17] allows a simplified stability analysis that may be performed as follows. Let $\{\tau_0, \ldots, \tau_r\}$, be a sorted set of candidate sampling periods suitably distributed in $\mathscr{T}$. Then, one may solve the

following finite set of LMIs:

$$L_{\tau_i}(P) \leq -\alpha\mathbb{I}, \;\; i = 0,\ldots,r, \;\; \text{s.t.} \;\; P = P^\top > 0, \tag{7.27}$$

for a fixed $\alpha \in \mathbb{R}^+$. In case that the problem is feasible and a solution, $P = P_G$, is encountered, the negative-definite character of $L_{T_k}(P_G)$ is to be checked for intermediate values of T_k in each open subinterval (τ_i, τ_{i+1}). If this fails to be accomplished, (7.27) has to be solved again for a finer grid of $\mathscr{T}$. Otherwise, the procedure should be relaunched for a new interval $\mathscr{T}' \subset \mathscr{T}$.

In practice, it would be necessary to assure stability in the frequency interval $[45, 65]$ Hz. A line frequency variation of $\pm 10\%$ of the nominal value is assumed, which encompasses the requirements in international standards and many practical scenarios [13, 22, 21]. Indeed, frequency fluctuations up to $\pm 6\%$ of the nominal value are considered in the literature for different scenarios such as, for example, wind farms [21, 3], photo-voltaic generators [1] and microgrids [8], the usual being $\pm 2\%$ and below. Therefore, recalling the relation $T_n = N \cdot T_s$, one finds out that $\mathscr{T} = \left[(55N)^{-1}, (45N)^{-1}\right]$. However, it is worth pointing out that wider frequency variations may occur in specific situations, such as island grids [21]. In this case the internal stability should be verified according to the expected frequency variation interval.

Thus, applying the expected variation interval, 40 uniformly distributed points are selected in $\mathscr{T} = \left[5.55 \cdot 10^{-5}, 3.8461 \cdot 10^{-5}\right]$ s. These points are used to construct the set of LMIs (7.27), and a feasible solution $P = P_G$ with $\alpha = 100$ is obtained. Figure 7.24 depicts the maximum modulus eigenvalue of $L_{T_k}(P_G)$, detailing with a star the 40 points leading to the LMI formulation. The maximum modulus eigenvalue of $L_{T_k}(P_G)$ corresponding to a finer grid consisting of 50000 uniformly distributed point are also drawn in Figure 7.24. These points are used to check the sign of $L_{T_k}(P_G)$ in the intervals between the points defining the LMI set. It can be seen that $L_{T_k}(P_G) < 0$ for every point in this finer grid of the interval $\mathscr{T}$; hence, stability is dynamically preserved therein.

7.5.3 Experimental results

With this information, the sampling period T_s is updated to maintain the ratio $N = 400$. Figure 7.25 and 7.26 show the steady-state behaviour in case of the nonlinear load at 48 Hz and 53 Hz, respectively: the shape of the source current is nearly sinusoidal with a THD of 0.4 and $cos\phi$ at the port are unitary. Figure 7.27 shows the system behaviour when the source frequency changes from 48 Hz to 53 Hz in a 40 cycles ramp manner. Notice that the source current is preserving the required sinusoidal shape and adapting to the variable source voltage frequency.

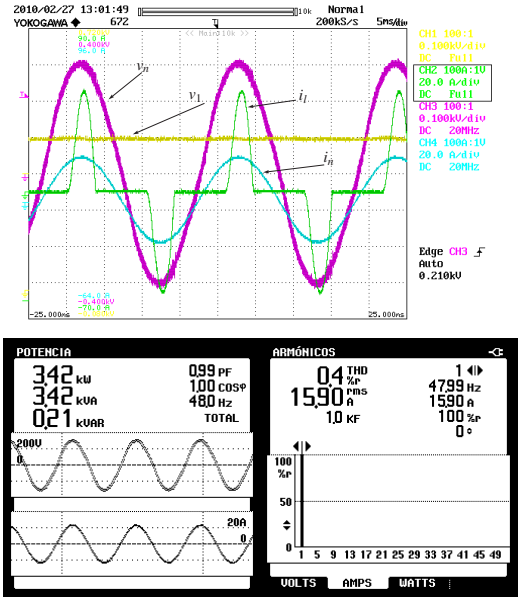

Fig. 7.25 Nonlinear load with active filter connected to the ac source working at 48 Hz with pre-compensation scheme. Top: v_n, v_1, i_l and i_n. Bottom: PF, $\cos\varphi$ and THD for i_n.

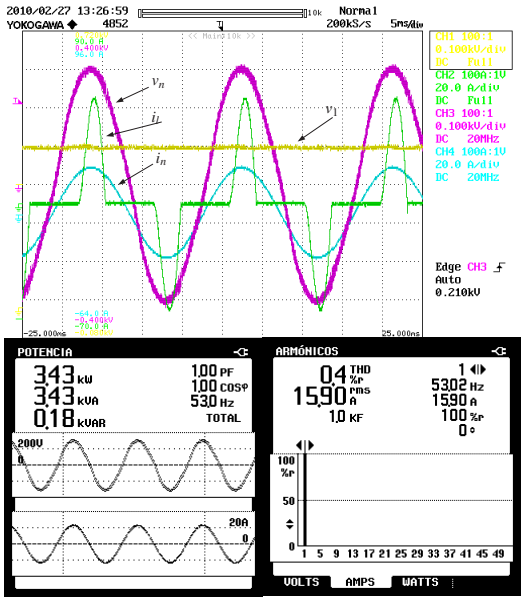

Fig. 7.26 Nonlinear load with active filter connected to the ac source working at 53 Hz with pre-compensation scheme. Top: v_n, v_1, i_l and i_n. Bottom: PF, $\cos\varphi$ and THD for i_n.

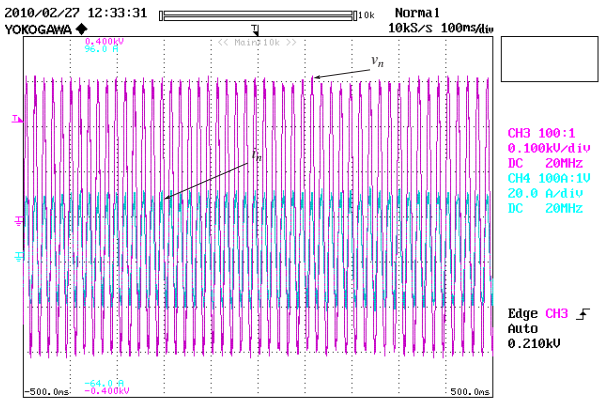

Fig. 7.27 Nonlinear load with active filter with pre-compensation scheme when the network frequency changes from 48Hz to 50Hz: v_n, i_n.

7.6 Robust design

A μ-synthesis approach can take advantage from the problem structure. Using the latter, the following controller is obtained for $T_s \in \mathscr{T} = \left[(55N)^{-1}, (45N)^{-1}\right]$, with $N = 400$:

$$\tilde{G}_x(z) = \frac{3.182z^7 - 6.432z^6 + 0.3002z^5 + 6.54z^4 - 3.791z^3 - 0.1361z^2 + 0.3089z + 0.02804}{z^7 - 0.2715z^6 - 1.165z^5 - 0.1143z^4 + 0.04983z^3 + 0.3138z^2 + 0.1596z + 0.02804}. \tag{7.28}$$

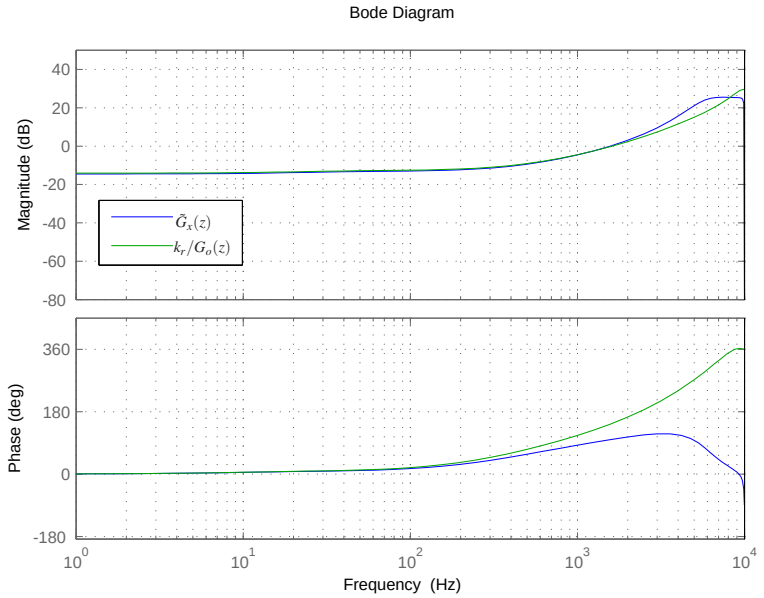

Fig. 7.28 Frequency response comparison between $\tilde{G}_x(z)$ and of the original controller $G_x(z) = k_r G_o^{-1}(z)$, with $k_r = 0.197$

Remark 7.1. Figure 7.28 shows that, for $T_s = \bar{T}$, the frequency responses of $\tilde{G}_x(z)$ and of the original controller, i.e. $G_x(z) = k_r G_o^{-1}(z)$, with $k_r = 0.197$ instead of the original $k_r = 0.7$, are very similar in the low and medium range[7]. Hence, aiming at maintaining the controller order as low as possible, in this case the practical implementation keeps the original structure for $G_x(z)$, with the adjusted parameter value $k_r = 0.197$.

It is worth to note that the μ-synthesis design seeks a causal filter $\tilde{G}_x(z)$ for a given frequency variation interval, while the standard design, in case of $G_o(z)$ a minimum phase system, uses $G_x = k_r/G_o(z)$ which is a non causal transfer function.

[7] In this application, it is expected to deal with currents with relevant harmonic components until the 13th or 15th harmonics which corresponds to 650 Hz and 750 Hz. Therefore the harmonic compensation is intended to take place within this region which is considered as the medium range in this remark

Finally, it is worth mentioning that, according to the Internal Model Principle, steady-state performance will be guaranteed when T_n (and, consequently, T_s) remains constant for sufficiently large time intervals.

Figures 7.29 and 7.30 show the open loop and sensitivity function frequency response of the odd-harmonic RC designed in Section 7.3 and the robust design of this section using $\tilde{G}_x(z)$. It can be seen that the tracking/rejection action is lower when using $\tilde{G}_x(z)$ as it represents a lower gain K_r, also with $\tilde{G}_x(z)$, the sensitivity function frequency response shows a better behaviour at the inter-harmonic frequencies.

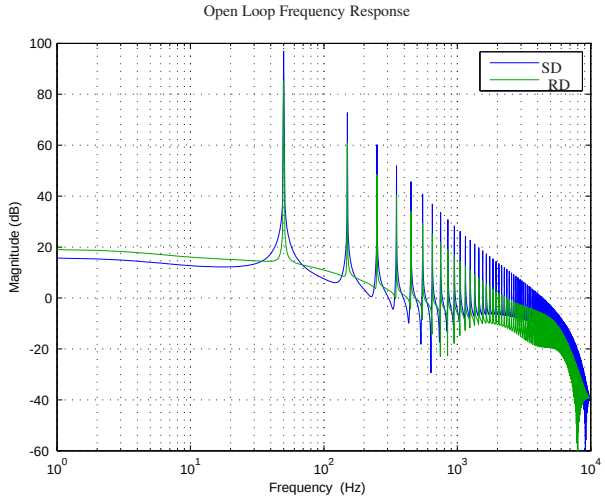

Fig. 7.29 Open loop magnitude response of function $G_l(z)$. Standard design (SD) and robust design (RD) comparison.

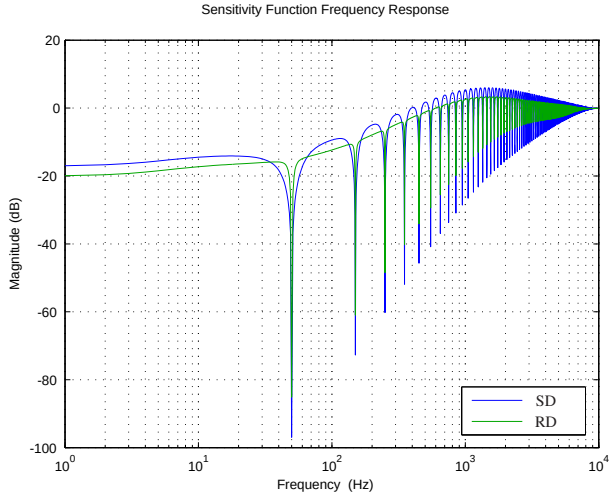

Fig. 7.30 Sensitivity function magnitude response. Standard design (SD) and robust design (RD) comparison.

7.6.1 Experimental results

Figures 7.31 and 7.32 show the system response when the network frequency is 49 Hz and 51 Hz, respectively, and the sampling period of the active filter repetitive controller is adapted as described in this Section. Notice that the performances are similar to the ones reported in Subsection 7.3.1 when both the network frequency and the controller sampling period work at nominal values (see Figure 7.8).

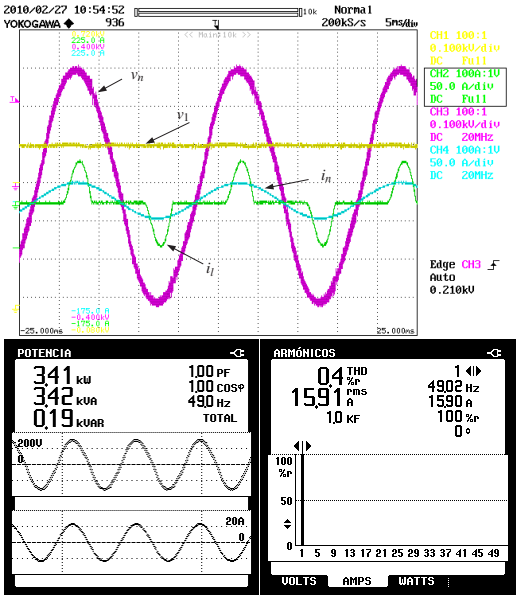

Fig. 7.31 Nonlinear load with active filter connected to the ac source working at 49 Hz using the robust design. Top: v_n, v_1, i_l and i_n. Bottom: PF, $\cos\varphi$ and THD for i_n.

The last experiment consist of a step change in frequency from 50 Hz to 51 Hz. Figure 7.33 shows that after a small transient the system performance is reached again.

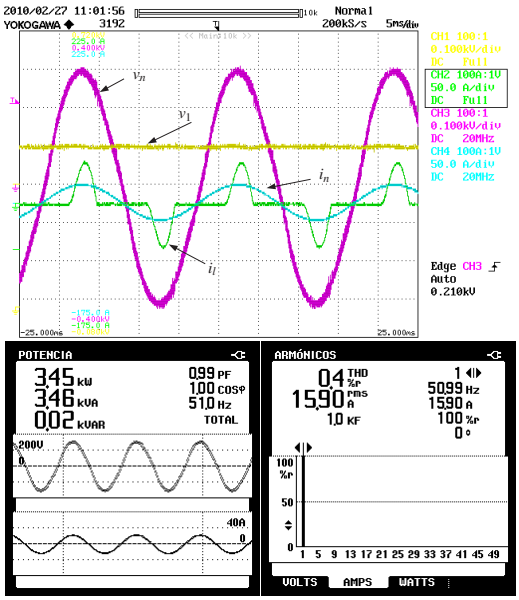

Fig. 7.32 Nonlinear load with active filter connected to the ac source working at 51 Hz using the robust design. Top: v_n, v_1, i_l and i_n. Bottom: PF, $\cos\varphi$ and THD for i_n.

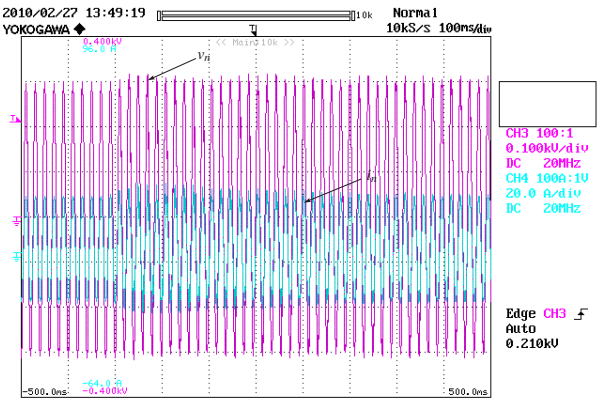

Fig. 7.33 Nonlinear load with active filter connected to the ac source using the robust design. v_n and i_n with a step change in the network frequency from 50 Hz to 51 Hz.

7.7 HORC

7.7.1 Experimental setup

The settings are the same used in Section 7.3.1 but using $k_r = 1$, changing the standard internal model by the second order odd-harmonic internal model described in Section 5.3.5:

$$I_{hodd}(z) = -\frac{\left(2z^{-\frac{N}{2}} + z^{-N}\right) H(z)}{1 + \left(2z^{-\frac{N}{2}} + z^{-N}\right) H(z)}$$

and defining

$$H(z) = 0.06241z^{-3} + 0.1293z^{-2} + 0.1963z^{-1} + 0.2239 + 0.1963z + 0.1293z^2 + 0.06241z^3.$$

Remark 7.2. In the active filter application, it is desirable to separate the dynamics of the two existing loops: the current loop and the energy shaping loop, where the current loop must be the fastest one. In this way the second-order odd-harmonic internal model, which is slower than the standard one, should be designed as fast as possible which is done using $k_r = 1$.

With this controller, the obtained open loop and sensitivity function magnitude response are shown in Figure 7.34 and 7.35, respectively. Also a comparison with the odd-harmonic repetitive control designed in Section 7.3 is shown in these Figures. Both Figures show the robustness improvement in face to frequency variations attained by the odd-harmonic HORC. In Figure 7.35, it is shown that the sensitivity function of the odd-harmonic HORC has a higher maximum gain in the high frequency range than the odd-harmonic RC, which can be considered as the cost of enhancing the robustness. However, the filter $H(z)$ has been designed to have a lower cut-off frequency to avoid problems due to the high gain in the highest frequency interval.

7.7.2 Experimental results

In the first experiment a rectifier is connected to the ac source, v_s, which is set to 50 Hz. The rectifier current, i.e. the load current i_l, has a total harmonic distortion (THD) of 62.6% and an RMS value of 19.56A. As shown in Figure 7.36, with the active filter connected in parallel with the rectifier, the shape of the current at the source port, i_n, is nearly sinusoidal, with a THD of 0.6%, while the power factor (PF) and $\cos\phi$ at the port are unitary. The figure also shows that the mean value of v_1 is maintained almost constant[8]. In the next experiment the same nonlinear load is connected to the ac source, v_s, now set to 49.5 Hz. As Figure 7.37 shows, the PF and the $\cos\phi$ remain close to unitary values and the THD for i_n is 1.7%. Although there is a small degradation this is considerably lower than the one presented in case of standard RC (see Figure 7.11) which shows the successful robustness improvement.

[8] v_2 is not shown due the limited number of channels in the instrumentation.

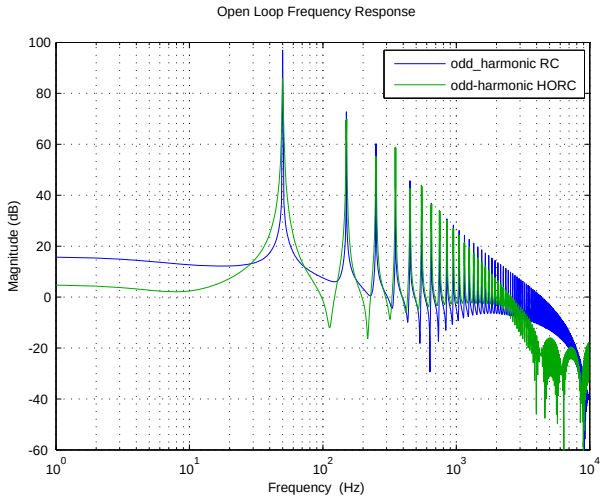

Fig. 7.34 Open loop magnitude response of function $G_l(z)$. Odd-harmonic RC and HORC design comparison.

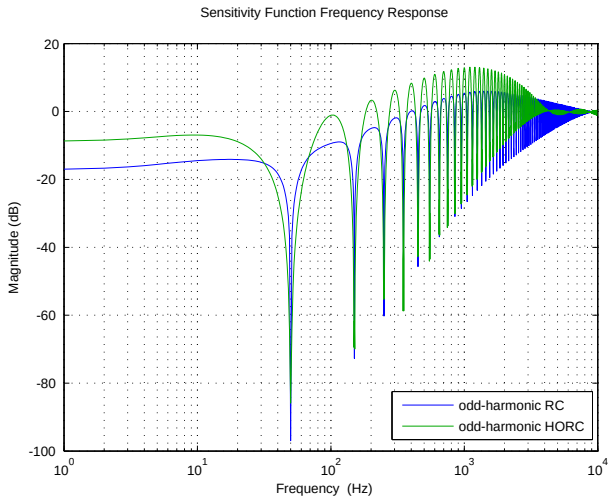

Fig. 7.35 Sensitivity function magnitude response. Odd-harmonic RC and HORC design comparison.

Figure 7.38 shows the results with the source configured to 50.5 Hz. As can be seen, also in this case the degradation is kept small with the PF and the $\cos\phi$ almost unitary and the THD of i_n with a value of 2.2%. It is also worth to note that, in all cases the THD is maintained below the one demanded in the current related normative, as standards IEC-61 000-3-$\{3,4\}$ and IEEE-519.

Finally, in Figure 7.39, a transition from 49.5 Hz to 50.5 Hz in the voltage source is depicted. The whole variation has been performed linearly in 40 cycles. It can

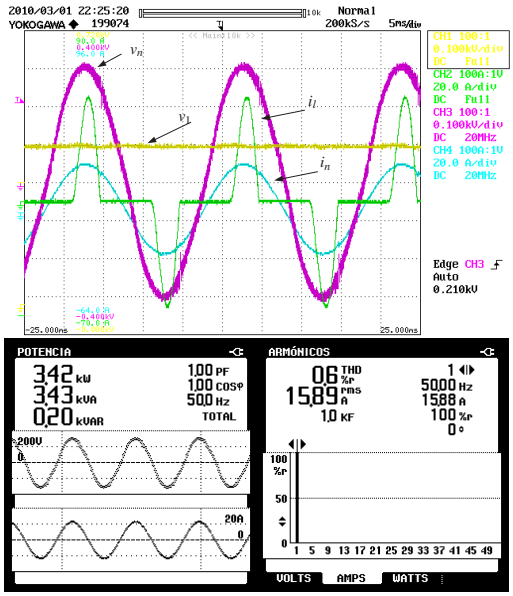

Fig. 7.36 Nonlinear load and the active filter connected to source (50 Hz) using the odd-harmonic HORC. (top) v_n, i_n, i_l and v_1 *vs* time; (bottom) PF, $\cos\phi$ and THD for i_n.

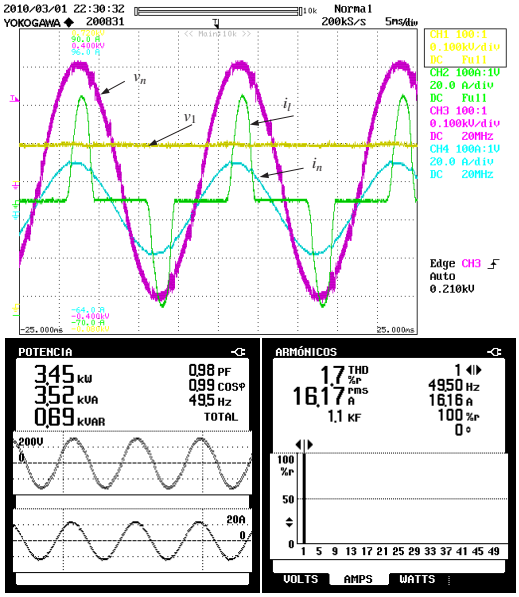

Fig. 7.37 Nonlinear load and the active filter connected to source (49.5 Hz) using the odd-harmonic HORC. (top) v_n, i_n, i_l and v_1 *vs* time; (bottom) PF, $\cos\phi$ and THD for i_n.

be noticed, that the control system maintains the performance during the complete transition.

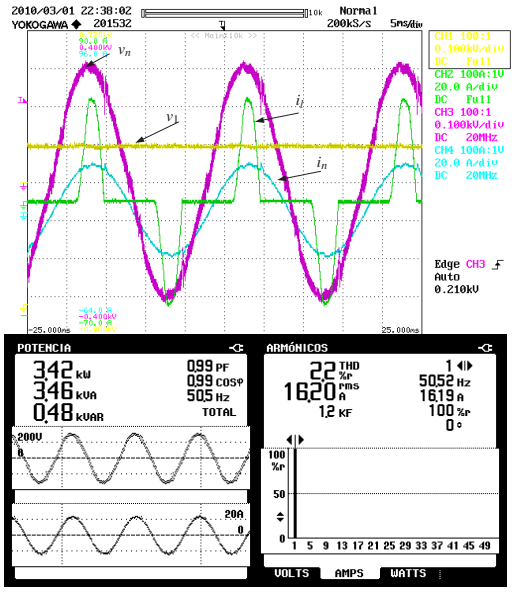

Fig. 7.38 Nonlinear load and the active filter connected to source (50.5 Hz) using the odd-harmonic HORC. (top) v_n, i_n, i_l and v_1 *vs* time; (bottom) PF, $\cos\phi$ and THD for i_n.

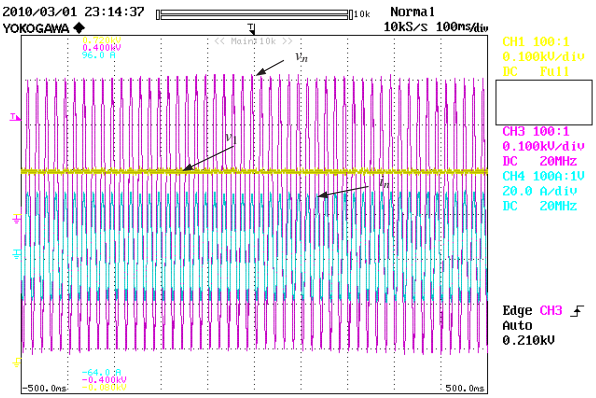

Fig. 7.39 Nonlinear load and the active filter connected to source using the odd-harmonic HORC. Frequency transition from 49.5 Hz to 50.5 Hz. v_n, i_n, and v_1 *vs* time.

For the next experiments, the capacitive-resistive load is connected to the ac source and the network frequency is set at 51 Hz and 49 Hz. Figures 7.40 and 7.41 show that the system performance is kept similar to the one obtained for the nominal frequency providing a unitary PF and $cos\phi$.

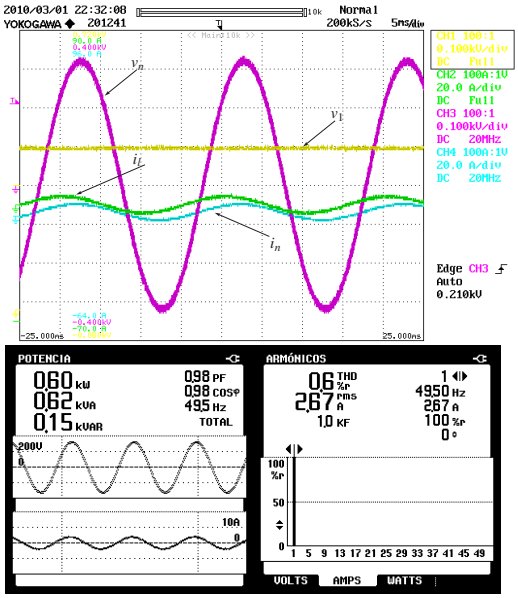

Fig. 7.40 Linear load and the active filter connected to source using the odd-harmonic HORC (49.5 Hz). (top) v_n, i_n, i_l and v_1 *vs* time; (bottom) PF, cos ϕ and THD for i_n.

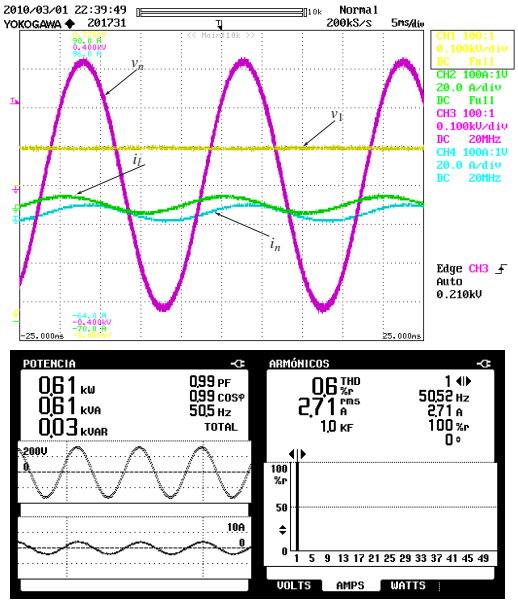

Fig. 7.41 Linear load and the active filter connected to source using the odd-harmonic HORC (50.5 Hz). (top) v_n, i_n, i_l and v_1 *vs* time; (bottom) PF, cos ϕ and THD for i_n.

7.8 Conclusions

This work shows the architecture, some design issues and a stability analysis for an active filter digital controller based on repetitive control.

The odd-harmonic RC with time varying sampling period designed in Section 7.4 includes an adaptive mechanism that follows the time-variation of the electrical network frequency in such a way that the well-known advantages of repetitive control are kept also maintaining its low computational cost. Theoretical and experimental results prove that the controlled system has a good performance and that, using the frequency adaptation mechanism, it is able to cope with more aggressive frequency changes than the usual ones in electrical distribution networks. However, the variation of the sampling period makes harder both the practical implementation and the theoretical stability analysis.

The controller in Section 7.5, besides the sampling period adaptation, includes an adaptive pre-compensation procedure to follow possible network frequency variations without losing the performance of the repetitive controller. This technique assures inner-loop invariance and, consequently, outerloop stability, independently of sampling period variations and of the frequency observer dynamics.

Section 7.6 presents a strategy based on the sampling period adaptation showed in previous sections. However, as this operation may negatively affect closed-loop stability, the controller was obtained through a small-gain theorem-based robust control design technique that assures BIBO stability in the required sampling period interval, with no restrictions on its rate of change. This interval is set from the expected interval of variation of the network frequency, which is assumed to be known. Theoretical and experimental results showed good performance of the controlled system.

Also, it is worth recalling the relationship between the stabilizing controller (7.28) designed in Subsection 7.6 and the original stabilizing controller (7.13) derived in Section 7.3, which was pointed out in Remark 7.1. This seems to be in accordance with the discussion in [19] for the constant sampling period case, where it is conjectured that the traditional scheme for $G_x(z)$ is quite close to the optimum controller structure. Further research will study the problem in the time-varying sampling period framework.

A second order internal model for HORC has been also implemented. Although, this repetitive controller achieves a narrower frequency range of operation without reducing its performance it does not employs a frequency observer nor an adaptive mechanism. Finally, the second order odd-harmonic HORC has similar computational cost compared with the standard full-harmonic RC and the stability analysis of this controller remains in the LTI systems frame. A new stable second order internal model for repetitive controllers has been proposed and studied in Section 7.7. This controller has been validated experimentally in the current loop of the shunt active filter providing a robustness improvement. Although, this repetitive controller achieves a narrower frequency range of operation without reducing its performance it does not employ a frequency observer nor an adaptive mechanism as the precedent controllers. Furthermore, the stability analysis of this controller remains in the LTI systems frame. Additionally, the implementation complexity turns out to be similar when comparing the order and computational cost of the standard (full-harmonic) repetitive controller and the second order odd-harmonic repetitive controller proposed here.

Finally, notice that in this work the current reference signal is constructed from the carrier extractor, which yields the voltage source normalized fundamental component. This component could be shifted, by an appropriate filtering before constructing the current reference. This procedure would allow the use of the proposed controller architecture for phase shift control purposes. Thus, in upcoming applications it would be possible to provide a controllable phase shift in the fundamental current which may be used to contribute to voltage control in the distribution network.

References

1. M. Ali, J. Tamura, and B. Wu. Smes strategy to minimize frequency fluctuations of wind generator system. In *Industrial Electronics, 2008. IECON 2008. 34th Annual Conference of IEEE*, pages 3382 –3387, nov. 2008.
2. P. Apkarian and R. Adams. Advanced gain-scheduling techniques for uncertain systems. *IEEE Transactions on Control Systems Technology*, 6(1):21–32, 1998.
3. S. Bolik. *Modelling and Analysis of Variable Speed Wind Turbines with Induction Generator during Grid Fault*. Ph.D. Thesis, Aalborg University, 2004.
4. D. Bruijnen, M. van de Molengraft, and M. Steinbuch. Efficient IIR notch filter design via multirate filtering targeted at harmonic disturbance rejection. In *Proceedings of the 4th IFAC Symposium on Mechatronic Systems*, pages 318–323, Heidelberg, Germany, 2006.
5. S. Buso, L. Malesani, and P. Mattavelli. Comparison of current control techniques for active filters applications. *IEEE Transactions on Industrial Electronics*, 45:722–729, october 1998.
6. V. Corasaniti, M. Barbieri, P. Arnera, and M. Valla. Hybrid active filter for reactive and harmonics compensation in a distribution network. *IEEE Transactions on Industrial Electronics*, 56(3):670 –677, 2009.
7. R. Costa-Castelló, R. Griñó, R. Cardoner Parpal, and E. Fossas. High-performance control of a single-phase shunt active filter. *IEEE Transactions on Control Systems Technology*, 17(6):1318–1329, Nov. 2009.
8. M. Datta, T. Senjyu, A. Yona, T. Funabashi, and C.-H. Kim. A frequency-control approach by photovoltaic generator in a pv-diesel hybrid power system. *IEEE Transactions on Energy Conversion*, 26(2):559 –571, june 2011.
9. F. Freijedo, J. Doval-Gandoy, O. Lopez, P. Fernandez-Comesana, and C. Martinez-Penalver. A signal-processing adaptive algorithm for selective current harmonic cancellation in active power filters. *IEEE Transactions on Industrial Electronics*, 56(8):2829 –2840, 2009.
10. H. Fujioka. Stability analysis for a class of networked-embedded control systems: A discrete-time approach. In *Proceedings of the American Control Conference*, pages 4997–5002, 2008.
11. S. Galeani, S. Tarbouriech, M. Turner, and L. Zaccarian. A tutorial on modern anti-windup design. *European Journal of Control*, 15:418 440, 2009.
12. P. Hippe. *Windup in Control: Its Effects and Their Prevention*. Advances in Industrial Control. Springer, 1st edition, May 2006.
13. IEC. Electromagnetic compatibility part 2-4: Environment compatibility levels in industrial plants for low-frequency conducted disturbances. *IEC 6100-2-4:2002*, 2002.
14. C. Lascu, L. Asiminoaei, I. Boldea, and F. Blaabjerg. Frequency response analysis of current controllers for selective harmonic compensation in active power filters. *IEEE Transactions on Industrial Electronics*, 56(2):337 –347, 2009.
15. P. Mattavelli. A closed-loop selective harmonic compensation for active filters. *IEEE Transactions on Industry Applications*, 37(1):81–89, january 2001.
16. Y. S. Ryu and R. Longman. Use of anti-reset windup in integral control based learning and repetitive control. In *Proceedings of the IEEE International Conference on Systems, Man, and Cybernetics, 1994. 'Humans, Information and Technology'*, volume 3, pages 2617 –2622 vol. 3, oct 1994.
17. A. Sala. Computer control under time-varying sampling period: An LMI gridding approach. *Automatica*, 41(12):2077–2082, 2005.
18. D. Sbarbaro, M. Tomizuka, and B. L. de la Barra. Repetitive control system under actuator saturation and windup prevention. *Journal of Dynamic Systems, Measurement, and Control*, 131(4):044505, 2009.

19. S. Songschonc and R. W. Longman. Comparison of the stability boundary and the frequency response stability condition in learning and repetitive control. *International Journal of Applied Mathematics and Computer Science*, 13(2):169–177, 2003.
20. Y. S. Suh. Stability and stabilization of nonuniform sampling systems. *Automatica*, 44(12):3222–3226, 2008.
21. R. Teodorescu, M. Liserre, and P. Rodrguez. *Grid converters for photovoltaic and wind power systems*. Adaptive and Learning Systems for Signal Processing, Communications and Control Series. John Wiley & Sons, Ltd., August 2011.
22. U C T E. Technical paper: Definition of a set of requirements to generating units. 2008.
23. A. Varschavsky, J. Dixon, M. Rotella, and L. Moran. Cascaded nine-level inverter for hybrid-series active power filter, using industrial controller. *IEEE Transactions on Industrial Electronics*, 57(8):2761 –2767, 2010.

Chapter 8
Conclusions and future work

8.1 Conclusions

A wide range of control applications in engineering must deal with periodic signals which usually enter the system as input references or disturbances. At the same time many of these applications operate with periodic signals whose frequency must change by specification or experiences variations due to the application intrinsic characteristics or abnormal functioning. In this context, repetitive control has been proven to be an efficient technique to deal with constant period signals, nevertheless, its performance decays importantly when the frequency of the signals is not accurately known or varies with time. This thesis presents some contributions to the topic of repetitive control working under varying frequency conditions. These contributions are summarized as follows:

- **Stability analysis methods for repetitive control with varying sampling time**. Two stability analysis techniques have been presented: an LMI gridding analysis and a robust control theory approach. Both techniques are useful to verify the stability of repetitive controllers that adapt their sampling period in order to follow period changes in the reference/disturbance signal. The allowable sampling period variation is expressed as an interval. In general, the results show that the obtained interval is larger when using the robust control theory analysis. Although the LMI analysis renders necessary conditions for a sufficient stability condition, it is found that in applications where the varying sampling period is set by a digital clock, the stability can be assured within the interval when the possible sampling periods resulting from the clock resolution are included in the analysis. The robust control approach gives sufficient conditions for stability, this due to the intrinsic conservatism in the small gain theorem.
  Although several proposals reported in the literature make use of repetitive controllers working with varying sampling period, the stability analysis scenario had not been properly established. Therefore, this results contribute to the stability analysis framework for repetitive control applications that operate with varying sampling period.

- **Design methods of repetitive controllers dealing with varying frequency conditions**. Two designs methodologies aimed at finding a RC which assures performance and stability for a given variation in the frequency of the periodic signals are presented. In both schemes the performance preservation is achieved us-

ing the sampling period variation approach. To ensure stability within the given frequency variation interval, a pre-compensation scheme and a robust synthesis approach has been proposed. The pre-compensation scheme assures the stability annihilating the structural changes caused by the sampling period variations through a LTV compensator, thus transforming the LTV stability framework into an LTI one. The robust synthesis design is achieved considering the sampling period variation and the delay element in the IM as an norm bounded uncertainties. Using the known frequency interval the norm of the uncertainty due to the sampling period variation can be calculated. As a result, a new stabilizing filter is obtained which assures the stability of the system for the given interval. The obtained controller results to be similar to the standard design in that the obtained stabilizing filter frequency response may resemble the standard filter one with slight differences. However, the new design method differs form the standard one in that the obtained filter is defined to be proper from design.
These design methods are innovative in the sense they offer a varying sampling period based strategy for RC that assures the stability and performance within a predefined frequency variation interval of the signals to be tracked or rejected.

- **Robust performance of repetitive control using high order internal models**. Following a different concept, the existing HORC has been modified to obtain an IM intended to deal with periodic signals with only odd-harmonic frequency components. Thus, the odd-harmonic HORC is introduced. The IM design provides action for wider interval around the odd-harmonic and fundamental frequencies for which the controller has been set, thus providing robustness in face to frequency changes. As a difference with other methods including the preceding ones in this thesis, this strategy does not need any frequency observer or estimation.
  This design contributes to the field of study in RC in that the odd-harmonic HORC obtains an important reduction of the computational burden. This is because the order of the internal model is twice as low as the conventional full-harmonic HORC. In fact, the computational load is similar to the one obtained with standard RC, i.e. the standard internal model.
  Additionally, the stability of the IM used in HORC has been analysed. It is found that several internal models may result BIBO unstable. Although, this fact does not affect the closed loop stability it is well known that it makes the practical implementations harder. For that reason, taking into account the actuator saturation, an AW strategy has been proposed. This is based on a MRAW scheme and the design incorporates an optimal LQ procedure looking for obtaining a deadbeat transition to recover the system. As a result, this AW technique achieves smaller error per period when compared with similar proposals.
  Only few AW strategies for RC have been reported. This AW strategy designed for RC is innovative since it provides: 1) a simple and low order design, 2) thanks to the use of the MRAW scheme, the RC is isolated from the saturation effects avoiding transients and convergence problems in the IM, 3) a deadbeat transition is sought using an optimal LQ procedure which provide a faster transition to recover the system.

- **Experimental validation**. Two experimental applications have been utilised to perform the experimental validation of the presented analysis and control strategies. A mechatronic plant called Roto-magnet and an active power filter.
  The Roto-magnet application is an educational platform designed to demonstrate the internal model principle in case of periodic disturbances. The purpose of using this plant to validate the approaches in this thesis is to cover the extensive field of rotating machinery applications where repetitive control can be used. The control goal is to maintain the desired speed rejecting the periodic disturbances. To obtain varying frequency conditions in the experiments a varying speed reference profiles were applied. The stability analysis and design strategies for RC working under varying sampling period lead to successful results facing varying frequency disturbances. The frequency intervals defined in the design and obtained in the analysis allow a wide range of speed operation. The harmonic components of the disturbance are effectively rejected within the speed interval achieving a performance that is practically the same as that of the nominal design. Also the proposed optimal LQ AW design has been implemented to be used in the HORC case. It is shown that tracking and rejection tasks can benefit from this compensation when actuator saturation occurs. The obtained error is lower compared with other techniques while the controller control action remains unaffected by the actuator saturation.
  The active power filter is an industrial-oriented application. The interest in this field of engineering has been growing importantly due to creation of new demanding needs and applications, e.g. the increment of alternative energy sources connected to the network and new needs in hybrid and electrical transportation. Thus, the control objective in the active power filter application is focused on power factor correction and harmonic compensation. The varying frequency conditions are caused by the network behaviour and the power factor and harmonic distortion are consequence of the loads connected to the grid. The experimental results show that the RC with varying sampling period adaptation achieves a very high performance despite frequency network changes. The analysis assures stability for the expected operating interval: $[45,\ 55]$ Hz, while the design strategies fulfil successfully the stability and performance requirements, i.e. PF close to 1 and low THD. Since the load current has in general odd frequency components, an odd-harmonic HORC has been implemented. The experimental results show that this scheme works efficiently maintaining a satisfactory performance for the given frequency interval. The efficiency relying on having lower computational burden compared with full action HORC and avoiding the use of any frequency observer/estimation device.

8.2 Future work

Chapter 3 analyses the stability of RC under a varying sampling period scheme. However, some conservatism exists due to the applied stability criteria, specially in the robust control theory approach. A research topic remains open in this field where additional criteria might be established to obtain some reduction in the conservatism. LTV systems framework might be considered as an important research line not only for the stability analysis, but also may be used in a formal transient

state study. The last topic is also relevant when considering the use of a frequency observer.

Chapter 4 present two design methodologies for RC dealing with varying frequency signals. A suggested research line involves the use of LTV systems theory to reduce the conservatism allowing for obtaining a better robust stability and performance trade off. Additionally, due to the structure of the RC, an interesting topic is the design of controllers that provide also robustness against plant uncertainties.

In Chapter 5 an odd-harmonic HORC is described. It was shown that high order internal models that incorporate the robustness filter $H(z)$ in a conventional design may result BIBO unstable. This fact limits the practical implementation specially for the third and higher order HORC. A research topic in the design of the robustness filter for HORC intended to generate BIBO stable IM might facilitate the practical implementation of these controllers.

In Section 5.4 an optimal LQ AW design has been presented. This design includes a condition to assure the internal stability of the system. Moreover, to derive the internal stability, the static non-linear saturation function is said to accomplish a so called sector condition. This condition entails some conservatism since the saturation function is considered to belong to the first and third quadrant. Upcoming research might be focused on finding a less conservative condition to improve the design methods of this AW compensator.

Appendices

Appendix A
Stabilizing filter implementation

Condition 2 of Proposition 2.1 should be fulfilled with an appropriate design of filter $G_x(z)$. The fundamental issue is to provide enough leading phase to cancel out the phase of $G_o(z)$ [1]. In general, it would be sufficient that $G_x(z)$ approximates the inverse of $G_o(z)$ in the passband of the filter $H(z)$ [1, 2].

In case of minimum phase systems $G_x(z)$ is implemented as the inverse of the complementary sensitivity function $G_o(z)$, then $G_x(z) = k_r G_o^{-1}(z)$. The causality issue is solved using the structure of the repetitive controller since $G_x(z)$ is in series with the memory loop element.

Thus, the implementation may follow the scheme in Figure A.1, where r_d stands for the relative degree of $G_o(z)$.

In case of non-minimum phase systems, the design follows the Zero Phase Error Tracking Controller (ZPETC) approach [3] applied to a prototype repetitive controller (PRC) [4]. Thus, using $G_o(z) = B(z)/A(z)$, where $B(z) = B^+(z)B^-(z)$, with $B^+(z)$ and $B^-(z)$ containing the minimum and non minimum phase zeros respectively, then $G_x(z)$ is defined as:

$$G_x(z) = k_r \frac{A(z)B^-(z^{-1})}{B^+(z)b_{max}}, \tag{A.1}$$

with $b_{max} = [B^-(1)]^2$, $B^-(z^{-1})$ comes from $B^-(z)$ substituting z for z^{-1}.

Thus, applying this design of $G_x(z)$ to the closed loop function $G_o(z)$ results:

$$G_x(z)G_o(z) = k_r \frac{B^-(z^{-1})B^-(z)}{b_{max}}.$$

To see how zero phase response is achieved we may express the frequency response of $B^-(z)$ as the sum of its real and imaginary components:

$$B^-(e^{j\omega}) = \mathrm{Re}(w) + j\,\mathrm{Im}(w).$$

With this, the frequency response of $B^-(z^{-1})$ may be written as follows

$$B^-(e^{-j\omega}) = \mathrm{Re}(w) - j\,\mathrm{Im}(w).$$

Then, in the frequency domain we have:

$$B^-(e^{-j\omega})B^-(e^{j\omega}) = \mathrm{Re}(w)^2 + \mathrm{Im}(w)^2,$$

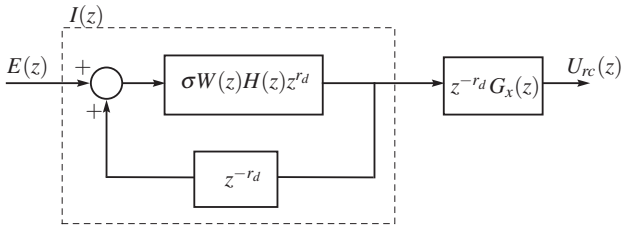

Fig. A.1 Implementation of $G_x(z)$ and the internal model, $W(z)$ is a delay function, $H(z)$ a null-phase low pass filter, and $\sigma \in \{-1, 1\}$.

which has zero phase for all ω. As a consequence, the ZPETC (A.1) compensates for the non minimum phase zeros and cancels the phase of $G_o(z)$. Furthermore, the term b_{max} is used to obtain gain close to 1 at low frequencies when $k_r = 1$.

Finally, it can be noted that the implementation also has the structure of Figure A.1 which is used to tackle the causality issue in $G_x(z)$.

References

1. T. Inoue. Practical repetitive control system design. In *Proceedings of the 29th IEEE Conference on Decision and Control*, pages 1673–1678, 1990.
2. G. Pipeleers, B. Demeulenaere, and S. Sewers. Robust high order repetitive control: Optimal performance trade offs. *Automatica*, 44:2628–2634, 2008.
3. M. Tomizuka. Zero phase error tracking algorithm for digital control. *Journal of Dynamic Systems, Measurements and Control*, 109:65–68, March 1987.
4. M. Tomizuka, T.-C. Tsao, and K.-K. Chew. Analysis and synthesis of discrete-time repetitive controllers. *Journal of Dynamic Systems, Measurement, and Control*, 111:353–358, September 1989.

Appendix B
Sampling period variation interval calculation

The robust control theory used to analyse the system stability in Section 3.4 yields an interval in which the sampling period variation is allowed preserving stability. The derivation of this interval involves the calculation of the exponential matrix norm $\|\Delta(\theta_k)\|$, see Theorem 3.1. Different norm bounds can be utilised to obtain the interval, each one entailing some degree of conservatism. In Section 6.4.3, taking advantage of having a first order plant, a direct calculation has been employed, while in Section 7.4.2, for a second order system, three norm bounds have been applied: a numerical calculation, the log norm of a matrix with respect to the 2-norm [2] and a Schur decomposition-derived bound [4]. This section, develops the procedure to obtain the results in Sections 6.4.3 and 7.4.2 to calculate the permissible sampling period variation interval. The above cited papers has been taken as a reference to describe the procedures. Other bounds and characteristics of the matrix exponential norm can be seen in [3].

Once the γ value of the system has been obtained:

$$\gamma_{\bar{T}} = (1+\varepsilon)\|G_{\bar{T}}(z)\|_\infty, \;\; \varepsilon > 0,$$

the variation internal is derived using the following stability condition (see Theorem 3.1):

$$\gamma_{\bar{T}}\|\Delta(\theta_k)\| \leq 1.$$

The following sections develop the procedures to obtain the variation intervals that assure system stability in the light of Theorem 3.1.

B.1 First order plant case

With the stability condition:

$$\|\Delta(\theta_k)\| = \|\Delta(T_k - \bar{T})\| \leq \gamma_{\bar{T}}^{-1}$$

and using

$$\Delta(\theta_k) = \int_0^\theta e^{At}dt = A^{-1}\left(e^{A\theta} - 1\right)$$

for $\theta > 0$,

the stability condition results:

$$A^{-1}\left(e^{A\theta}-1\right) \leq \frac{1}{\gamma}.$$

In case of first order plant we obtain:

$$\theta = T_k - \bar{T} \leq \frac{1}{A}\log\left(1+\frac{A}{\gamma_{\bar{T}}}\right).$$

Finally, we can directly have the upper limit of the interval:

$$T_u = \bar{T} + \frac{1}{A}\log\left(1+\frac{A}{\gamma_{\bar{T}}}\right).$$

Similar calculation can be done for $\theta < 0$, then we have

$$\Delta(\theta_k) = \int_{\theta}^{0} e^{At}dt = -A^{-1}\left(e^{A\theta}-1\right),$$

resulting the lower limit of the interval:

$$T_l = \bar{T} + \frac{1}{A}\log\left(1-\frac{A}{\gamma_{\bar{T}}}\right).$$

B.2 Higher order plants case

B.2.1 Numerical calculation

The numerical calculation procedure consist simply in obtain the matrix norm and calculate directly the stability interval. Thus, we have

$$\|\Delta(\theta_k)\| = \|\int_{0}^{\theta} e^{At}dt\| = \|A^{-1}(e^{A\theta}-1)\|,$$

then, to accomplish stability it is needed that

$$\|A^{-1}(e^{A\theta}-1)\| \leq \gamma_{\bar{T}}^{-1}.$$

Thus we need to find:

$$\theta_{max} = \max\{\theta \geq 0 \mid \|A^{-1}(e^{A\theta}-1)\| \leq \gamma_{\bar{T}}^{-1}\}$$

and

$$\theta_{min} = \min\{\theta < 0 \mid \|A^{-1}(e^{A\theta}-1)\| \leq \gamma_{\bar{T}}^{-1}\}.$$

After that, it is possible to calculate $T_{max} = \theta_{max} + \bar{T}$ and $T_{min} = \theta_{min} + \bar{T}$.

B.2.2 Log norm bound

Given a matrix $A \in \mathbb{R}^{nxn}$, the following is obtained [1]:

$$\|e^{At}\| \leq e^{\mu(A)t},\ \forall\, t \geq 0,$$

with

$$\mu(A) := max\left\{\mu \mid \mu \in eigenvalue\ of (A + A^T)/2\right\},$$

the log norm of A (associated with the 2-norm). A^T being the transpose of A.

Using the later and with $\theta > 0$ we have:

$$\|\Delta(\theta_k)\| \leq \int_0^{\theta} \|e^{At}\| dt \leq \int_0^{\theta} e^{\mu(A)t} dt,$$

thus,

$$\|\Delta(\theta_k)\| \leq \int_0^{\theta} e^{\mu(A)t} dt = \frac{1}{\mu(A)}(e^{\mu(A)\theta} - 1),$$

then, to accomplish the stability condition

$$\frac{1}{\mu(A)}(e^{\mu(A)\theta} - 1) \leq \gamma_{\bar{T}}^{-1}.$$

Thus, the upper limit can be obtained:

$$T_u = \bar{T} + \frac{1}{\mu(A)} \log\left(1 + \frac{\mu(A)}{\gamma_{\bar{T}}}\right).$$

A similar procedure for $\theta < 0$ can be used:

$$\|\Delta(\theta_k)\| \leq \int_0^{-\theta} \|e^{-At}\| dt \leq \int_0^{-\theta} e^{\mu(-A)t} dt,$$

thus,

$$\|\Delta(\theta_k)\| \leq \int_0^{-\theta} e^{\mu(-A)t} dt = \frac{1}{\mu(-A)}(e^{\mu(-A)(-\theta)} - 1),$$

then, to accomplish the stability condition

$$\frac{1}{\mu(-A)}(e^{\mu(-A)(-\theta)} - 1) \leq \gamma_{\bar{T}}^{-1}.$$

Therefore, the lower limit can be obtained:

$$T_l = \bar{T} - \frac{1}{\mu(-A)} \log\left(1 + \frac{\mu(-A)}{\gamma_{\bar{T}}}\right).$$

B.2.3 Schur decomposition-derived bound

Given the Schur decomposition of A,

$$Q^T AQ = D + N,$$

with Q an orthogonal matrix, $D = diag(\lambda_i)$, λ_i being the eigenvalues of A and $N = (n_{ij})$ a strictly upper triangular matrix, n_{ij} being the elements of A, where $n_{ij} = 0$ for $i \geq j$. We have (see the proof in [3]):

$$\|e^{At}\| \leq e^{\alpha_1 t} \sum_{k=0}^{n-1} \frac{\|Nt\|^k}{k!}, \ \forall\, t \geq 0,$$

with α_1 the maximum real part of the eigenvalues of A.

Then, using the definition for $\Delta(\theta_k)$ we can find the following:

$$\|\Delta(\theta_k)\| \leq \int_0^\theta \|e^{At}\| dt \leq \int_0^\theta e^{\alpha_1 t} \sum_{k=0}^{n-1} \frac{\|Nt\|^k}{k!} dt = \Lambda(\theta),$$

therefore

$$\|\Delta(\theta_k)\| \leq \Lambda(\theta),$$

with

$$\Lambda(\theta) = \begin{cases} \sum_{k=0}^{n-1} \|N\|^k \left(-\frac{(-1)^k}{\alpha_1^{k+1}} + \frac{e^{\alpha_1 \theta}}{\alpha_1} \sum_{l=0}^{k} \frac{(-1)^l \theta^{k-l}}{\alpha_1^l (k-l)!} \right), & if\ \theta \geq 0,\ \alpha_1 \neq 0 \\ \sum_{k=0}^{n-1} \|N\|^k \left(-\frac{(-1)^k}{\alpha_2^{k+1}} + \frac{e^{\alpha_2 \theta}}{\alpha_2} \sum_{l=0}^{k} \frac{(-1)^l \theta^{k-l}}{\alpha_2^l (k-l)!} \right), & if\ \theta < 0,\ \alpha_2 \neq 0 \\ \sum_{k=0}^{n-1} \frac{\|N\|^k}{(k+1)!} |\theta|^{k+1}, & otherwise \end{cases}$$

where α_2 is the maximum real part of the eigenvalues of $-A$.

Thus we are interested in finding $\theta_{max} = \max\{\theta \geq 0 \mid \Lambda(\theta) \leq \gamma_{\bar{T}}^{-1}\}$ and $\theta_{min} = \min\{\theta < 0 \mid \Lambda(\theta) \leq \gamma_{\bar{T}}^{-1}\}$ and calculate $T_{max} = \theta_{max} + \bar{T}$ and $T_{min} = \theta_{min} + \bar{T}$.

References

1. G. Dahlquist. *Stability and Error Bounds in the Numerical Integration of Ordinary Differential Equations*. Kungl. Tekniska Högskolans Handlingar. Almqvist & Wiksells, 1959.
2. H. Fujioka. Stability analysis for a class of networked-embedded control systems: A discrete-time approach. In *Proceedings of the American Control Conference*, pages 4997–5002, 2008.
3. C. V. Loan. The sensitivity of the matrix exponential. *SIAM Journal on Numerical Analysis*, 14(6):971–981, 1977.
4. Y. S. Suh. Stability and stabilization of nonuniform sampling systems. *Automatica*, 44(12):3222–3226, 2008.

Appendix C
Optimal LQ design in LMI form

The conventional optimal LQ procedure to obtain a state feedback design can be put in terms of an LMI [2, 1]. We are interested in finding the expression of the following problem into an LMI frame:

$$\min_K \sum_{k=0}^{\infty} \chi_k^T Q_p \chi_k$$

subject to:

$$\begin{aligned} \chi_{k+1} &= A\chi_k - B\sigma_{2,k} \\ \sigma_{2,k} &= K\chi_k, \end{aligned}$$

where $Q = Q^T > 0$. Thus, using the candidate Lyapunov function $V(\chi_k) = \chi_k^T P \chi_k$ for the system $\chi_{k+1} = (A - BK)\chi_k$ we have that:

$$V(\chi_{k+1}) - V(\chi_k) = \chi_k^T ((A - BK)^T P(A - BK) - P)\chi_k. \tag{C.1}$$

Using the $S-$procedure we can state the following:

$$V(\chi_{k+1}) - V(\chi_k) + \chi_k^T Q_p \chi_k < 0, \tag{C.2}$$

resulting

$$\chi_k^T ((A - BK)^T P(A - BK) - P + Q_p)\chi_k < 0. \tag{C.3}$$

Summing both sides of equation (C.2) from 0 to ∞, it is obtained

$$\sum_{k=0}^{\infty} \chi_k^T Q_p \chi_k < -(V(\chi_\infty) - V(\chi_0)),$$

then, assuming that the candidate Lyapunov function $V(\chi_\infty) = 0$ we have

$$\sum_{k=0}^{\infty} \chi_k^T Q_p \chi_k < \chi_0^T P \chi_0,$$

which constitutes the upper bound for the cost function. If we minimize $\chi_0^T P \chi_0$ then the cost function $\sum_{k=0}^{\infty} \chi_k^T Q_p \chi_k$ is minimized and we obtain an equivalent formulation of the LQ problem. Furthermore, the procedure to minimize $\chi_0^T P \chi_0$ can be formulated as a minimization problem in the variable γ that includes the condition $P < \gamma I$.

Now, equation (C.2) can be put in an LMI form. Thus, using equation (C.2), (C.1) we have the following matrix form:

$$-P + \begin{bmatrix} (A-BK)^T & I \end{bmatrix} \begin{bmatrix} P & 0 \\ 0 & Q_p \end{bmatrix} \begin{bmatrix} (A-BK) \\ I \end{bmatrix} < 0,$$

then Schur−complement implies

$$\begin{bmatrix} -P & (A-BK)^T & I \\ (A-BK) & -P^{-1} & 0 \\ I & 0 & -Q_p^{-1} \end{bmatrix} < 0.$$

We can perform the following variable change

$$\begin{bmatrix} P^{-1} & 0 & 0 \\ 0 & I & 0 \\ 0 & 0 & Q^{-1} \end{bmatrix} \begin{bmatrix} -P & (A-BK)^T & I \\ (A-BK) & -P^{-1} & 0 \\ I & 0 & -Q_p^{-1} \end{bmatrix} \begin{bmatrix} P^{-1} & 0 & 0 \\ 0 & I & 0 \\ 0 & 0 & Q^{-1} \end{bmatrix} < 0,$$

thus resulting that

$$\begin{bmatrix} -P^{-1} & P^{-1}(A-BK)^T & P^{-1}Q_p \\ (A-BK)P^{-1} & -P^{-1} & 0 \\ Q_pP^{-1} & 0 & -Q_p \end{bmatrix} < 0,$$

then, using $Q = P^{-1}$, $X_1 = KQ$ the following is obtained

$$\begin{bmatrix} -Q & QA^T - X_1^T B^T & QQ_p \\ AQ - BX_1 & -Q & 0 \\ Q_pQ & 0 & -Q_p \end{bmatrix} < 0.$$

Finally $P < \gamma I$ may be expressed as:

$$\begin{bmatrix} \gamma I & I \\ I & -Q \end{bmatrix} > 0.$$

Thus, the LQ design problem can be stated as:
$\min \gamma$
s.t.
$$\begin{bmatrix} \gamma I & I \\ I & -Q \end{bmatrix} > 0,$$

$$\begin{bmatrix} -Q & QA^T - X_1^T B^T & QQ_p \\ AQ - BX_1 & -Q & 0 \\ Q_pQ & 0 & -Q_p \end{bmatrix} < 0,$$

where $Q = Q^T > 0$ and $X_1 = KQ$.

References

1. D. Balandin and M. Kogan. Synthesis of linear quadratic control laws on basis of linear matrix inequalities. *Automation and Remote Control*, 68:371–385, 2007.
2. S. Boyd, L. E. Gahoui, E. Ferron, and V. Balakrishnan. *Linear Matrix Inequalities in System and Control Theory*, volume 15 of *SIAM Studies in Applied Mathematics*. SIAM, Philadelphia, 1994.

Appendix D
Remote laboratory with the Roto-magnet plant

The Rotomagnet plant has been taken as a basis for the creation of a virtual/remote laboratory. This application has been built using EJS software and LABVIEW. Its features are oriented to realize the limited performance of classic PID control [9, 1] towards the rejection of non-constant disturbances and, at the same time, to show the effectiveness of the IMP for the rejection of periodic disturbances by means of resonators and repetitive control. The laboratory has been integrated in the Automatl@b network, a Spanish interuniversity network of web-based laboratories devoted to distance learning of control engineering [4].

This appendix describes briefly the virtual/remote laboratory features including some operational aspects.

D.1 Application structure

The virtual/remote laboratory application has been built using Easy JAVA Simulations (EJS), which is a JAVA-based software tool for the simulation of physical systems [5]. EJS allows the development of a powerful Graphic User Interface (GUI) (see Figure D.3), thus yielding an interactive illustration of the time and frequency characteristics of a system. The virtual setting is completely developed in EJS using an existing mathematical model of the plant [13] and a GUI designed with EJS. The remote setting has been created using EJS and Laboratory Virtual Instrumentation Engineering Workbench (LABVIEW), which is an application from National Instruments (NI). Both settings have been designed in a homogeneous manner, so few differences exist between the two interfaces.

D.2 EJS-LABVIEW connection

LABVIEW allows a local interaction with the plant and the development of controllers in a simple and straightforward way (see Figure D.1).

LABVIEW includes the feature of Remote Panels, by which the front panel of the application is published on the Internet. This allows the remote control of the LABVIEW application over the web. The drawback of this method is that the remote

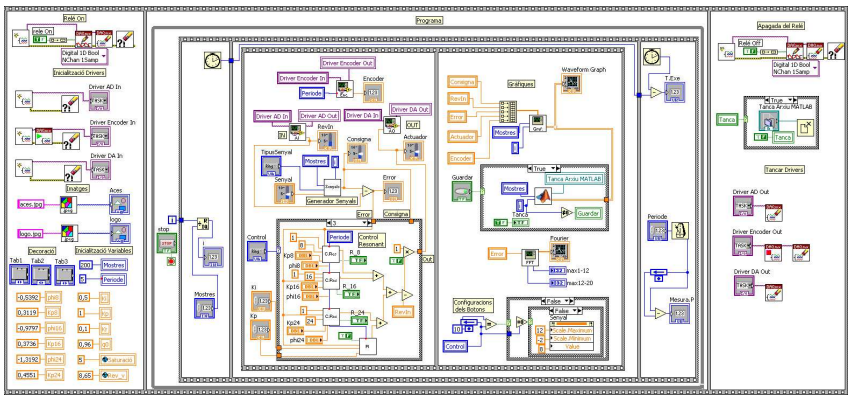

Fig. D.1 Main local control program in LABVIEW.

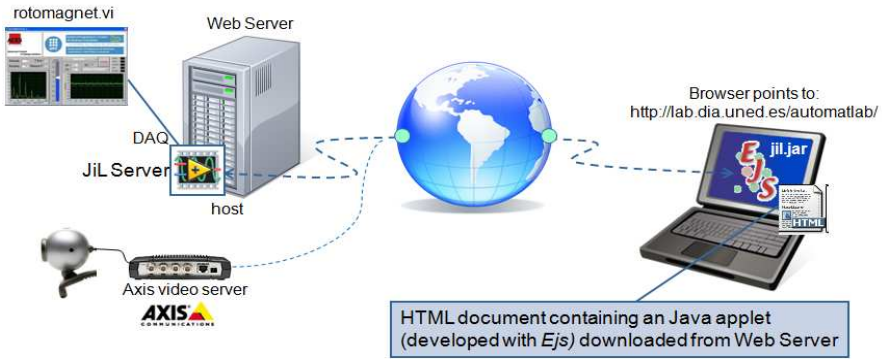

Fig. D.2 Laboratory architecture with JIL server.

user needs to install an additional software in the client machine, the so-called *run-time engine*, provided by NI.

Aiming at providing a solution, the Department of Computer Science and Automatic Control of the UNED[1] has produced a set of software applications that allows the development of virtual and remote laboratories using EJS and LABVIEW [10, 12]. Figure D.2 depicts the communication structure used in this approach. It is based on a JAVA-Internet-LABVIEW (JIL) software module called *JIL server*. This server provides of a plain way to communicate JAVA applets or applications with LABVIEW applications running in remote computers. With this, an EJS application can be integrated with the ability of monitoring, changing and manipulating variables and parameters of a remote LABVIEW application. This setup is combined with a camera and Axis video server (Axis-2400) integrated in the EJS application which provides of visual feedback for the experiments.

[1] Universidad Nacional de Educación a Distancia is a distance learning university in Spain

D.3 Virtual and remote environments

The laboratory application consists of two homogeneous settings:

- The virtual laboratory: in this framework, the plant model is used to compute the time evolution of the system. As shown in Figure D.3, the plant is represented by a geometric scheme. Through the virtual setting the students are introduced for the first time to the system features and serves as a validation tool for analytical calculations. This setting does not consume network resources, operates locally and with no access restrictions.
- The remote laboratory: in this framework it is possible to work with the real plant located in a remote laboratory. In order to ease the use of this setting the GUI is the same used in the virtual laboratory, but the graphic schematic representation of the physical system is here combined with the video streaming of the real plant. The setting also includes an augmented reality [2] display option, in which the simulation model is superimposed to the camera view of the plant (see Figure D.6). This aims at compensating for possible video transmission delays.
  The access to the remote lab is restricted to students who have previously passed the activities performed with the virtual lab, which results in a substantial decrease of the experimentation time required in this setting.

The settings may operate in two ways:

- Manual mode: this mode allows one to carry out open-loop experiments with two main educational purposes. Firstly, to get acquainted with the time and frequency characteristics of the plant and disturbances and, secondly, to understand the need for closed-loop control.
- Automatic mode: this mode allows closed-loop experimentation with different controllers. The experiments are oriented to show the limited performance of PID control for the rejection of non-constant disturbances and to illustrate the IMP benefits for such purpose by means of resonators and repetitive control. Also, the limitations of both control techniques can be tested in this mode.

D.4 Practical example

In this section, the virtual/remote laboratory capabilities are illustrated by means of a practical example which involves a PI controller, resonant control and repetitive control.

The GUI of the virtual/remote laboratory is divided in two main parts (see Figure D.3). The left hand side hosts the representation window, where the system scheme is portrayed. The right hand side, where the evolution of the main system variables are shown both graphically and numerically, contains the system evolution window.

When the plant receives a constant voltage input, its steady-state speed describes a periodic signal (recall Figure D.3). Its specific shape depends on the features of the magnets and on its geometrical distribution, while the frequency depends on the input voltage. In the Device tab, four sliders are shown and four actions can be taken through them in order to modify the geometry and distribution of the fixed and mobile magnets of the plant, thus generating different disturbance shapes. Therefore, the possible actions are:

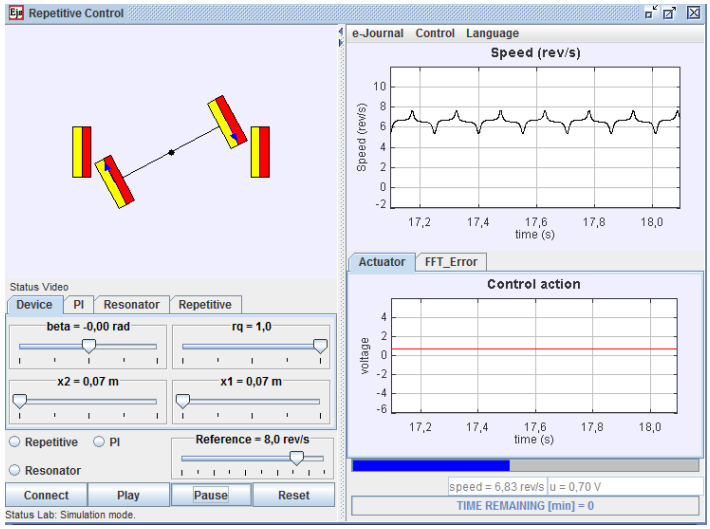

Fig. D.3 Rotomagnet Virtual Laboratory View (open-loop experiments)

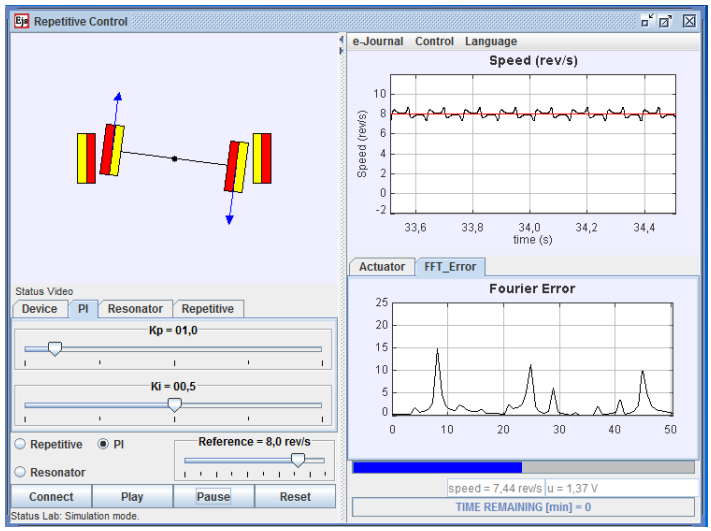

Fig. D.4 PI control (closed-loop experiments): frequency response.

- Close/move away the fixed magnets to/from the axis system
- Rotate the left hand side fixed magnet a certain angle (β)
- Reduce the magnetic pole intensity of one mobile magnet (rq)

All these changes are reflected in the plant scheme.

The limited performance of classic PI control towards the rejection of periodic disturbances can be shown by means of the virtual laboratory. Indeed, Figure D.4 depicts the steady state speed error Fourier transform of the PI controlled plant when the reference speed is set at 8rev/s . Notice that the error frequency components are distributed around 8 Hz and its harmonics. The tab PI allows to tune the proportional and integral gains.

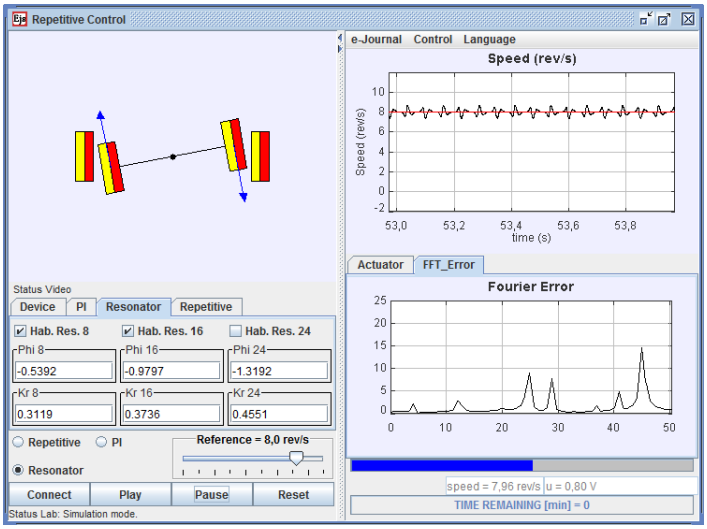

Fig. D.5 Resonant control (closed-loop experiments): frequency response.

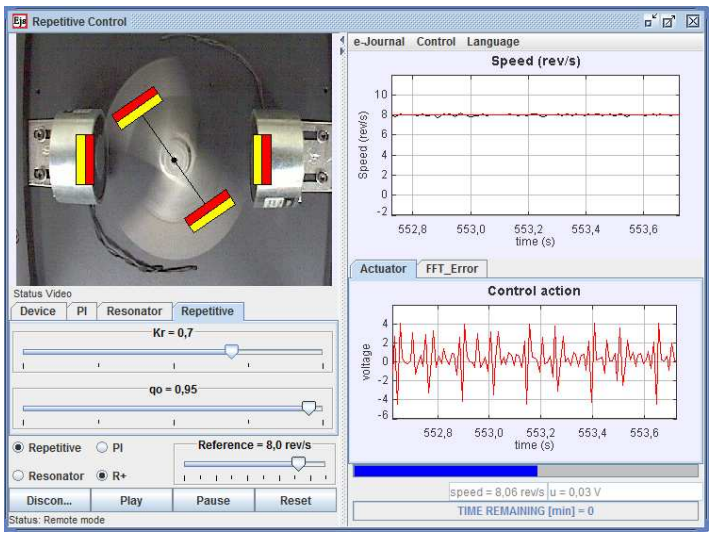

Fig. D.6 Repetitive control in remote setting (closed-loop experiments): time response

The use of a resonant controller composed of two resonators, placed at frequencies of 8 Hz and 16 Hz, allows to overcome the problem. This may be realized from Figure D.5, where the steady-state error Fourier transform shows no components at these frequencies. Furthermore, with the inclusion of additional resonant elements the error could be almost zeroed. The virtual/remote laboratory contains a Resonator tab which allows to apply and modify each resonator implemented for frequencies of 8, 16 and 24 Hz and, thus, to observe separately its effect on the system dynamics. The shift phase and gain parameters can be set independently for each resonator.

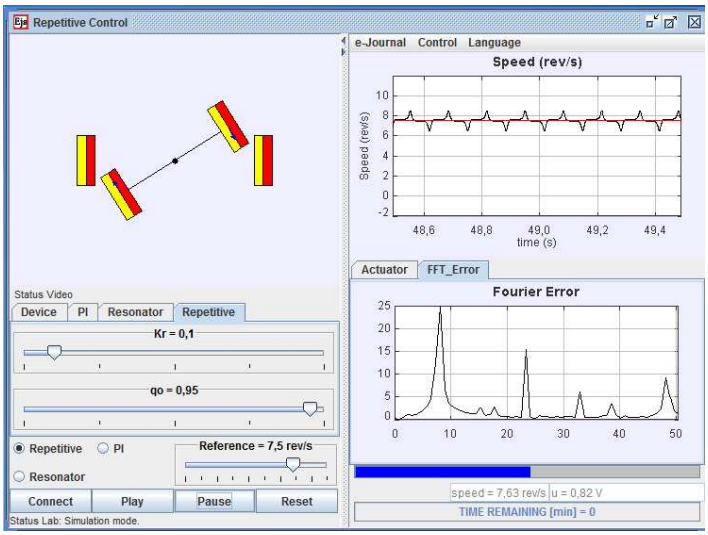

Fig. D.7 Repetitive control with reference different from nominal (closed-loop experiments)

Alternatively, Figure D.6 shows the speed steady state behaviour in remote setting when applying a repetitive controller. As it can be seen, disturbances are completely rejected, while the control action contains the harmonic components. The Repetitive tab allows to tune the repetitive controller, namely, the gain k_r, which can take values in the interval $[0,1]$, and the parameter q_0 of the filter $H(z) = \frac{1-q_0}{2z} + q_0 + \frac{(1-q_0)z}{2}$, which can be adjusted to obtain different frequency responses.

Also, with the Device tab it is possible to change the disturbance shape. In this case it is important to emphasize that performance is maintained, because it depends on the frequency of the disturbance and not in its specific shape.

However, the most important weak point of resonant and repetitive controllers is the need to known the reference/disturbance frequency. As an example, Figure D.7 shows the steady state speed when the reference frequency is 7.5 Hz, while the design frequency of the repetitive controller is 8 Hz. Notice that the control action cannot reject the disturbance effect, and the steady state error becomes a periodical signal. In fact, the results remind those obtained with a regular PI controller (see Figure D.4). Resonant-based controllers show a similar performance if the frequency of the reference/disturbance does not match any of the frequencies of the resonators. This problem can be addressed by means of adaptive schemes [8, 7].

D.5 Educational context

D.5.1 The Automatl@bs network

The Automatl@bs project [4, 11] is a Spanish interuniversity experience that aims at the design, development and exploitation of a network of virtual and remote laboratories for the distance learning of automatic control. Its origin can be traced back

to 2004 when, having in mind the challenging educational changes derived from the European Higher Education Space (EHES), the Education in Automatic Control group of the Spanish Automatic Control Committee boosted the research on improvement and adaptation of the teaching-learning quality in Automatic Control to the EHES requirements.

The laboratories that constitute the Automatl@bs network have been developed by the groups that are involved in the project, which belong to the Universities of Alicante, Almería, León, Miguel Hernández (Elche), UNED, Technical University of Catalonia and Politechnical University of Valencia [11, 6, 3]. The labs offer an integrated environment where to carry out practical activities at different levels. As it provides of a common working setting and of a time booking system to perform the remote experiments, Automatl@bs can be regarded as a single laboratory despite the fact that the plants are physically located in different places.

References

1. O. Arrieta and R. Vilanova. Performance degradation analysis of controller tuning modes: application to an optimal pid tuning. *International Journal of Innovative Computing, Information and Control*, 6(10):4719–4730, 2010.
2. R. Azuma, Y. Baillot, B. MacIntyre, R. Behringer, S. K. Feiner, and S. Julier. Recent advances in augmented reality. *IEEE Computer Graphics and Applications*, 21(6):34–47, 2001.
3. R. Costa-Castelló, M. Vallés, L. M. Jiménez, L. Diaz-Guerra, A. Valera, and R. Puerto. Integración de dispositivos físicos en un laboratorio remoto de control mediante diferentes plataformas: Labview, matlab y c/c++. *Revista Iberoamericana de Automática e Informática Industrial*, 7(1):23–34, 2010.
4. S. Dormido, H. Vargas, J. Sánchez, R. Dormido, N. Duro, S. Dormido-Canto., and F. Morilla. Developing and implementing virtual and remote labs for control education: The UNED pilot experience. In *Proceedings of the 17th IFAC World Congress*, pages 12655–12660, 2008.
5. F. Esquembre. *Creación de Simulaciones Interactivas en Java. Aplicación a la Enseñanza de la Física*. Pearson Prentice Hall. Educación, 2005.
6. J. L. Guzman, M. Domínguez, M. Berenguel, J. J. Fuentes, F. Rodríguez, and P. Reguera. Entornos de experimentación para la enseñanza de conceptos básicos de modelado y control. *Revista Iberoamericana de Automática e Informática Industrial*, 7(1):10–22, 2010.
7. J. Olm, G. Ramos, and R. Costa-Castelló. Stability analysis of digital repetitive control systems under time-varying sampling period. *Control Theory Applications, IET*, 5(1):29 –37, 6 2011.
8. J. M. Olm, G. A. Ramos, and R. Costa-Castelló. Adaptive compensation strategy for the tracking/rejection of signals with time-varying frequency in digital repetitive control systems. *Journal of Process Control*, 20(4):551 – 558, 2010.
9. C. Pedret, A. Ibeas, R. Vilanova, and M. de la Sen. Reduced-order modeling based on generalized holds: application to digital pid control. *International Journal of Innovative Computing, Information and Control*, 6(7):3053–3066, 2010.
10. H. Vargas, J. Sánchez, N. Duro, R. Dormido, S. Dormido-Canto, G. Farias, S. Dormido, F. Esquembre, C. Salzmann, and D. Gillet. A systematic two-layer approach to develop web-based experimentation environments for control engineering education. *Intelligent Automation & Soft Computing*, 14(4):505–524, 2008.
11. H. Vargas, J. Sánchez, C. A. Jara, F. A. Candelas, O. Reinoso, and J. L. Díez. Docencia en automática: Aplicación de las TIC a la realización de actividades prácticas a través de internet. *Revista Iberoamericana de Automática e Informática Industrial*, 7(1):35–45, 2010.
12. H. Vargas, J. Sánchez-Moreno, S. Dormido, C. Salzmann, D. Gillet, and F. Esquembre. Web-enabled remote scientific environments. *Computing in Science and Engineering*, 11(3):36–46, 2009.
13. E. Xargay and R. Costa-Castelló. Modelado de una planta diseñada para ilustrar el principio del modelo interno. In E. por J.A. Somolinos, editor, *Proceedings of the XXV Jornadas de Automática*, Ciudad Real, Septiembre 2004. ISBN 84-688-7460-4. Dep Legal: CR-388-2004.

List of Publications

Articles in Journals

1. J.M. Olm, G.A. Ramos, and R. Costa-Castelló. Stability Analysis of Digital Repetitive Control Systems Under Time-Varying Sampling Period. *IET Control Theory & Applications.*, vol.5, no.1, pp.29-37, 2011.

   - Contributions related with Sections 3.4 and 6.4.

2. J.M. Olm, G.A. Ramos, and R. Costa-Castelló. Adaptive compensation strategy for the tracking/rejection of signals with time-varying frequency in digital repetitive control systems, *Journal of Process Control*, vol. 21(4), pp. 551-558, 2010.

   - Contributions related with Sections 4.3 and 6.6.

3. G.A. Ramos, J.M. Olm, and R. Costa-Castelló. Digital repetitive control under non-uniform sampling: an LMI stability analysis, *Mathematical Problems in Engineering*, vol. 2011, pp. 16 pages, 2011.

   - Contributions related with Sections 3.3 and 6.4.

4. R. Costa-Castelló, J.M. Olm, and G.A. Ramos. Design and analysis strategies for digital repetitive control systems with time-varying reference/disturbance period, *International Journal of Control*, vol. 84(7), pp. 1209-1222, 2011.

   - Contributions related with Sections 3.3, 3.4, 4.3, 6.4 and 6.6.

5. G.A. Ramos, J.M. Olm, and R. Costa-Castelló. A survey of repetitive control in varying frequency conditions, *Ingeniería e Investigación*, vol. 31(2), pp. 29-37, 2011.

   - Contributions related with Chapter 2.

6. R. Costa-Castelló, J.M. Olm, H. Vargas, and G.A. Ramos. An educational approach to the internal model principle for periodic signals, *International Journal of Innovative Computing, Information and Control*, in press, 2011.

   - Contributions related with Appendix D.

7. G.A. Ramos and R. Costa-Castelló. Power factor correction and harmonic compensation using second-order odd-harmonic repetitive control. *IET Control Theory & Applications.*, in press, 2012.

   - Contributions related with Chapter 5 and Section 7.7.

8. G.A. Ramos, R. Costa-Castelló and J.M. Olm. Analysis and Design of a Robust Odd-Harmonic Repetitive Controller for an Active Filter under Variable Network Frequency. *Control Engineering Practice.*, in press, 2012.

   - Contributions related with Sections 4.2, 7.2 and 7.6.

Articles in conference proceedings

1. G.A. Ramos and R. Costa-Castelló. An optimal anti-windup strategy for repetitive control systems. IEEE Conference on Decision and Control. *Proceedings of the 50th IEEE Conference on Decision and Control and European Control Conference*. Orlando: December, 2011, pp. 6043-6048

2. R. Costa-Castelló, G.A. Ramos, and J.M. Olm. A comparative study of repetitive control techniques for active power filters under network frequency variations, *Proc. IV Seminar for Advanced Industrial Control Applications*, pp. 116-121, November, 2011

3. G.A. Ramos, J.M. Olm, and R. Costa-Castelló. Repetitive control of an active filter under varying network frequency: power factor correction, *Proc. IEEE XI Latin American Robotics Competition & Colombian Conference on Automatic Control*, October, 2011

4. R. Costa-Castelló, G.A. Ramos, J.M. Olm, and M. Steinbuch. Second-order odd-harmonic repetitive control and its application to active filter control. In *49th IEEE Conference on Decision and Control*, pages 6967-6972, Hilton Atlanta Hotel in Atlanta, Georgia USA, December 15-17 2010.

5. G.A. Ramos, R. Costa-Castelló, and J.M. Olm. Anti-windup schemes comparison for digital repetitive control. In *15th IEEE International Conference on Emerging Technologies and Factory Automation*, pages 1-7, Bilbao, September 13-16 2010.

6. R. Costa-Castelló, J.M. Olm, G.A. Ramos, and R. Cardoner-Parpal. Odd-harmonic repetitive control of an active filter under varying network frequency: Practical considerations. In *Proceedings of the IEEE International Conference on Control Applications Part of 2010 IEEE Multi-Conference on Systems and Control*, pages 398-403, Yokohama, Japan, September 8-10 2010.

7. J.M. Olm, G.A. Ramos, R. Costa-Castelló, and R. Cardoner. Odd-harmonic repetitive control of an active filter under varying network frequency: Control design and stability analysis. In *American Control Conference (ACC'10)*, pages 1749-1754, Baltimore, MD (USA), June 30-July 02, 2010.

8. R. Costa-Castelló, J.M. Olm, and G.A. Ramos. Design and analysis strategies for digital repetitive control systems with time-varying reference/disturbance period. In *Symposium on Learning Control at IEEE CDC 2009*, December 2009.

9. L. Diaz, G.A. Ramos, H. Vargas, and R. Costa-Castelló. A virtual/remote laboratory to illustrate the internal model principle for periodical signals. In *8th IFAC Symposium on Advances in Control Education (ACE2009)*, October 2009.

10. J.M. Olm, G.A. Ramos, and R. Costa-Castelló. Análisis de estabilidad de controladores repetitivos con periodo de muestreo variable mediante técnicas de control robusto. In *JA2009 Jornadas de Automática 2009*, September 2009.

11. G.A. Ramos, J.M. Olm, and R. Costa-Castelló. Adaptive compensation strategy for the tracking/rejection of signals with time-varying frequency in digital repetitive control systems. In *ETFA 2009 - 14th IEEE International Conference on Emerging Techonologies and Factory Automation*, September 2009.

12. G.A. Ramos, J.M. Olm, and R. Costa-Castelló. Anlisis de estabilidad de un sistema de control repetitivo digital con periodo de muestreo variable. In *SAAEI09 Seminario Anual de Automtica, Electrónica Industrial e Instrumentación*, July 2009.

13. G.A. Ramos, J.M. Olm, and R. Costa-Castelló. Digital repetitive control under time-varying sampling period: An lmi stability analysis. In *Control Applications, (CCA) & Intelligent Control, (ISIC), 2009 IEEE*, pages 782-787, July 2009.